EXPERIMENTAL INVESTIGATION AND MODELING OF DROPWISE CONDENSATION ON A HORIZONTAL GOLD COATED TUBE

A THESIS SUBMITTED TO
THE GRADUATE SCHOOL OF NATURAL AND APPLIED SCIENCES
OF
MIDDLE EAST TECHNICAL UNIVERSITY

BY

ORHAN SERDAR

IN PARTIAL FULFILLMENT OF THE REQUIREMENTS
FOR
THE DEGREE OF MASTER OF SCIENCE
IN
MECHANICAL ENGINEERING

DECEMBER 2004

Approval of the Graduate School of Natural and Applied Sciences

_____
Prof. Dr. Canan ÖZGEN
Director

I certify that this thesis satisfies all the requirements as a thesis for the degree of Master of Science.

_____
Prof. Dr. S. Kemal İDER
Head of Department

This is to certify that we have read this thesis and that in our opinion it is fully adequate, in scope and quality, as a thesis for the degree of Master of Science.

_____
Assoc. Prof. Dr. Cemil YAMALI
Supervisor

Examining Committee Members

Prof. Dr. Demir BAYKA _____

Assoc. Prof. Dr. Cemil YAMALI _____

Prof. Dr. Kahraman ALBAYRAK _____

Asst. Prof. Dr. Tahsin ÇETİNKAYA _____

Prof. Dr. Ercan ATAER _____

I here declare that all information in this document has been obtained and presented in accordance with academic rules and ethical conduct. I also declare that, as required by these rules and conduct, I have fully cited and referenced all material and the results that are not originial to this work.

Orhan SERDAR

ABSTRACT

EXPERIMENTAL INVESTIGATION AND MODELING OF

DROPWISE CONDENSATION ON A HORIZONTAL GOLD COATED TUBE

SERDAR, Orhan

M.S., Department of Mechanical Engineering

Supervisor: Assoc. Prof. Dr. Cemil Yamalı

December 2004, 141 pages

The phenomenon dropwise condensation on a horizontal gold coated tube is investigated by both analytical and experimental methods in this study. A computer program is prepared to calculate the dropwise condensation heat transfer rate on the horizontal gold coated tube. An experimental setup was also manufactured to measure the dropwise condensation heat transfer rate.

The effects of flow rate, temperature of cooling water and also steam to wall temperature difference have been analytically investigated by using Mathcad computer program. Experiments were carried out at different inlet temperatures of

cooling water. Effects of cooling water at different flow rates are also experimentally investigated. Results of the experiments are compared to those of the literature and the analytical results.

Keywords: Dropwise condensation, horizontal tube, dropsize distribution, sweeping, departure size, experimental study, analytical study.

ÖZ

ALTIN KAPLI YATAY BİR BORU ÜZERİNDE
DAMLACIK YOĞUŞMASININ MODELLENMESİ VE DENEYSEL OLARAK İNCELENMESİ

SERDAR , Orhan

Yüksek Lisans, Makina Mühendisliği Bölümü

Tez Yöneticisi: Doç. Dr. Cemil Yamalı

Aralık 2004, 141 sayfa

Bu çalışmada, yüzeyi altın ile kaplı yatay bir boru üzerinde su buharının yoğuşması problemi analitik ve deneysel yöntemlerle incelenmiştir. Altın kaplı yatay boru üzerindeki damlacık yoğuşmasını analiz eden bir bilgisayar programı yazılmıştır. Yoğuşma problemini gözlemleyebilmek için bir deney düzeneği de hazırlanmıştır.

Soğutma suyu giriş sıcaklığı, akış debisi ve buhar ile boru yüzeyi arasındaki sıcaklık farkının etkileri, Mathcad bilgisayar programı yardımıyla incelenmiştir. Deneyler; soğutma suyunun, farklı giriş sıcaklıklarında gerçekleştirilmiştir. Soğutma suyunun farklı akış oranlarının etkileri de deneysel olarak incelenmiştir. Deneylerden

elde edilen sonuçlar, literatürdeki sonuçlar ve analitik araştırmadan elde edilen sonuçlarla karşılaştırılmıştır.

Anahtar Kelimeler: Damlacık yoğuşması, yatay silindir, damlacık dağılımı, süpürme, damlacık ayrılma boyutu, deneysel çalışma, analitik çalışma.

To my parents , whom I owe my existence,

And to Mr. Beşir ERAKİ ,

who will always be remembered with respect and love

(May He Rest In Peace)

ACKNOWLEDGEMENTS

I express my sincere appreciation to Assoc. Prof. Dr. Cemil Yamalı for his guidance, support, understanding and valuable contributions throughout the research.

Thanks are extended to the examining committee members for sparing time to read this thesis and for their valuable suggestions and comments.

I gratefully acknowledge Mustafa Yalçın, Mustafa Topsakal for their technical assistance in manufacturing and operating the setup and Sir Ramazan Büyükpoyraz and Lady Feray Koca for their valueable ideas.

My special thanks are for the managing staff of Electronic Research and Development Center of Turkish Railway for giving me valuable time accomplish this study.

I. express my deepest gratitude to my mother Halise Eraki Serdar and my father Hasan Serdar, not only because they supported me throughout my education life, as well as during this study, but also they provided me good living and working conditions.

TABLE OF CONTENTS

PLAGIARISM.....iv

ABSTRACT.....iv

ÖZ.....vii

ACKNOWLEDGEMENTS.....ix

TABLE OF CONTENTS.....x

LIST OF TABLES..... xiii

LIST OF FIGURES.....xv

LIST OF SYMBOLS.....xviii

CHAPTER

1. INTRODUCTION.....1

    1.1 Condensation……...……...1

2. LITERATURE SURVEY.....5

    2.1 Drop Size Distribution.....10

    2.2 Conduction Through Droplets.....13

    2.3 Effects of Non-condensable Gases.....13

    2.4 Promoting Dropwise Condensation.....16

3. ANALYTICAL MODEL…….…….....…..…….....27

    3.1 Conduction Through a Single Droplet.....31

    3.2 Heat Flux in Dropwise Condensation Excluding The Effect of Sweeping.....36

3.3 Heat Flux in Coalescence Range..... 37

3.4 Variation of Departing Size of a Droplet on The Cylindrical Surface..... 44

4. EXPERIMENTAL STUDY.....51

4.1 Cooling Water Tank.....56

4.2 Boiler.....57

4.3 Test Section.....58

4.4 Working Fluid.....63

4.5 Test Piece.....64

4.6 Temperature Measurement System 66

4.6.1Measuring of The Condenser Surface Temperature 68

4.7 Experimental Procedure..... 72

5. RESULTS AND DISCUSSIONS.....74

5.1 Analytical Results.....74

5.1.1 Effect of Steam to Wall Temperature Difference on Condensation Heat Transfer.....76

5.2 Experimental Results.....83

5.2.1 Results of the Experiments Performed at Different Flow Rates and Cooling Water Inlet Temperatures.....84

5.3 Comparison of Analytical and Experimental Results 88

5.3.1 Comparison of Experimental Results with Literature.....88

5.3.2 Comparison of Experimental Results with Analytical Results.....92

5.4 Effect of Fractional Area (f_{co}) on Condensation Heat Transfer.....102

6. CONCLUSIONS.....106

6.1 Recommendations for Future Work.....107

REFERENCES.....108

APPENDICES

A. RESULTS OF THE EXPERIMENTS.....116

B. MATHCAD PROGRAM SOURCE.....119

LIST OF TABLES

TABLE

2.1 Condensation mode criteria.....24

3.1 Variation of departing size droplet with angle α for cylindrical surface 49

4.1 The temperature values of thermocouples $[T_1, T_2, T_3]$, the equations of temperature distribution $[T(r)]$, condenser surface temperature $[T_s]$.....71

5.1 Variation of local heat transfer rate on the condenser surface at different surface subcooling (ΔT) with departing droplet radius (r_{dep}).....77

5.2 Variation of local heat transfer coefficient on the condenser surface at different surface subcooling ΔT with departing droplet radius (r_{dep}).....77

5.3 Variation of mean heat transfer rate, heat flux and heat transfer coefficient for entire condenser surface with surface subcooling (ΔT). 79

5.4 Filmwise condensation heat transfer coefficient 82

5.5 Variation of mean heat transfer coefficient by experiments at different cooling water inlet temperatures with surface subcoolings (ΔT). 87

5.6 Contact angle for various surfaces 89

5.7 Condensation modes for various surfaces 90

5.8 Variations of mean heat transfer rate, heat flux, and heat transfer coefficient for constant value of $r_{dep} = 0.159 \times 10^{-2}$ with surface subcooling.....93

5.9 Comparison of mean heat transfer coefficient for different surface subcooling (ΔT) with constant departing droplet radius $r_{dep} = 0.159 \times 10^{-2}$ and varying $r_{dep} = 0.16 \times 10^{-2} mK\ 1.2 \times 10^{-2} m$. 96

5.10 Comparison of heat transfer coefficient for different surface subcooling (ΔT) with departing droplet radius (r_{dep}). 98

5.11 Comparison of heat transfer coefficient for different surface subcoolings (ΔT) with coalescence size droplet radius (r_{co}) 100

A.1 Experimental Data and Results for $T_{in} = 20°C$ 116

A.2 Experimental Data and Results for $T_{in} = 30°C$ 116

A.3 Experimental Data and Results for $T_{in} = 40°C$ 117

A.4 Experimental Data and Results for $T_{in} = 50°C$ 117

A.5 Experimental Data and Results for $T_{in} = 60°C$ 117

A.6 Experimental Data and Results for $T_{in} = 70°C$ 118

LIST OF FIGURES

FIGURE

2.1 Reflectance spectrum for very slow steam rate.....6

2.2 Reflectance spectrum of the position between two drops for very slow steam rate.....7

2.3 Comparison of drop distribution between random fractal model and photography.....12

2.4 Variation of overall heat transfer coefficient with the row number of cylindrical tubes.....16

2.5 The behaviour of water droplet on the different surfaces.....21

2.6 Surface energy and equilibrium contact angle of water for different coating systems.....22

2.7 The behaviour of water droplet on the different surfaces 23

2.8 The CAM-100 contact angle measuring equipment.....25

2.9 The contact angle data for plain copper tube.....26

2.10 The contact angle data for stearic asit coated tube.....26

3.1 Coalescence of two water drops on the condenser surface.....30

3.2 Droplets at 5700 times magnification.....30

3.3 Model for heat conduction through a droplet.....33

3.4 Drop distribution over the condenser surface during steam condensation cycle obtained by a theoretical model…….....38

3.5 Maximum droplet radius and isolated droplet radius vs. time.....39

3.6 The droplet on vertical surface acting gravity.....45

3.7 Gravitational force acting on a droplet resting on a cylindrical surface.....46

3.8 Variation of departure sizeon the condenser surface.....47

3.9 Variation of departure size with angle of α.....50

4.1 Schematic presentation of the apparatus.....52

4.2 General view of the experimental setup.....54

4.3 Schematic layout of the experimental setup.....55

4.4 General view of the cooling water tank.....56

4.5 General view of the boiler 57

4.6 General view of the test section.....58

4.7 Front view of the test section.....59

4.8 Drawing of the gauge and the metal rings.....60

4.9 Drawing of the teflon component.....61

4.10 Drawing of the test section - front view.....62

4.11 Drawing of the test section - lateral view.....63

4.12 Dropwise condensation on the gold coated condenser surface.....65

4.13 The condenser surface - lateral view.....66

4.14 The condenser surface - front view 66

4.15 Temperature measurement system.....67

4.16 The positions of thermocouple holes on the condensation tube.....69

4.17 A typical variation of temperature value $[T_1, T_2, T_3]$ inside condensation tube with respect to the distance of thermocouple holes from the center of the condensation tube (11.5 - 15 -18mm).....70

5.1 Variation of local heat transfer coefficient with departure size.....78

5.2 Variation of local heat transfer coefficient with angle 78

5.3 Variation of mean heat flux with surface subcooling (ΔT).....80

5.4 Variation of mean heat transfer coefficient with surface subcooling (ΔT).....81

5.5 Variation of filmwise condensation heat transfer coefficient with surface subcooling (ΔT) 83

5.6 Variation of mean heat flux with surface subcooling.....85

5.7 Variation of mean heat transfer coefficient with surface subcooling ……86

5.8 Comparison of mean heat transfer coefficient with surface subcooling.....91

5.9 Comparison of mean heat flux with surface subcooling.....92

5.10 Comparison of mean heat flux with surface subcooling.....95

5.11 Comparison of the mean heat transfer coefficient with surface subcooling.....97

5.12 Comparison of mean heat transfer coefficient for different fractional area coefficient n with departing size droplet radius (r_{dep}).....99

5.13 Comparison of heat transfer coefficient for different fractional area coefficient n with coalescence size droplet radius (r_{co}).....101

5.14 Variation of fractional area with coefficent n.....103

5.15 Variation of heat transfer coefficient for different coalescence size drop radius with respect to fractional area constant n 104

5.16 Variation of fractional area with drop radius at different fractional coefficient n.....105

LIST OF SYMBOLS

C_p	Specific heat at constant pressure	[J/(kg.K)]
g	Gravity	[m/s^2)
h	Heat transfer coefficient	[W/(m^2.K)]
h_{fg}	Latent heat of evaporation	[J/kg]
k	Thermal conductivity	[W/(m.K)]
L	Length	[m]
q"	Heat flux	[W/m^2]
Q	Heat transfer rate	[W]
r	Radius of the droplets	[m]
T	Temperature	[°C]
fco	Fraction of Area	
n	Fractional Area Coefficient	
R	Radius of Curvature	[m]
P_v^*	Saturation Pressure	[N/m²]
G	Gas Constant	[J/kg.K]
Ti	Temperature of Liquid-Vapor Interface	[°C]
$\dot{m}$	Mass Flow Rate	[kg/s]

σ	Surface Tension	[N/m]
γ	Condensation Coefficient	
ρ	Density	[kg/m^3]
θ	Contact Angle	[rad]

Subscripts

cond	Condensation
f	Fluid
g	Water vapor
i	Loop variable
in	Inlet
out	Outlet
sat	Saturation
v	Vapor
w	Wall
max	Maximum
co	Coalescence
l	Liquid
s	Surface
d	Droplet
T	Total
dc	Direct Condensation

CHAPTER 1

INTRODUCTION

1.1 Condensation

Condensation is a phenomena frequently encountered in nature, defined as the phase change from the vapor state to the liquid or the solid state. This can take place within a bulk vapor when its temperature is below the saturation temperature corresponding to its pressure, or on a solid surface whose temperature is below the saturation temperature of the vapor. In the latter case the vapor temperature itself may be either at saturation or superheated. In any case, condensation requires a certain amount of subcooling.

During the phase change process energy in the form of the latent heat must be removed from the region of condensation, either by convection, diffusion or radiation. A pressure decrease occurs in the region where condensation is taking place, as a result mass diffuses toward this region. The condensation phenomenon can be classified as:

1) Bulk condensation

2) Surface condensation

Bulk condensation takes place within the bulk of the vapor away from any solid or liquid boundaries.

Surface condensation is the condensation taking place on a subcooled solid surface when exposed to vapor. Because of its wide application in industry, it is the

most important one from the engineering point of view. Surface condensation can be classified further as either dropwise or filmwise condensation. Depending upon the characteristics of the condenser surface employed, either one or both of these can take place on a surface.

Filmwise condensation is the most widely observed mode, and occurs if the liquid wets the condenser surface, resulting in the coverage of the surface by a liquid condensate film. This film is removed from the surface under the action of the gravity , acceleration or other body forces and/or shear stresses due to vapor flow.

Dropwise condensation occurs if the condensate does not wet the condenser surface. In this type of condensation vapor in contact with a subcooled surface form microscopic droplets on the surface, which then grow by the direct condensation on the droplets and by coalescences between the droplets, until a certain size is reached. The drops then leave the surface by the action of body forces and/or vapor shear. It has been noted that the heat transfer coefficient with dropwise condensation is an order of magnitude larger than that with filmwise condensation. This would seem to make dropwise condensation a very attractive mechanism in for industrial applications.

No satisfactory means of sustaining dropwise condensation over a long period of time could be found, which has hindered industrial applications of this efficient heat transfer mechanism.

Film condensation occurs when the liquid wets the surface and the condenser surface is blanketed by a condensate film. This film represents a thermal resistance to heat transfer and a temperature gradient exists in the film.

Dropwise condensation occurs on a surface which is coated with a substance that inhibits wetting. Heat transfer rates in dropwise condensation may be ten times higher than in film condensation. Since very high heat transfer rates can be obtained,

it is desired to have dropwise condensation in applications. It is possible to reduce the heat transfer area half or less in a condenser system by using dropwise condensation.

Various surface coatings, such as gold, silicones and teflon, have been used in the industry to maintain dropwise condensation but none of these methods has reached any considerable success. The effectiveness of such coatings gradually decreases due to oxidation and fouling and film condensation occurs after a period of time. Another reason of losing the effectiveness of dropwise condensation is the accumulation of droplets on the condenser surface. Heat transfer rate sharply decreases because of the accumulated droplets. Therefore, most condensers are designed on the assumption that film condensation will take place on the surface.

Unlike filmwise condensation, the physical processes taking place in dropwise condensation are complex and random when viewed on a detailed scale. Moreover the parameters affecting dropwise condensation are more difficult to control (e.g. the number of nucleation sites, and non-condensable gases). The major portion of the heat transfer with dropwise condensation takes place on droplets of microscopic sizes.

In early studies the majority of research workers produced dropwise condensation by means of chemical promoters. Recent studies showed that coating the condenser surface with noble metals, particularly gold, may be the ultimate solution of the problem of sustaining dropwise condensation over long periods of time. It has been suggested that an optimum coating thickness, thick enough to obtain dropwise condensation and at the same time thin enough to keep the coating expenses to a minimum, can be found.

Dropwise condensation is essentially a cyclic process. The many droplets that cover the surface pass through the same cycle of subprocesses. A drop cycle begins

with the nucleation of single droplets at preferred nucleation sites (1). These droplets grow by direct condensation only, up to a size on the order of magnitude of the distance between neighboring nucleation sites. Beyond this point coalescences between neighboring drops can take place and the subsequent growth of the drops may be considered to occur by the combination of direct condensation and by coalescence. As a result of the coalescences, the number of droplets per unit area decreases as the drop sizes increase, while the condensing surface area covered by these drops increases. Coalescences between droplets provides a continuous source of nucleation sites, since the movement of the droplets expose bare areas on which these sites may exist.

When a drop reaches a size at which the body forces exceed the surface tension forces holding the drop to the solid surface, the drop departs and sweeps the surface clear, permitting new nucleation sites to become available in the sweeping path.

The understanding and description of dropwise condensation thus depends upon a careful analysis of the cyclic subprocesses which begin with the nucleation of droplet, continues with growth and seemingly random coalescences and ends with the drop departing and sweeping the surface.

The size at which drops are removed from the surface is called the departure size. The departure size is an important parameter in dropwise condensation: By intuition it can be concluded that a decrease in the departure size results in an increase in heat transfer coefficients. Since the departure size is related to the drop size distribution and the sweeping frequency, a study of the influence of departure size on dropwise condensation heat transfer can be expected to improve the understanding of this phenomenon.

CHAPTER 2

LITERATURE SURVEY

The higher heat transfer performance due to dropwise condensation as compared with filmwise condensation has been of considerable interest to many researchers around the world since the first paper on dropwise condensation heat transfer was published by Schmidt et al. (2) in 1930.

Historically, there are two opposite hypotheses on the mechanism of the formation of the initial droplet: the film fracture hypothesis and the nucleation hypothesis. The latter one has been supported by most of the workers since microscopic observations provided by McCormic and Westwater (3) indicated that there was no visible condensate liquid film existing among droplets. However, Song et al. (4) have put forward a droplet and condensate film coexisting mechanism of the formation of droplets during dropwise condensation.

They proposed that a thin condensate film exists on the area among the droplets and also that a condensate film exists at the spots from which the droplets departed.

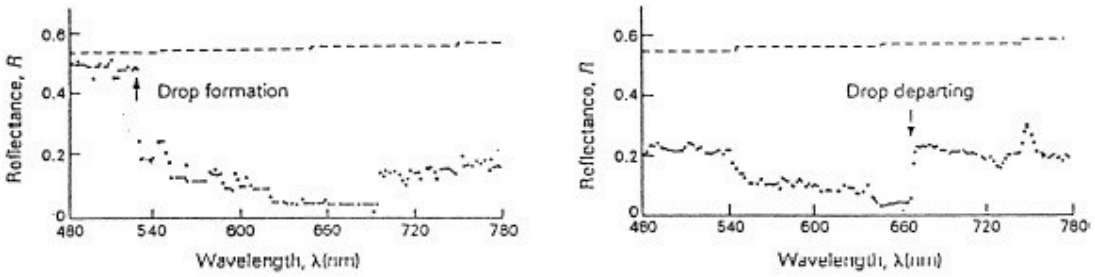

(a) (b)

Figure 2.1 Reflectance spectrum for very slow steam rate (a- Location between two drops, and b- Spot of departing drop).

They also experimentally demonstrate the existence of condensate film by comparing the measured reflectance spectra of certain locations on the condensation surface in the condensation environment with the standard reflectance spectrum, i.e. the reflectance spectrum on the plain surface without contacting the steam or condensate liquid (the dashed line at the top area in Figs. 2.1 and 2.2), as shown in Figs. 2.1 and 2.2. The experiments were conducted at the atmospheric pressure with surface subcooling temperature difference ranging from 1 to 5 K. In the case of low steam flow rate , it can be seen from Fig. 2.1 that the reflectance spectra at locations where the droplet was formed before (on the left-hand side of the arrow in Fig. 2.1a) or the droplet departed later (the arrow position in Fig. 2.1b), were below the standard reflectance spectrum. This indicated that condensate film exists on the condensation surface all along. From Fig. 2.2, similar results were also found for the case of normal steam flow rate except that the frequency of droplet formation was much faster than that of the situation in Fig. 2.1.

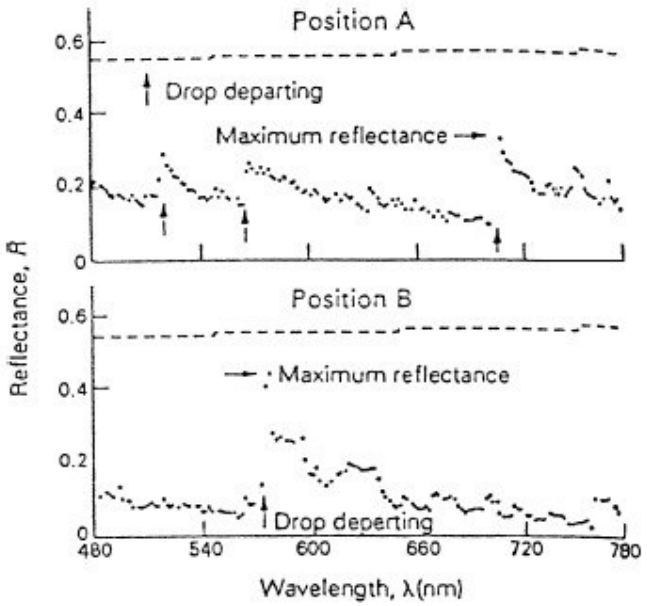

Figure 2.2 Reflectance spectrum of the position between two drops for very slow steam rate

Regarding the mechanism for the nucleation process, Jakob (5) also proposed that the process begins with the formation of a very thin layer of condensate on the bare surface. This film grows quickly in thickness from zero to some critical value, at which time it fractures and forms droplets. A new layer begins to grow in the bare area left by the fractured film. He also speculated that the critical thickness of the film from which the drops are formed has a certain value. He concluded that in order for the heat transfer coefficient with dropwise condensation to be much larger than that with film condensation, the film between the droplets must be extremely thin. Approximate calculations of Jakob(5) showed the mean thickness of the film between, the droplets to be on the order of 0.001 mm. According to the film fracture model, then, all condensation is of a film type. However, with "dropwise"

condensation , a definite limitation exists on the maximum possible thickness of this film, which ruptures to form the subsequent drops.

Emmons (6) attempted to account for the large heat transfer rates associated with dropwise condensation as being a result of a reevaporation process between the droplets. According to this model, condensing and reevaporating vapor molecules form a supersaturated vapor blanket on the bare area between droplets. When this supersaturated vapor comes into contact with the drop, condensation occurs. Erb and Thelen (7), like Emmons, also assumed a reevaporation process but modified the mechanism slightly. According to this model the heat transfer is explained as a two step process. In the first step vapor is supercooled by heat transfer with the condenser surface. Part of the supercooled vapor is condensed on a drop while the remainder is heated by the heat of vaporization released and becomes saturated. This cooling and heating cycle repeats itself. Although both models consider that the final condensation occurs directly on the droplets themselves, they give the impression that the major portion of the heat transfer takes place in the area between the droplets, subcooling the vapor.

Eucken(8) proposed a diffusion mechanism in which an absorbed layer of vapor molecules on the bare surface between the droplets is presumed to exist. The temperature of this layer varies from the saturation temperature near the droplet to the condensation surface temperature far away from the droplet, and is thus subcooled.

In order to form an experimental basis to describe the mechanism of dropwise condensation, Welch and Westwater (9) made high speed motion pictures through a microscope. The films showed that numerous coalescences took place between the

extremely small drops. When a coalescence took place a distinct flash of light was observed at the portion of the surface cleaned as a result of the coalescence. The luster disappeared in about one millisecond, and they concluded that this disappearance of the luster was associated with the formation of a thin film.

McCormick and Baer (1) provided the first experimental evidence on the nucleation character of dropwise condensation. They conducted repetitive condensation test on a given surface; drops were condensed, then evaporated and condensed again. It was observed, that even after a number of repetitions; drops appeared to grow from the same site. The magnification used was 600 fold. As part of this study, fifty control drops were randomly chosen and their location on the surface marked on a projection screen. In subsequent runs the number of control drops appearing in the same location varied between 25 and 50, being closer to 50 most of the time. These observations would appear to weaken the film fracture hypothesis considerably. However, it is also conceivable that upon the fracture of a "film", that surface tension would draw the film together at a more or less fixed location, which may then be identified as a nucleation site. The nucleation hypothesis is further strengthened by the observations in this work that droplets form along scratches on the surface, and that the surface roughness definitely effects the population of primary droplets. Primary drop densities were observed to vary from 1.7×10^4 drops/cm² for very smooth surfaces up to 22×10^4 drops/cm² for very rough surface. Since the overall temperature difference was maintained constant in the experiments, these variations could not be due to changes in temperature difference.

Umur and Griffith (10) show, theoretically and experimentally, that no condensate film on the surface thicker than a monolayer can form. They reasoned that if a film forms on a surface, this can occur only by one of two ways; Either it forms by condensation between drops, or a sliding drop leaves a film residue behind.

Further evidence for the nonexistence of a condensate film between droplets was furnished by Ivanovskii et. al. (11), using a different fluid. By measuring the electrical resistance between two electrodes embedded in a glass surface on which dropwise condensation of mercury was taking place, they concluded that no thin condensate layer existed between the droplets.

As a result of their photographic study of dropwise condensation, McCormick and Westwater (33) appear to confirm that dropwise condensation is indeed a nucleation phenomenon. Photographs taken through a microscope with magnifications of up to 400 showed nucleating and growing droplets which eventually coalesce with neighboring large droplets. They observed that new drops form on the sites vacated by the coalescing droplets. Consequently, recent analytical models have assumed that droplets form on nucleation sites, neglect any heat transfer taking place between these drops, assume that condensation occurs only on the surface of the droplets, and that the latent heat is transferred through the droplets to the solid surface.

2.1 Drop Size Distribution

The seemingly random nucleation, growth and departure of droplets results in a certain size distribution of droplets on the condenser surface. It is essential that this size distribution be known for the analytical formulation of the dropwise condensation phenomena, and can be considered as an important geometrical parameter for this specific heat transfer problem.

The drop size distribution is treated in the literature in two different ways: a) Many consider a surface area reasonably large relative to the largest drops, with drops departing and sweeping the surface periodically, and define a spacially averaged size distribution over this entire area. Measurements of drop size distributions with random

still photographs satisfy such a definition (54), and include the effects of the sweeping process. Since this distribution depends on how frequently the condenser surface is swept by departing drops, it should be a function of the heat flux. b) Others consider the transient development of the size distribution, beginning with a newly swept region and continuing to an arbitrary time corresponding to a maximum size(15). The local distribution at this maximum size becomes a steady distribution, but does not incorporate the sweeping effect.

For the cases where the distance between nucleating sites is large relative to the nucleation size, which is assumed to be the case, droplets grow by direct condensation only up to a size on the order of the distance between the nucleation sites. In this domain the drop size distribution is thus governed by a mechanism different than the growth mechanism in the larger drop size range, where growth also takes place by coalescence. One therefore can expect a completely different form for the drop size distribution function in this size range. The analytical studies of Glicksman and Hunt (12) and Graham and Griffith (13) clearly showed that the drop size distributions are quite different at very small sizes. Since the droplets in this size range can exist only at the nucleation sites, these drops are not closely packed, and considerable distance exists between them during the early stages of growth. It may therefore be expected that the droplets in this size range contribute little to the averaged total heat flux. Unlike the droplets in the coalescence size range, the drop size distribution in the direct condensation range is determined by the condensation on and conduction through the droplets, and thermal properties therefore influence the process. All drop size distribution measurements made were in the coalescing droplet range, and therefore very little is known about the size distribution in the direct condensation range, where the primary drops exist.

Le Fevre and Rose (14) suggested that an expression of the form

$$f_{co(r/r_{max})} = 1 - (r/r_{max})^n \qquad (2-1)$$

can be used for the time average size distribution where f_{co} is the fraction of area occupied by droplets in the size range from a radius r to the maximum radius r_{max}. The theoretical study of Tanaka (15) showed that n should be around 1/3. Le Fevre and Rose (14) used the same value in order to compare heat transfer measurements with their analytical model, which incorporates Eq. (2-1).

Yu-Ting Wu (60) presented the random fractal model to simulate the drop size and spatial distribution in dropwise condensation. They find that the photographs of dropwise condensation taken at different instant or in different scale are similar and a whole photograph can be obtained by enlarging properly a local photograph. These features indicated that dropwise condensation appears with self-similarity which is one of the most important feature of fractal. In addition, drop spatial distribution possesses randomicity. The random fractal model and a condensing photograph are given in Fig. 2.3.

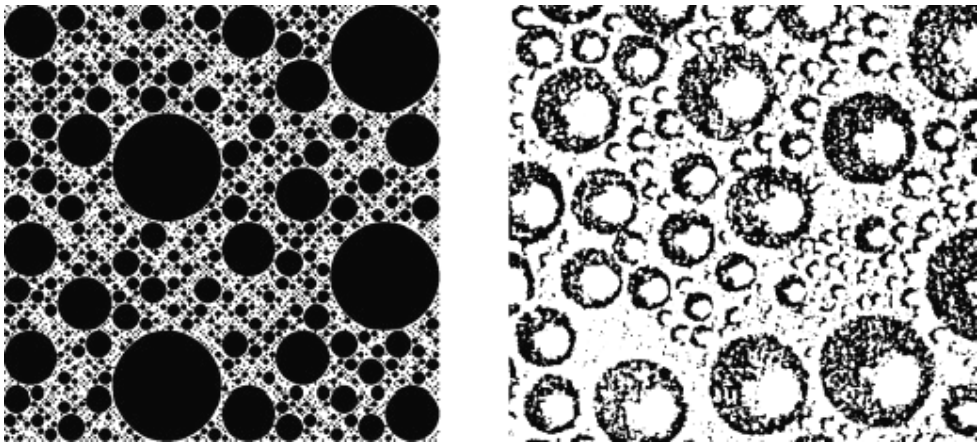

Figure 2.3 Comparison of drop distribution between random fractal model and photography (a- Drop distribution constructed by using the random fractal model. b- Close-up photography of condensing surface).

2.2 Conduction Through The Droplets

The drop size distribution and the heat transfer through the individual droplets must be known in order to calculate the heat flux with dropwise condensation.

The first model for conduction heat transfer through a droplet was proposed by Fatica and Katz (16), and assumed that the surface and base temperatures of the droplet are uniform and constant, equal to the vapor and condenser surface temperatures , respectively . The majority of heat transfer actually takes place through a region very close to the periphery of the drop, the triple interface between the solid, liquid and vapor. At small sizes the surface tension forces in drops are dominant relative to gravitational forces, and the distortion of droplets from a spherical shape is negligible, except perhaps for droplets close to the departure size. This has been demonstrated by the calculation of drop shapes (17).

Numerical solutions closely agree with the experimental results, and show that 83 to 98 percent of the calculated total heat transfer through a droplet goes through the corner element of the edge of the droplet. This points to the importance of the edge of the droplet as far as the total heat transfer is concerned.

2.3 Effects of Non-condensable Gases

Industrial systems in which condensation takes place usually contain some amount of non-condensable gases. The working fluid might decompose in some systems, liberating non-condensable gases. For example, alcohol condensing on copper decomposes into hydrogen and aldehyde, while water, at elevated temperatures, liberates hydrogen gas when it comes in contact with stainless steel .

Both filmwise and dropwise condensation are affected by non-condensable gases present in the vapor, but is most significant for the case of dropwise

condensation. Non-condensable gases carried to the condenser surface by the condensing vapor accumulate and cause a reduction in heat transfer coefficient by reducing the vapor partial pressure. This reduction might be large enough to offset the gains of dropwise condensation. Therefore, the removal of non-condensable gases may become necessary to improve the heat transfer coefficient. On the other hand, in certain applications such as the production of liquified petroleum gases, liquid nitrogen and liquid oxygen, condensation must take place in the presence of non-condensables, because of the nature of the specific process.

Othmer (19) was the first to study the effect of non-condensable gases on heat transfer systematically. He measured filmwise condensation of steam-air mixtures on a horizontal tube, and observed that a significant decrease in heat transfer coefficient occurs with an increase in the amount of non-condensable gases present. It was concluded that the non-condensable gases which reach the tube surface remain there and become an obstacle to condensation.

Furman and Hampson (20) examine the effects of non-condensable gas on filmwise and dropwise condensation on a horizontal copper tube with a steam-nitrogen mixture. It was noted that the dropwise condensation heat transfer coefficient reduced drastically with an increase in the amount of nitrogen, especially at low steam flow rates.

Tanner et. al. (21) made measurements of dropwise condensation of steam-nitrogen mixtures at low system pressures, and observed a sharp reduction in heat transfer coefficient with an increase in non-condensable content. Since non-condensable gases impair the heat transfer rate, researchers try to eliminate them from their systems in order to achieve reproducible results. Prolonged boiling of the water prior to making measurements, in order to replace the gases by vapor within the system was employed by several investigators (21 , 22). It was observed that blowing vapor to the atmosphere through a vent for a long period of time can reduce the amount of non-condensables considerably, but

can never eliminate them completely. In one case (22), the boiler and steam chamber are flooded completely to eliminate air before boiling began. It was observed that even this was not sufficient to eliminate gases from the system.

The Engineering Physical Sciences Research Council (69) presented an experimental study to provide experimental data on the effect of non-condensables, and falling condensate on the thermal performance of a bundle of tubes.

A purpose-built test facility was constructed and used to generate data for filmwise and dropwise condensation from pure steam and steam-air mixtures flowing downwards across a 15x5 bundle of tubes. Data were obtained at conditions typical of those found in the UK electricity generating industry. Steam was supplied at a pressure of 50mbar, and steam to cooling water temperature difference is 4K.

Typical results are shown in Fig. 2.4, and demonstrate the properties of high-quality dropwise condensation. The dropwise coefficients are significantly larger than their filmwise equivalents and, for pure vapours, the dropwise values remain approximately constant throughout the bundle, while the filmwise values decrease.

Both pure steam and steam-air mixtures were tested. These showed that it was not sufficient just to produce dropwise condensation; a high-quality dropwise condensation must be produced. This is characterised by the rapid growth and departure from the surface of small, spherical drops.

The data also showed that the pure-vapour heat transfer coefficients were reasonably independent of bundle position, at least until row 15.

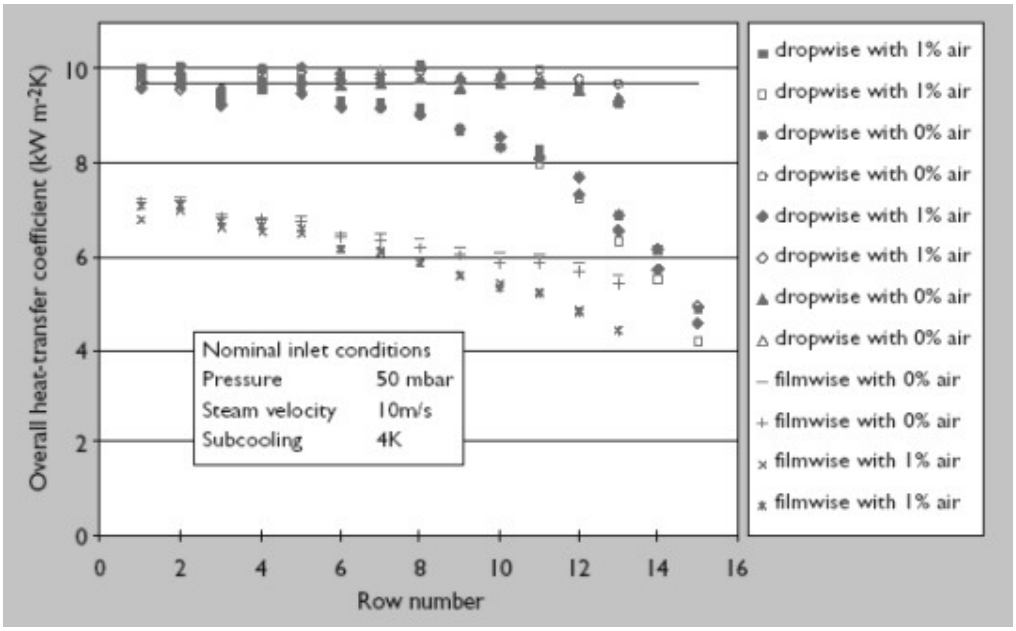

Figure 2.4 Variation of overall heat transfer coefficient with the row number of cylindrical tubes.

2.4 Promoting Dropwise Condensation

Although dropwise condensation gives heat transfer coefficients an order of magnitude larger than filmwise condensation, its industrial application is hindered because of the hydrophilic nature of commercial metals. Most vapours condense in filmwise condensation mode on most common metal surfaces. Therefore, a solid metal surface must be modified in order to promote the dropwise condensation mode. Dropwise condensation has been obtained on these types of surface by one of three methods of surface preparation to make the surface hydrophobic:

i) Coating the surface with certain chemical substances called promoters
ii) Coating the surface with a solid hydrophobic non-metallic material
iii) Coating the surface with a noble metal, usually gold.

A good promoter should be long lasting, easy to apply, nontoxic and must be compatible with the system in which it is used, i.e., it should not impair the proper functioning of the other parts of the system.

Promoting the surface by chemical means has not produced permanent dropwise condensation up to this point in time; it eventually reverts to the filmwise mode as the promoter is washed away. Another factor contributing to the failure of the promoter is the accumulation of fouling matter that may be present in vapor (11); the promoter becomes submerged beneath the fouling matter.

Fatty acids and other organic compounds have been used as promoters in the early stages of dropwise condensation research. Later, promoters containing sulphur and selenium and long-chain hydrocarbons have been developed and tested. Such promoter compounds falling in this category are xanthates, selenium, disulphide, thiosilanes and thiophosphor compounds (23). Tests show that thiosilanes and xanthate compounds are the most promising sulphur bearing promoters for copper alloys, and the "life" obtained with these varies from 8 to 21 weeks. These results were confirmed by Bromley and Read (24), who also found that tetrakis dodecylthio silane is the best promoter among those that were tested, as far as the promoter life is concerned. Some of the promoters were tested in commercial applications, in ship board (25) and stationary power station (23) condensers. Good to fairly good dropwise condensation was reported using tetrakis (dodecane thio) silane for a period of 9 months under intermittent operation (25).

Zhang et al. (26, 27) used various surface processing methods including mechanical polish, ion plating, and ion plating and ion-beam mixing technology, to modify the micro structure of the metal surface layer in order to form a amorphous-state surface layer, which has low surface free energy. The Cu–Cr surface prepared by

ion plating and ion-beam mixing combination technique maintained dropwise condensation for 8500 h. Zhao et al. (28) studied the effects of different ion-implanted elements and processing conditions on the dropwise condensation heat transfer characteristics. It was found that the processing condition for different implanted elements had considerable impact on the dropwise condensation heat transfer.

Song et al. (29) investigated condensation heat transfer characteristics of steam on brass tubes having chromium surfaces prepared with three kinds of surface processing techniques, i.e. ion plating, electroplating, and ion plating with ion-beam mixing. The ion-plated tubes were sorted into three sets for experimental tests. The first set of tubes was used to conduct experiments in the laboratory immediately after the surface was treated. This kind of surface maintained dropwise condensation for 50 h. The tubes of the second set were installed in a large scale steam–water heat exchanger in a power station which operated for one and half years. Then, one of the tubes was taken from the heat exchanger and used in condensation experiments in the laboratory. Film condensation only was obtained. The third set of tubes which had been exposed to the air for about 2 years also failed to promote dropwise condensation. The chromium surfaces prepared by ion plating technique were of very high purity due to the vacuum operation for surface processing. The freshly treated surface gives rise to dropwise condensation of steam due to the organic substances adsorbed from the environment. One electroplated chromium surface maintained dropwise condensation in the laboratory even after the surface was exposed to the air for 1 year. As noted earlier by Finnicum and Westwater (30) dropwise condensation on electroplated chromium surfaces is due to impurities from the surface processing technique rather than the metal itself. The ion plating with ion-beam mixing

technology transforms the chromium surface layer into an amorphous state which possesses low surface free energy, hence, resulting in dropwise condensation.

Some researchers also tried to prepare the metal organic compound film on the metal substrate in the laboratory. Liu and Xu (31) prepared a metal-organic compound film on a copper tube. The surface maintained dropwise condensation of steam for about 2000 h. They also found that this surface enhanced filmwise condensation heat transfer of ethanol and ethylene glycol vapours to some extent. Guo et al. (32) coated PTFE on an electrochemically eroded porous surface and tested steam dropwise condensation on the surface. Yang and Cheng (33) investigated dropwise condensation of steam on Ni-PTFE composite plated surfaces. Xin and Xia (34) experimentally studied the heat transfer performance of dropwise condensation in two-phase closed thermosiphones using the oleic acid as the promoter. Dropwise condensation of steam was maintained for 11,340 h.

For liquids with high surface free energy (or surface tension) such as water and ethanol, metal organic compound surface layers, which have good adhesion with the substrate, would be expected to maintain dropwise condensation mode for a long period of time to meet the requirements of industrial applications. However, for most organic vapours, which are widely used in petrochemical processes, a polymer film on the metal substrate may be the only approach for promoting dropwise condensation. The difficulties for the polymer lie in its much lower thermal conductivity and poor adhesion with metal substrates. The different thermal expansivities of metal and polymer film, and the weak binding effect between the two materials lead to the polymer film peeling after a period of time. In the laboratory test, dropwise

condensation of steam on a copper tube with 10mm o.d. and 100mm long, which was coated with a PTFE polymer film has been maintained for about 1000 h so far (35).

Experimental investigations of the condensation heat transfer of steam indicated that the surface processing conditions have a significant effect on the dropwise condensation heat transfer characteristics and the adhesion of the polymer film with the metal substrate. This implied that the physico-chemical properties and the purity of the polymer film were dependent on the surface processing conditions. The optimum surface processing conditions for different systems of polymer film and metal substrate remains a key problem before the dropwise condensation on polymer film can be realised in practical applications.

The thickness of the promoter layer on the condensation surface also affects the type of condensation, as was reported by Tanner et.al. (36). Over a certain range of promoter thickness, the quality of the condensation does not change with thickness, but if the layer is too thin filmwise condensation occurs. Excessive amounts of promoter increases the wettability of the surface, and is considered to be due to the disordering of the promoter molecules.

The disadvantage of producing dropwise condensation by chemical promoters is that the dropwise condensation so obtained has a limited life. To produce continuous dropwise condensation then, promoter must be injected repeatedly into the condenser at certain intervals.

Dropwise condensation has been obtained by coating the condenser surface with a thin layer of teflon (PTFE)(37). If the coating is too thin, it wears away in a very short period of time. On the other hand, if it is too thick the thermal resistance

introduced circumvents the gains of dropwise condensation. Selecting the correct thickness, therefore, is crucial for the effective use of this procedure for obtaining dropwise condensation.

Although considerable research has been conducted with dropwise condensation on gold surfaces, the hydrophobic nature of gold is still a subject of controversy. Many researchers conclude that gold is hydrophobic, having a contact angle of around 65° with water. Nevertheless, the results of other studies are in disagreement with this, and claim that truly clean gold is hydrophilic in nature. The controversy arises because of the difficulty of keeping the gold surface pure and free from contaminations; even a minute amount of contamination on the gold surface appears to effect its wettability. It was found that two groups of contaminants exist which can effect the wettability of the surface in opposite directions (38); organic contamination make the surface hydrophobic whereas oxygen or oxides have the tendency to render it hydrophilic. A difficulty common to all of these studies lies in the definition of a "clean" surface, since it is not possible to have a surface completely free of foreign atoms or molecules. The behaviour of water droplet on the different surfaces shown in Fig. 2.5.

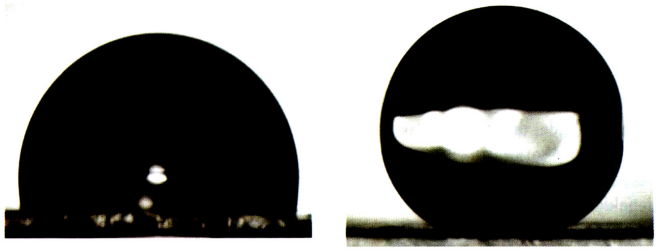

Fig 2.5 The behaviour of water droplet on the different surfaces (a- A droplet on the horizantal polipropilen (PP) surface, b- A droplet on the horizantal super-hydrophobic PP surface).

Contact angle has sometimes been used to predetermine the condensation mode on a specific solid surface. However, the contact angle measured at room temperature and in equilibrium with an air environment has been proven not to be useful for determining the wettability of systems where mass transfer takes place. For example, the contact angle of water on a polytetrafluoroethylene (PTFE) surface is 88° under the condensation condition at atmospheric pressure but 108° at room temperature with an air environment (39). The difference was caused mainly by the difference of the condensate surface free energies at different measurement temperatures. Fig.2.6 shows the surface energy and the contact angle at equilibrium which can be obtained for such systems (61).

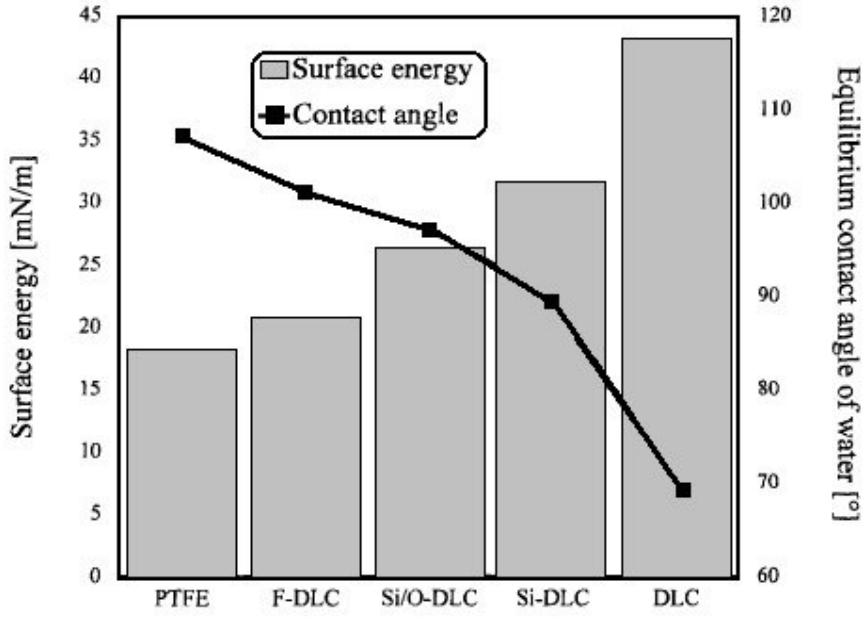

Figure 2.6 Surface energy and equilibrium contact angle of water for different coating systems.

PTFE : Polytetrafluoroethylene

F : Fluorine

Si : Silicon

Si/O : Silicon/oxygen

DLC : Diamond –like carbon

According to θ contact angle , the behaviour of water droplet on the different surfaces shown in Fig. 2.7.

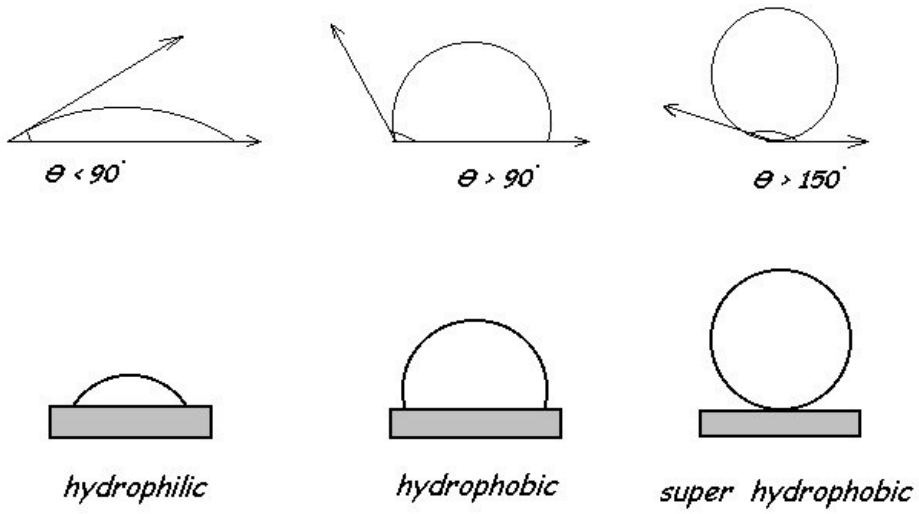

Figure 2.7 The behaviour of water droplet on the different surfaces

Ma (40) put forward a surface free energy criterion, i.e. the surface free energy difference between the condensate liquid at the condensation temperature and the

solid surface, defined as $\Delta\gamma_{l-s}$ (l and s denote the surface free energies of liquid and solid, respectively) to predict whether filmwise or dropwise condensation of a vapour will occur on a solid surface. In a conservative manner, the critical surface free energy difference was considered to be 0.0333 J/m² according to an empirical correlation between contact angle and surface free energy difference (41). The surface free energy of a solid depends only on its composition and chemical structure and can be calculated from the measured contact angles at room temperature (42) for low surface-free-energy solid surfaces like polymer films. Consequently, it is more convenient and accurate to use the surface free energy rather than the contact angle to predict condensation mode because the surface free energy criterion is not affected by the measuring temperature of the contact angles. The new surface free energy difference criteria and comparison with contact angle method are shown in Table 2.1.

Table 2.1 Condensation mode criteria

Surface free energy difference criterion	Contact angle method	Condensation mode
$\Delta\gamma \leq 0$	–	Filmwise
$0 \leq \Delta\gamma < 0.0333$	$0° \leq \theta < 90°$	Mixed condensation
$\Delta\gamma \geq 0.0333$	$\theta \geq 90°$	Dropwise

The contact angle can also be measured by using some special equipments(62). The Cam-100 is one model of these equipments shown in Fig. 2.8. Some measurement samples with software program are shown in Fig. 2.9, Fig. 2.10.

The equipment has wide lenses to focus on the droplet which stands on the surface. Since the droplets has a simetric shape for left and right sides on the surfaces, it is expected to measure the same contact angle values for both side of them. The final value of contact angle is obtained by taking average of data measured for both side of the droplet.

The contact angle data for plain copper tube and stearic asit coated tube are measured as 33.3° in Fig. 2.9 and 155° in Fig. 2.10, respectively.

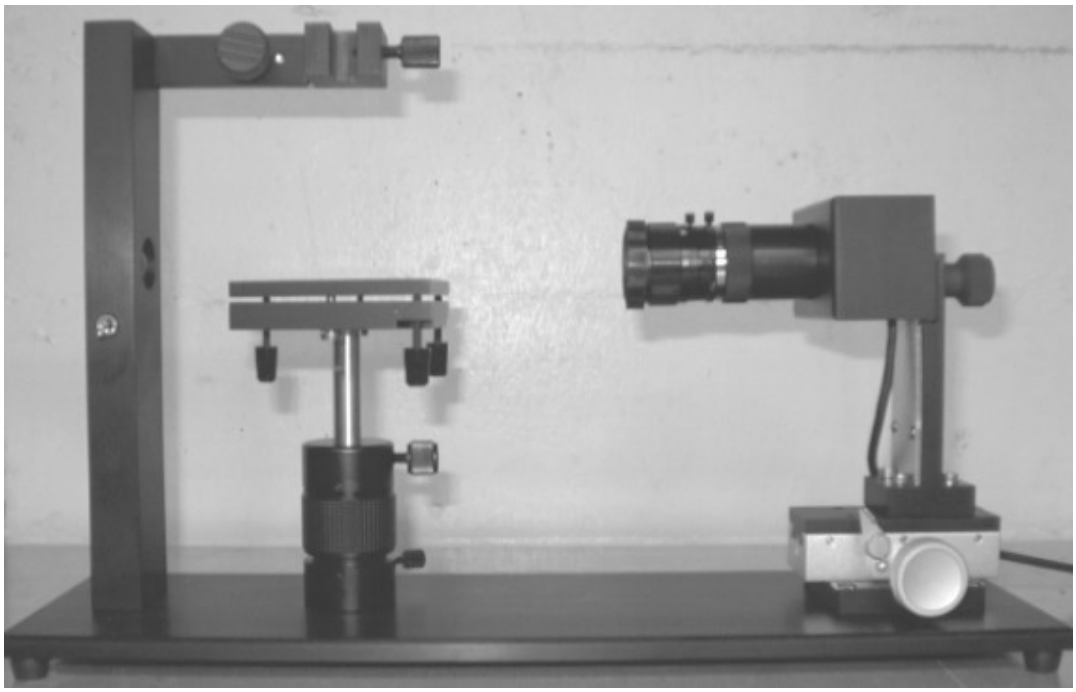

Figure 2.8 The CAM-100 contact angle measuring equipment

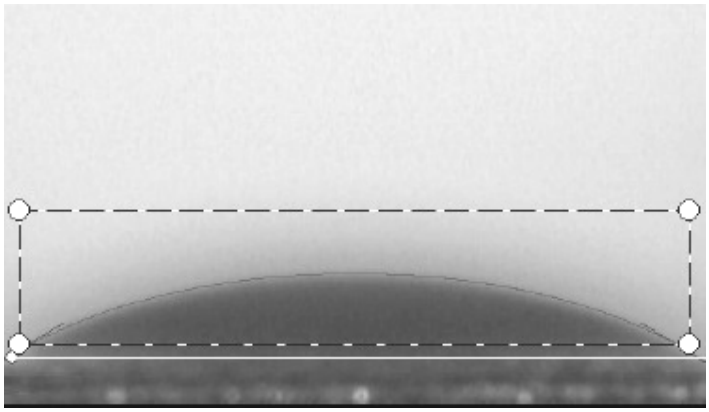

Figure 2.9 The contact angle data for plain copper tube

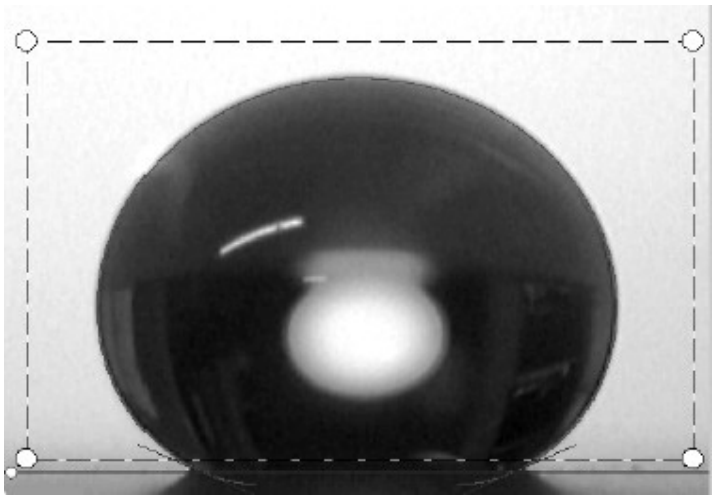

Figure 2.10 The contact angle data for stearic asit coated tube

CHAPTER 3

ANALYTICAL MODEL

The condensation of steam on a horizontal gold coated tube is investigated by both analytical and experimental methods in this study. A computer program is implemented in order to analyze the problem. The program calculates the heat flux and the heat transfer coefficient on the surface of a cylinder on which dropwise condensation is taking place.

Following assumptions are made in the analysis of this study :

- The vapor is at uniform temperature.
- Heat transfer from vapor to liquid is carried out only by condensation. Convection effect is neglected.
- The droplets form at specific sites on the surface.
- The area between the droplets can be considered as thermally insulated.
- Only gravity forces are acting on the condensate, and the shear effect of the vapor is neglected.

The analytical formulation of dropwise condensation requires careful understanding of the processes taking place. The most fundamental question that

should be asked before proceeding with the analytical description is how the droplets form in the first place. The Micro-cine studies of McCormick-Westwater (44), Peterson-Westwater (45) and the experimental studies of Umur and Griffith (10) and Ivanovskii et. al. (11) removed doubts about the origin of the smallest drops on the surface; it has been concluded that the droplets form by a nucleation process at specific locations called nucleation sites. In the model to be developed here therefore it will be assumed that droplets form at specific sites on the surface, the so-called nucleation sites associated with pits and surface scratches, and it also will be assumed that the area between the droplets can be considered as thermally insulated .

If the thermal conductivity of the condenser surface substrate material is low, the interaction between the droplets is expected to influence significantly the overall heat transfer behavior. In such a case the small droplets surrounding a large one disturb the temperature distributions in the neighborhood of the periphery of the large droplet due to their much smaller effective thermal resistance. With high conductivity condenser materials, such as copper employed in the experimental part of the present work, these interactions are expected to have little effect.

Considerable progress has been made in the calculation of the heat transfer rates through single droplets. Beginning with the steady conduction models for a spherical surface with constant temperature boundary conditions at the base and liquid-vapor interface, the model has been improved gradually by taking the interfacial resistance, curvature, substrate material and thermocapillary flow effects (10,46,47,48) into account. These studies result in two important conclusions:

i) The majority of the heat transfer in a drop takes place within a narrow region close to the perimeter of the drop, due to the very small thermal resistance existing there (49).

ii) The majority of the heat transfer in dropwise condensation takes place through droplets of very small sizes (13), because of their small thermal resistances and large numbers.

Following the droplets formation on nucleation sites, it is considered that the early stage of growth of droplets takes place by the direct condensation of vapor on the liquid-vapor interface. These primary droplets are anchored to the nucleation sites and are far apart from one another, considering that the critical size of the nucleating droplets are much smaller than the average distance between nucleation sites. Once the droplets begin coalescing their physical location is no longer limited to specific nucleation sites on the surface. The droplets move about as a result of coalescences, and can be located at virtually any point on the solid surface, occupying as much surface area as may be permitted by the capillary attraction forces between the droplets.

Coalescence of two water drops in a condensation chamber experiment at a short time scale is shown in Fig 3.1. Photos are taken with a fast camera on a silicon substrate (63).

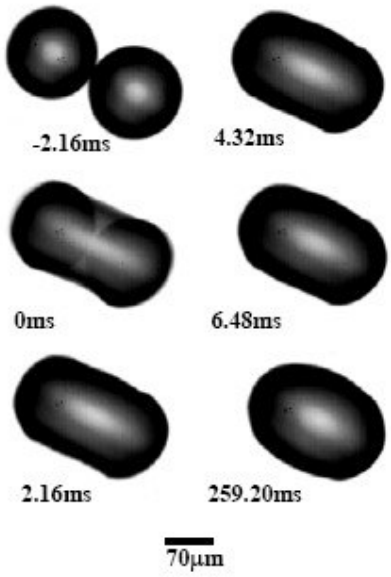

Figure 3.1 Coalescence of two water drops on the condenser surface.

Droplets in the coalescing region grow to be large enough to observe under the microscope (64). One image of droplets under microscope is shown in Fig. 3.2.

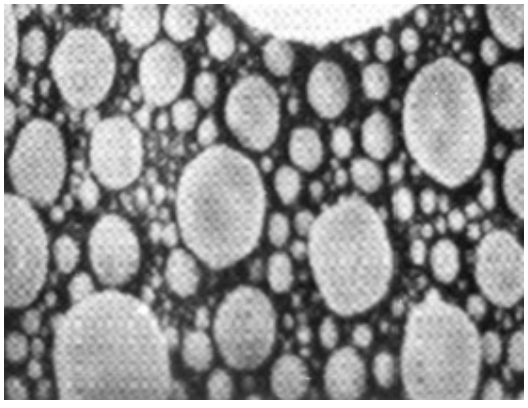

Figure 3.2 Droplets at 5700 times magnification.

When the size of a drop on a vertical surface reaches a certain critical value it departs and sweeps droplets along in its path.

The sweeping process by departing drops is an element of dropwise condensation that contributes significantly to making it a highly efficient heat transfer phenomena. The sweeping process essentially reduces the average size of the droplets on the surface, and therefore increases the heat transfer rate.

3.1 Conduction Through A Single Droplet

The interfacial heat transfer coefficient derived by Umur and Griffith (10) is used in the analysis below. The complete form of the equation, from Ref. (10), can be written as

$$h_e = \left(\frac{2\gamma}{2-\gamma}\right)\left(\frac{1}{2\pi}\right)^{1/2} \frac{h_{fg}^2 P_v^*}{G^{3/2} T_{sat}^{3/2} T_i}\left(1-\frac{R^*}{R}\right) \qquad (3-1)$$

where

$$R^* = \frac{2T_{sat}\sigma}{h_{fg}\rho_l}\cdot\frac{1}{\Delta T^*} \qquad (3-2)$$

where

γ : Condensation coefficient (fraction of molecules that strike a surface and condense)

h_{fg} : Latent heat of vaporization

P_v^* : Saturation pressure corresponding to vapor temperature

G : Gas constant

T_{sat} : Vapor saturation temperature

T_i : Temperature of liquid-vapor interface

σ : Surface tension

ρ_l : Liquid density

ΔT^* : Difference between the vapor and the interface temperatures $(T_{sat} - T_i)$

h_e : Equivalent heat transfer coefficient for the liquid-vapor interface at the point of interest.

R : The radius of curvature of the interface at the point of interest

Eq. (3-1) can be written in the following simple form:

$$h_e = \frac{K_1}{T_i}\left(1 - \frac{K_2}{R\Delta T^*}\right) \qquad (3-3)$$

where

$$K_1 = \left(\frac{2\gamma}{2-\gamma}\right)\left(\frac{1}{2\pi}\right)^{1/2} \frac{h_{fg}^2 P_v^*}{G^{3/2} T_{sat}^{3/2}} \qquad (3-4)$$

$$K_2 = \frac{2T_{sat}\sigma}{h_{fg}\rho_l} \qquad (3-5)$$

The geometry and nomenclature used for the drop conduction model is shown in Fig. 3.3.

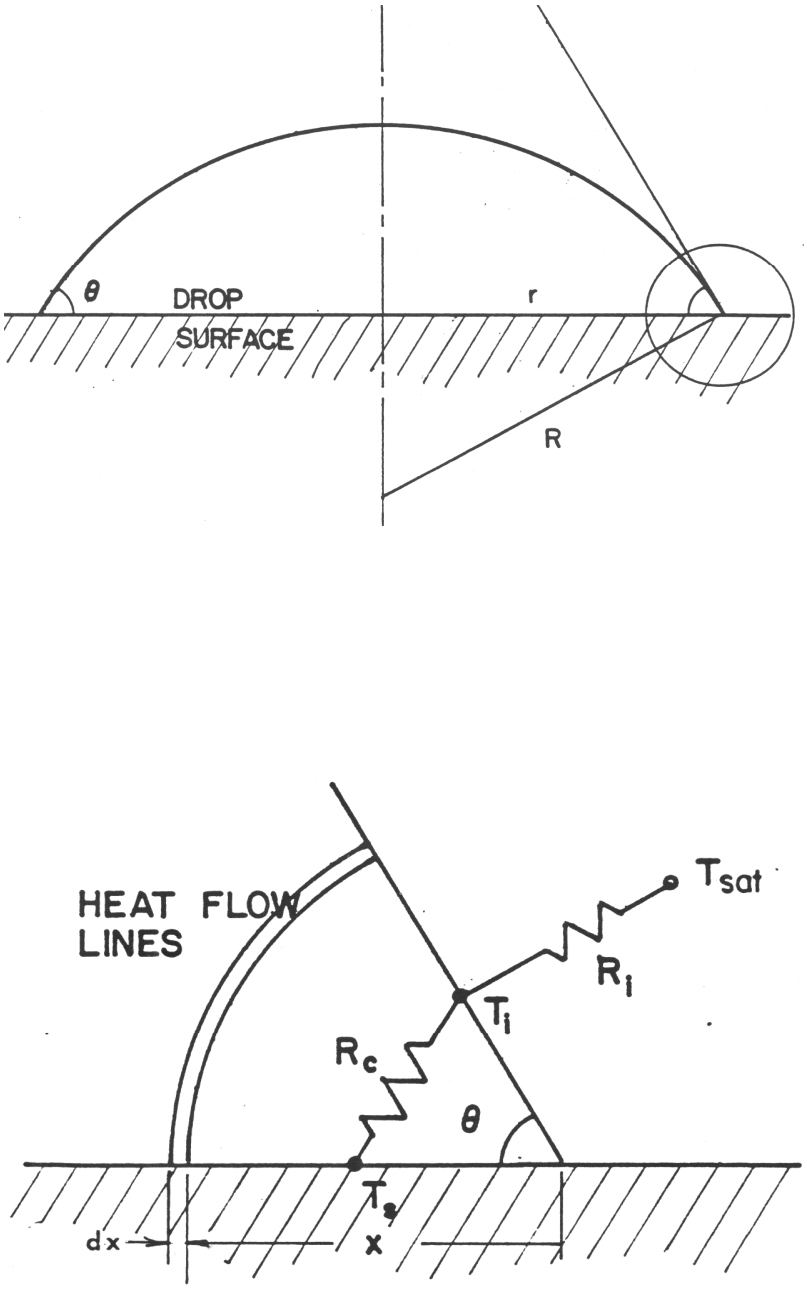

Figure 3.3 Model for heat conduction through a droplet

Assuming circular heat flow lines within the condensate in the vicinity of the triple interface line, the thermal resistance for the interfacial mass transfer can be expressed as (per unit cross sectional area of the differential element considered);

$$R_i = \frac{1}{h_e} \qquad (3-6)$$

This is in series with the thermal resistance of the condensate, given by;

$$R_c = \frac{x\theta}{k} \qquad (3-7)$$

where x and θ are shown in Fig. 3.3. Defining the following temperature differences:

$$\Delta T_t = T_{sat} - T_s \qquad (3-8)$$

$$\Delta T_s = T_i - T_s \qquad (3-9)$$

$$\Delta T^* = T_{sat} - T_i \qquad (3-10)$$

where T_s is the condenser surface temperature. The heat flux at any point on the surface of the drop can be expressed in terms of either Eq. (3-6) or Eq. (3-7) as:

$$\frac{q}{A} = h_e \Delta T^*$$

$$\frac{q}{A} = \left(\Delta T_t - \Delta T^*\right)\frac{k}{x\theta} \qquad (3-11)$$

where (q/A) is the heat flux within the differential element considered.Substituting h_e from Eq. (3-3) into Eq. (3-11) and taking $T_i \approx T_{sat}$ and rearranging to solve for ΔT^* gives:

$$\Delta T^* = \frac{\frac{\Delta T_t k T_{sat}}{\theta K_1} + \frac{K_2 x}{R}}{x + \frac{k T_{sat}}{\theta K_1}} \qquad (3-12)$$

As can be noted in Eq. (3-12), $\Delta T_t >> \Delta T^*$ for large droplets, and the interfacial resistance can be neglected. As R gets smaller, ΔT^* becomes comparable to ΔT_t. Although Eq. (3-12) contains a number of parameters, most have a constant value for a given vapor-liquid liquid combination, and Eq. (3-12) can be expressed more simply by;

$$\Delta T^* = \frac{A + C\frac{x}{r}}{x + B} \qquad (3-13)$$

where

$$A = \frac{\Delta T_t k T_{sat}}{\theta K_1} \qquad (3-14)$$

$$B = \frac{k T_{sat}}{\theta K_1} \qquad (3-15)$$

$$C = K_2 \sin\theta \qquad (3-16)$$

The total heat transfer rate through the droplet can be obtained by integrating the local heat flux over the drop base in Fig. 3.3 :

$$q_d(r) = \int_0^r h_e \Delta T^* 2\pi(r - x\cos\theta)dx \qquad (3-17)$$

Substituting h_e and ΔT^* from Eqs. (3-3) and (3-13) gives the total heat transfer rate for a drop of radius r as

$$q_d(r) = \frac{2\pi K_1}{T_{sat}}(Ar - BK_2\sin\theta)\left[-\cos\theta + \frac{r + B\cos\theta}{r}\ln\frac{r+B}{B}\right] \qquad (3-18)$$

The mean heat flux at the base of the droplet becomes:

$$q_d''(r) = \frac{q_d(r)}{\pi r^2}$$

$$q_d''(r) = \frac{2K_1 B}{r^2 T_{sat}}(r\Delta T_t - K_2\sin\theta)\left[-\cos\theta + \frac{r + B\cos\theta}{r}\ln\frac{r+B}{B}\right] \qquad (3-19)$$

3.2 Heat Flux in Dropwise Condensation Excluding The Effect of Sweeping

Observation of a surface on which dropwise condensation is taking place shows vertical regions in different stages of development. As soon as a region is swept by a departing drop, new droplets nucleate on the surface and begin growing by direct condensation and then by coalescences. The drop size distribution within a particular

swept area is uniform; that is, there is little difference between the regions at different elevations except for a very short period of time immediately following the sweeping. On the other hand on a surface randomly swept by departing droplets, the surface is covered by swept region at different stages of development and therefore an average dropsize distribution should be considered. If the sweeping rate is very high, the dropsize distribution would be significiant different than the dropsize distiribution given by Eq. (2-1) for an unswept area. In the present work, sweeping rate is not very high, therefore the dropsize distribution obtained in the experimental study is expected to be presented by Eq. (2-1).

3.3 Heat Flux in Coalescence Range

The drop size distribution in the portion of the coalescence region visible with suitable magnification has been measured (13, 51) and predicted from basic principles (15, 52). It is shown that a simple relations of the form given by Eq. (2-1) matches well to experimental measurements for values of n close to 1/3 (52). The function given in Eq.(2-1) is considered valid only for the coalescence region because it is based on measurements made in this region only.

This size distribution applies for drops within the size range from departure down to the order of magnitude of the half distance between nucleation sites. Below this size droplets grow by direct condensation, and begin coalescing when they grow sufficiently to a size equal to the spacing between nucleation sites.

Figs. 3.4a-d show the development of the dropsize distribution over the condenser surface obtained in a numerical study (65), corresponding to elapsed times of 0.07, 0.13, 0.19 and 0.21ms from the start. These figures reveal the complexity of the process of dropsize distribution development.

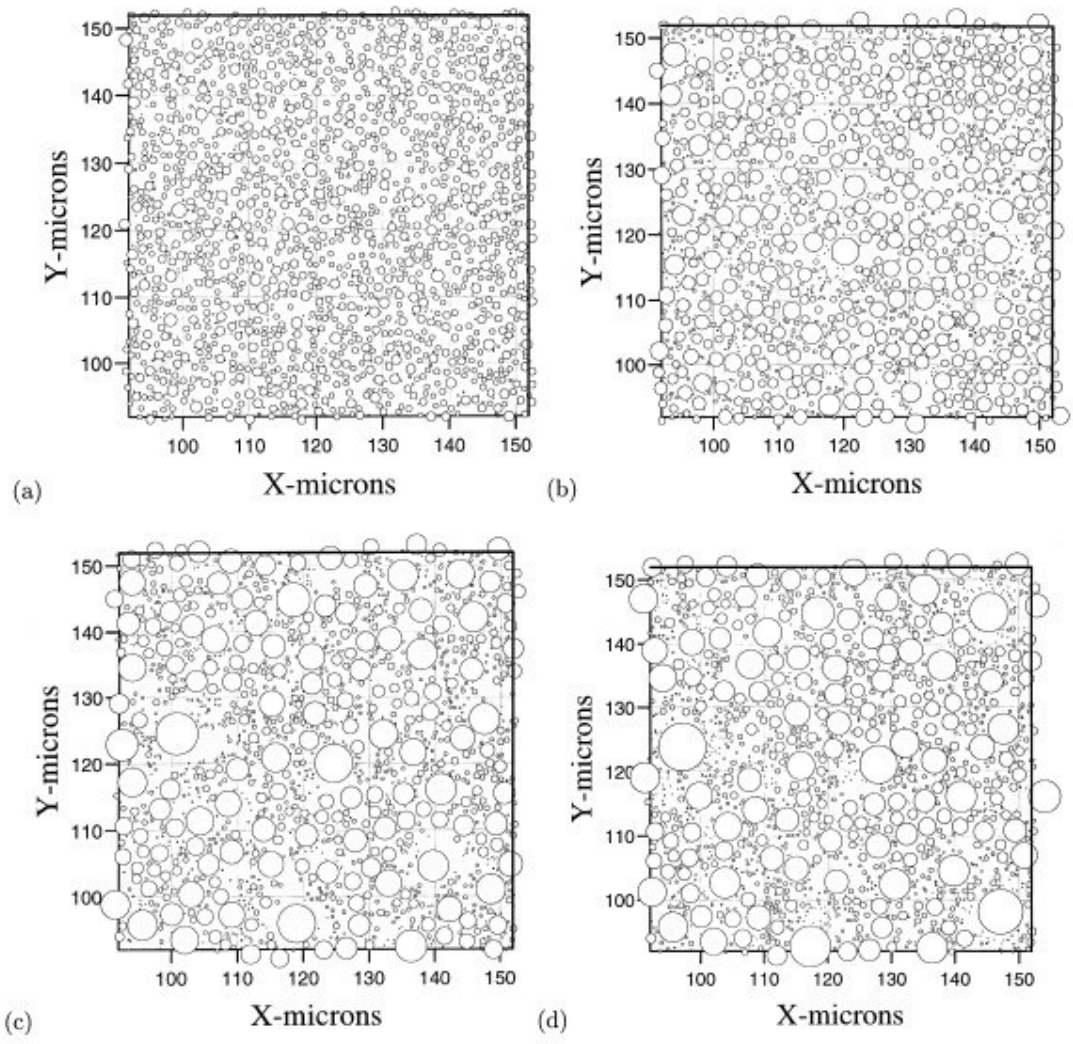

Figure 3.4 Drop distribution over the condenser surface during steam condensation cycle obtained by a theoretical model: (a) 0.07 ms (b) 0.13 ms (c) 0.19 ms (d) 0.21 ms after sweeping by a falling drop (T_{wall} =100 ℃, ΔT =3 K).

Fig. 3.5 shows the maximum drop radius in a dropsize distribution over a surface swept by a departing droplet as a function of time obtained in the theoretical study (65). Again, due to the randomness of drop coalescences, the rate of increase of r_{max} fluctuated with time.

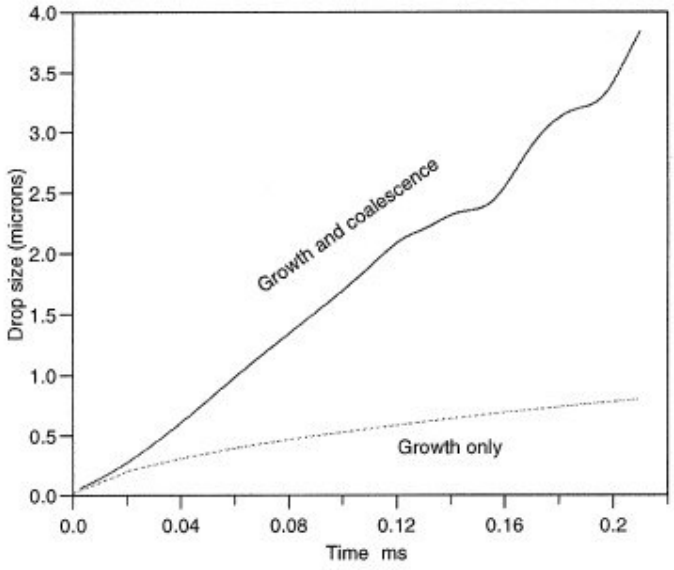

Figure 3.5 Maximum droplet radius and isolated droplet radius vs. time.

The radius of drops which do not coalesce (r_{growth}) is also plotted in Fig. 3.5. The influence of coalescence even at this early stage in the condensing cycle is clear. At time 0.21 ms the radius of a coalescing drop is four to fives times greater than the drop that grows by direct condensation four to five times that which would have occurred from growth alone is achieved.

The fraction of area occupied by droplets in the size range dr for the coalescing droplets becomes, from Eq. (2-1):

$$df_{co}(r) = n\left(\frac{r}{r_{max}}\right)^{n-1}\frac{dr}{r_{max}} \qquad (3-20)$$

where r varies from r_{co} to r_{dep}. To obtain the total dropwise condensation heat transfer incremental values of df_{co} should be obtained from r_{co} to r_{dep} by dividing this radius range to a suitable numbers of divisions at the corresponding radius values. While dividing the radius range of coalescing droplets care should be given to the fact that at smaller diameters heat flux is order of magnitude larger than the heat flux at large diameters. For that reason taking the increments of radius equal at each division would result in large round off error at smaller diamaeters. To eliminate this difficulty at smaller diameters increments are taken smaller and increased as the diameter is increased. To achieve this goal dr should be increased logarithmically to make the contributions of heat transfer at each drop radius to the total heat transfer at the same order.

If a gradually increasing increments in the drop radius range is targeted, a logarthimic variation such as the Eq. (3-21) for r given below may be employed

$$r_i = r_{co}e^{\frac{\ln(r_{dep})-\ln(r_{co})}{m}.i} \qquad (3-21)$$

where

m : The number of divisions between r_{co} to r_{dep} (taken as 10000 in this study)

i : 1,2,3.....10000

With such a scheme the discrete value of the drop radius in the colascing droplets range would be as follows:

$i = 0 \qquad r_0 = r_{co}$

$i = 1 \qquad r_1 = r_{co} e^{\frac{\ln(r_{dep}) - \ln(r_{co})}{10000}}$

$i = 2 \qquad r_2 = r_{co} e^{\frac{\ln(r_{dep}) - \ln(r_{co})}{5000}}$

.

.

.

$i = 10000 \qquad r_{10000} = r_{dep}$

from Eq. (3.20), area increments for colascing droplets, df_{co} can be expressed as;

$$r_{max} = r_{dep}$$

$$df_{co}(r_i) = n\left[\frac{\left[\frac{r_i + r_{i-1}}{2}\right]}{r_{dep}}\right]^{n-1} \frac{(r_i - r_{i-1})}{r_{dep}} \qquad (3-22)$$

By using the expression that gives the heat flux for an individual droplet, Eq. (3.19) and the contributions of fractional area for all drops that has radius varying from r_{co} to r_{dep} incremental values of heat flux of a droplet at an incremental value of the drop size can be written as:

$$q_d''(r_i) = \frac{2K_1 B}{r_i^2 T_{sat}} (r_i \Delta T_t - K_2 \sin\theta) \left[-\cos\theta + \frac{r_i + B\cos\theta}{r_i} \ln \frac{r_i + B}{B} \right] \quad (3-23)$$

in general.

Specifically, from Eq. (3.23), the mean heat flux at the base of the each droplet, $q_d''(r_i)$ then becomes :

$$q_d''(r_1) = \frac{2K_1 B}{r_1^2 T_{sat}} (r_1 \Delta T_t - K_2 \sin\theta) \left[-\cos\theta + \frac{r_1 + B\cos\theta}{r_1} \ln \frac{r_1 + B}{B} \right]$$

$$q_d''(r_2) = \frac{2K_1 B}{r_2^2 T_{sat}} (r_2 \Delta T_t - K_2 \sin\theta) \left[-\cos\theta + \frac{r_2 + B\cos\theta}{r_2} \ln \frac{r_2 + B}{B} \right]$$

$$q_d''(r_3) = \frac{2K_1 B}{r_3^2 T_{sat}} (r_3 \Delta T_t - K_2 \sin\theta) \left[-\cos\theta + \frac{r_3 + B\cos\theta}{r_3} \ln \frac{r_3 + B}{B} \right]$$

.

.

.

.

$$q_d''(r_{10000}) = \frac{2K_1 B}{r_{10000}^2 T_{sat}} (r_{10000} \Delta T_t - K_2 \sin\theta) \left[-\cos\theta + \frac{r_{10000} + B\cos\theta}{r_{10000}} \ln \frac{r_{10000} + B}{B} \right]$$

In the same fashion, by employing the Eq. (3-22), the fraction of area covered by droplets on the condenser surface area at each increment, $df_{co}(r_i)$:

$$df_{co}(r_i) = n\left[\frac{\left[\frac{r_i + r_{i-1}}{2}\right]}{r_{dep}}\right]^{n-1} \frac{(r_i - r_{i-1})}{r_{dep}} \quad \text{in general}$$

and

$$df_{co}(r_1) = n\left[\frac{\left[\frac{r_1 + r_0}{2}\right]}{r_{dep}}\right]^{n-1} \frac{(r_1 - r_0)}{r_{dep}}$$

$$df_{co}(r_2) = n\left[\frac{\left[\frac{r_2 + r_1}{2}\right]}{r_{dep}}\right]^{n-1} \frac{(r_2 - r_1)}{r_{dep}}$$

$$df_{co}(r_3) = n\left[\frac{\left[\frac{r_3 + r_2}{2}\right]}{r_{dep}}\right]^{n-1} \frac{(r_3 - r_2)}{r_{dep}}$$

.

.

$$df_{co}(r_{10000}) = n\left[\frac{\left[\frac{r_{10000} + r_{9999}}{2}\right]}{r_{dep}}\right]^{n-1} \frac{(r_{10000} - r_{9999})}{r_{dep}}$$

specifically.

Then the mean heat flux over the entire condensing surface due to the contributions of those drops in the coalescence region can be calculated as follows :

$$q''_{total} = df_{co(1)} q''_d(r_1) + df_{co(2)} q''_d(r_2) + df_{co(3)} q''_d(r_3) + ... + df_{co(10000)} q''_d(r_{10000}) \qquad (3-24)$$

The total heat flux for dropwise condensation without the sweeping effect is the sum of the contributions due to the droplets growing by direct condensation and the droplets that grow by colascing with neighboring droplets.

$$q''_T = q''_{dc} + q''_{co} \qquad (3-25)$$

In the equation above the contributions to the total heat transfer rate by droplets which are obtained by direct condensation will be neglected since their total number is negligibly small with respect to the droplets that grow by colascences.

3.4 The Variation of Departing Size of a Droplet on The Cylindrical Surface :

Experiments show that departing roplets is one of the important parameter that has an influence on the dropwise condensation heat transfer coefficient. Since the departing droplet radius changes with gravitational force and the component of the gravitational force acting on a droplet and parallel to the condenser surface changes along the surface on a condenser tube, the dropwise condensation heat transfer coefficient should also vary as a function of the angular position on the surface.

Departing size of a droplet changes on a horizantal cylindrical surface since the gravitational force acting on it change from the top to the bottom of the surface. At the top of the cylindrical surface, the departing size of droplet is theoretically infinity and it decreases and reaches the minimum when the gravitational force is parallel to the condenser surface.

It is concluded from dimensional analysis and from the analysis in Ref. (43) for a drop on a vertical surface that

$$D_{dep} \approx \frac{1}{\sqrt{g}} \qquad (3-26)$$

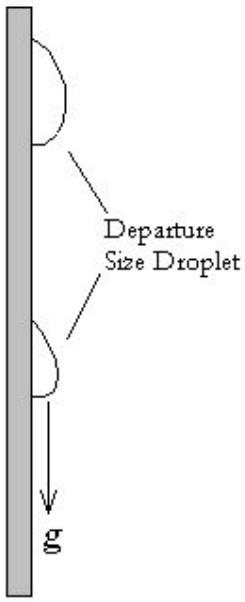

Figure 3.6 The droplet on vertical surface acting gravity

Gravity acts parallel to the surface and cause the deformation depicted in the Fig. 3.6 for a droplet on a vertical surfaces.. Since the component of the gravitational force parallel to the surface cause the droplet to depart, to determine the departing droplet radius this component should be given the consideration.. Eq. (3-26) for the horizantal tube then becomes

$$D_{dep} \approx 1/\sqrt{g\cos\alpha} \qquad (3-27)$$

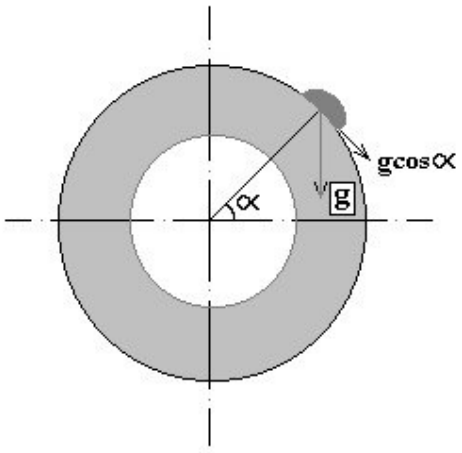

Figure 3.7 Gravitational force acting on a droplet resting on a cylindrical surface

To analyze the dropwise condensation on a cylindrical surface the condenser surface was divided into four regions as shown in Fig. 3.8. Since the radius of departing droplet on the condenser surface decreases with the parallel component of gravity, the radius of departing droplet will increase by increasing the angle from the top up to 90^o as shown in Fig. 3.8.

α : The angle between the vertical direction and the position of the droplet on the cylindrical surface.

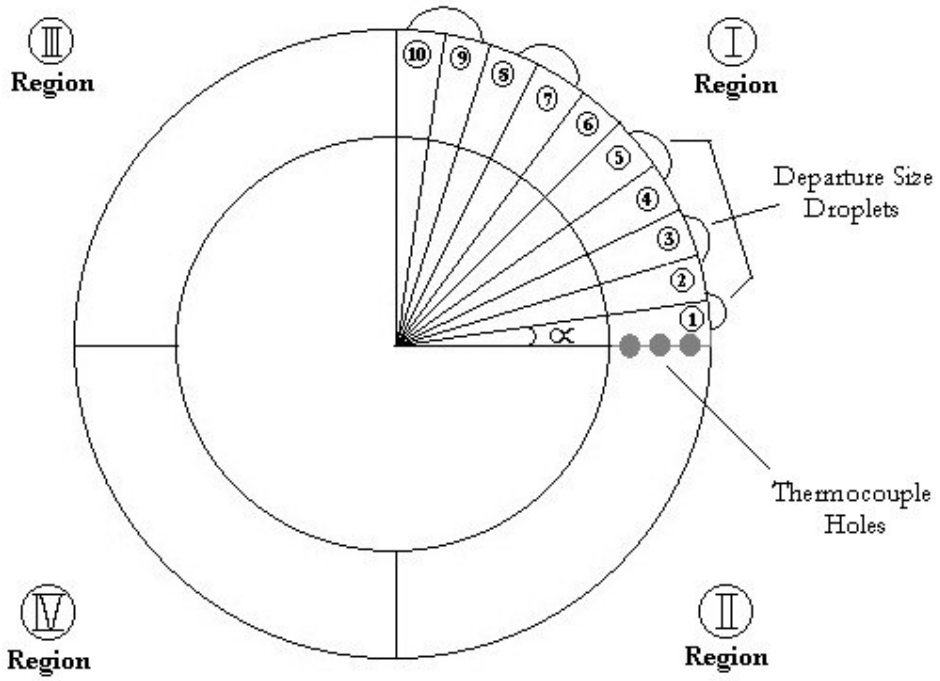

Figure 3.8 Variation of departure size on the condenser surface.

Due to the symmetry the variation of the departure size is the same for region I and III which means that Eq. (3-27), $D_{dep} \approx 1/\sqrt{g\cos\alpha}$ can be applied for both of the Regions I and III.

On the lower surface of the cylindrical surface both the parallel and perpendicular component of the gravitational force has an influence on the drop departure size. As one goes downward the parallel component decreases whereas the perpendicular component increases. Exact calculation of the drop shape and the departure size in this region of the condenser surface requires a complicated analysis of the surface tension and gravitational forces. Therefore in this study it will be assumed that decreasing effect of the vertical component and the increasing effect of the parallel component of the gravitational force on the departing droplet is such that the departure size do not change significantly from angular position of 90° and 180° and therefore for Region II and IV $D_{dep} \approx 1/\sqrt{g}$. Since the radius of departing droplet for vertical surfaces depends on gravity, it can be calculated as $r_{dep} = 0.159.10^{-2} m$.

For evaluation of the dropwise condensation on a cylindrical surface, the numerical technique was applied as follows: The Region I was divided 10 equal angles of 9° to take the variation of the radius of departing droplet into account. Then the departure size at each angle would be given by the Eq. (3-27), $D_{dep} \approx 1/\sqrt{g\cos\alpha}$ as shown in the following table.

Table 3.1 Variation of departure size with angle α for cylindrical condenser surface.

α	rdep*100
0	0.159
9	0.160
18	0.163
27	0.169
36	0.177
45	0.189
54	0.208
63	0.237
72	0.287
81	0.403
82	0.427
83	0.457
84	0.493
85	0.540
86	0.604
87	0.697
88	0.854
89	1.208

Variation of departure size with angle α for cylindrical condenser surface is also shown in Fig. 3.9 to gain a better insight. Fig. 3.9 gives important information about the variation of the departure size on a cylindrical surface. Up to an angle of 80°, variation is comparetively slow. Beyond this angle significant changes start taking place.

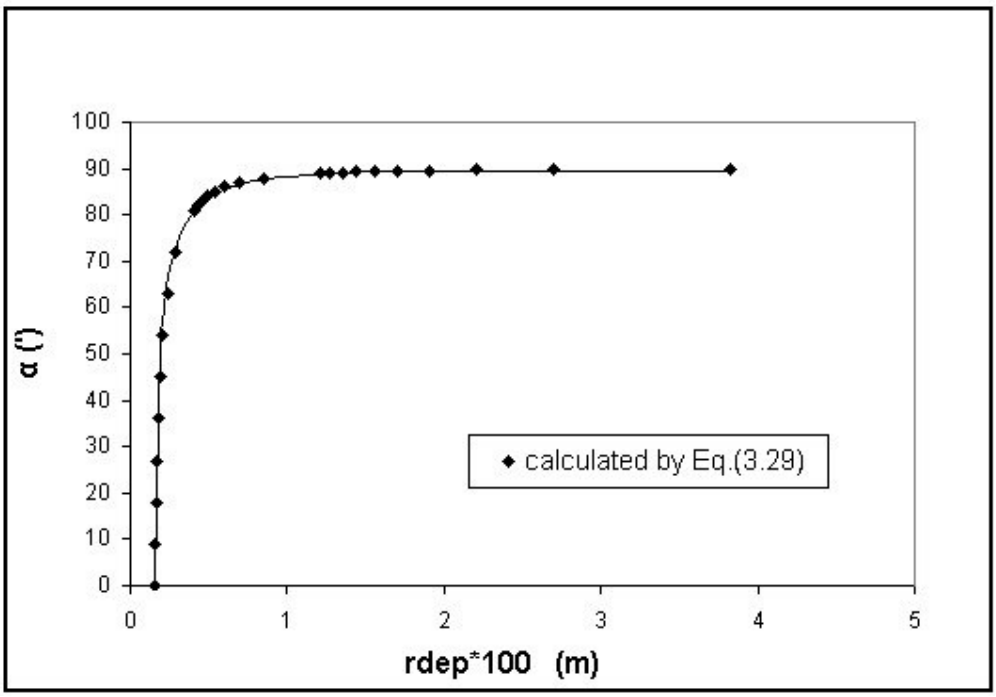

Figure 3.9 Variation of departure size with angle α.

CHAPTER 4

EXPERIMENTAL STUDY

Experimental investigation of this study was carried out in the heat transfer laboratory at the Mechanical Engineering Department of METU. Some parts of the apparatus were constructed by earlier researchers. A test section which has been newly designed to investigate dropwise condensation on a gold coated horizantal cylindrical tube was manufactured in Ankara - Turkish Railway Factory and put together on the existing apparatus.

Basic components of the setup are the following:

- Cooling water tank with electric heater to supply water at required temperatures.
- The boiler to generate steam.
- Test section.
- Temperature measurement system

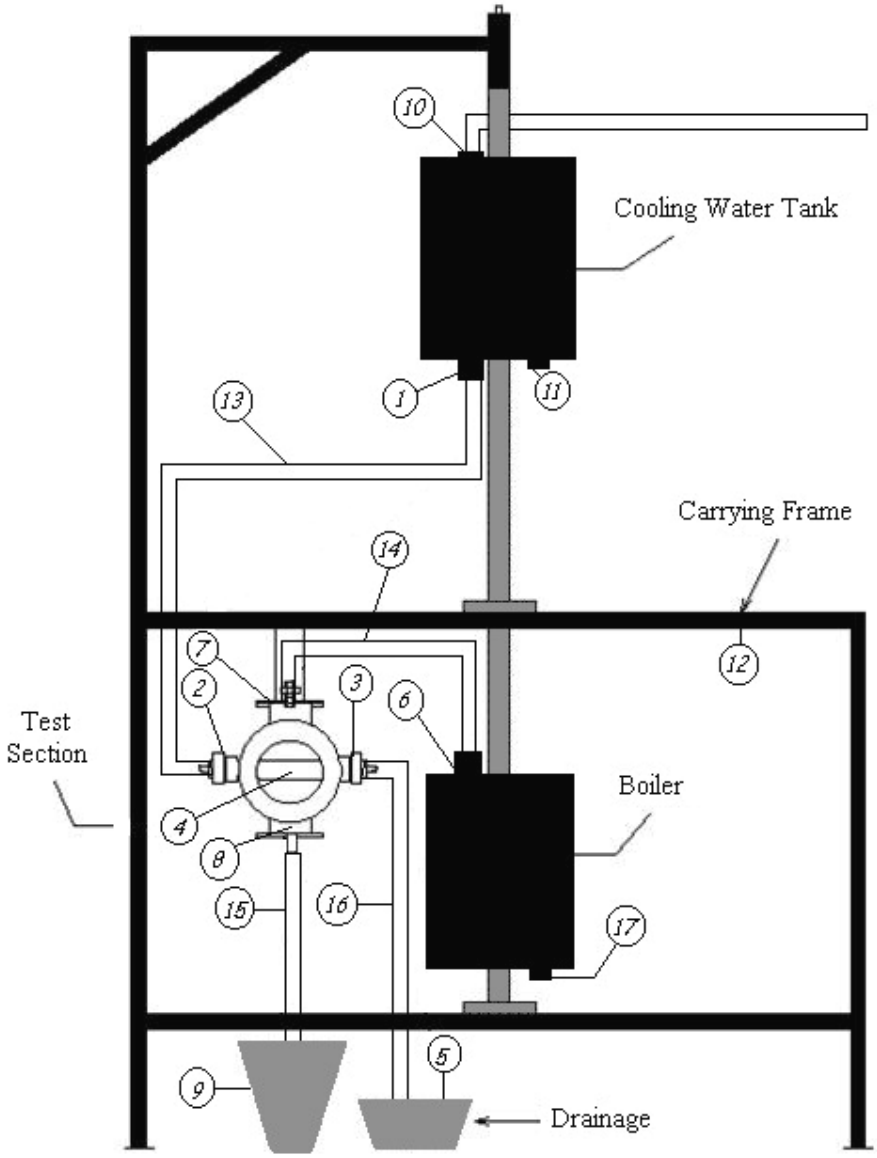

Figure 4.1 Schematic presentation of the apparatus

The components of the experimental setup shown in Fig 4.1 are the following:

1. Valve
2. Inlet of Test Section for Cooling Water
3. Exit of Test Section for Cooling Water
4. Gold Coated Horizantal Condensation Tube
5. Drainage for Cooling Water
6. Exit of Boiler
7. Inlet of Test Section for Steam
8. Exit of Test Section for Steam
9. Drainage for Condense Steam
10. Inlet of Cooling Water Tank
11. Electrical Heater
12. Carrying Frame
13. Elastic Hose
14. Copper Hose
15. Copper Hose for Condensed Steam
16. Elastic Hose for Cooling Water
17. Electrical Heater

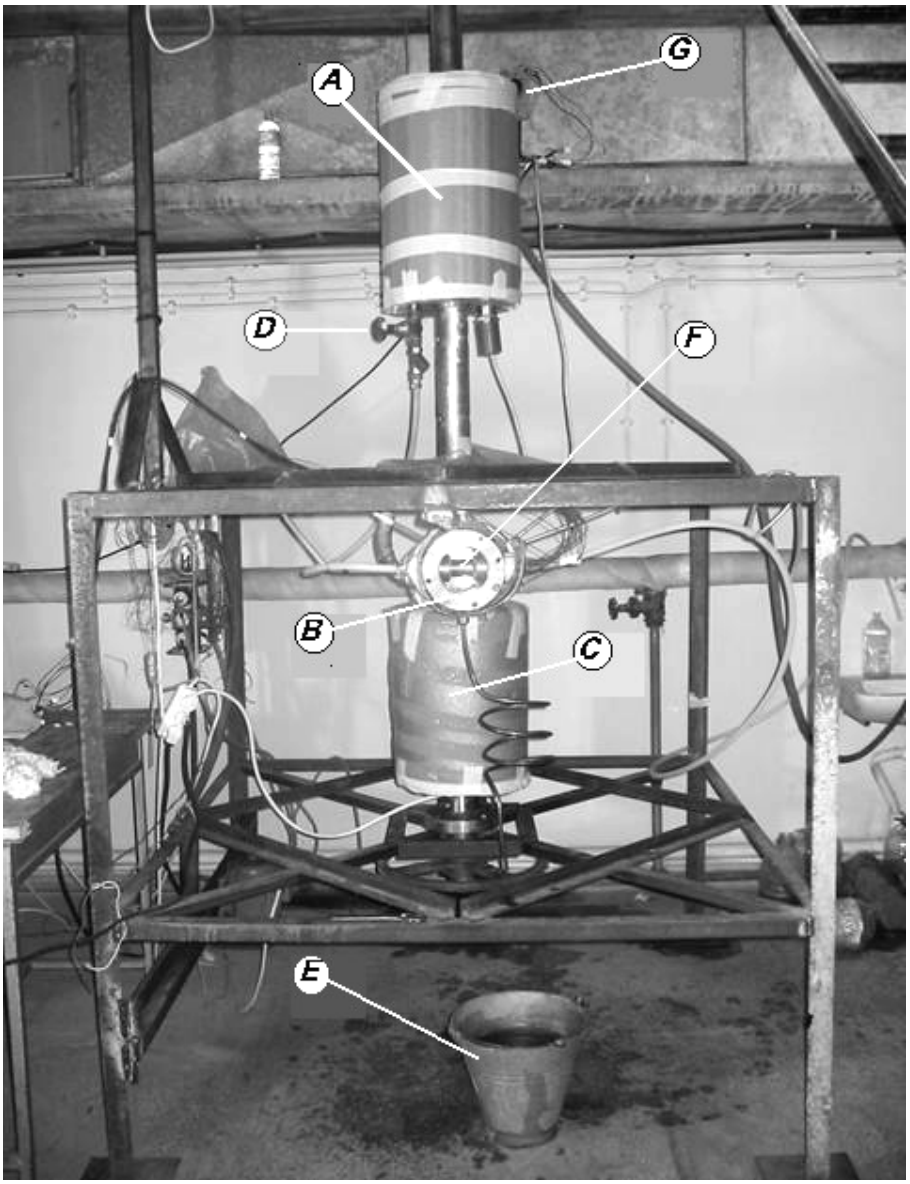

Figure 4.2 General view of the experimental setup

The main components of the experimental setup are shown in Fig 4.2.

- A - Cooling Water Tank
- B - Test Section
- C - Boiler
- D - Valve
- E - Drainage
- F - Gold Coated Horizantal Tube
- G – Thermostat

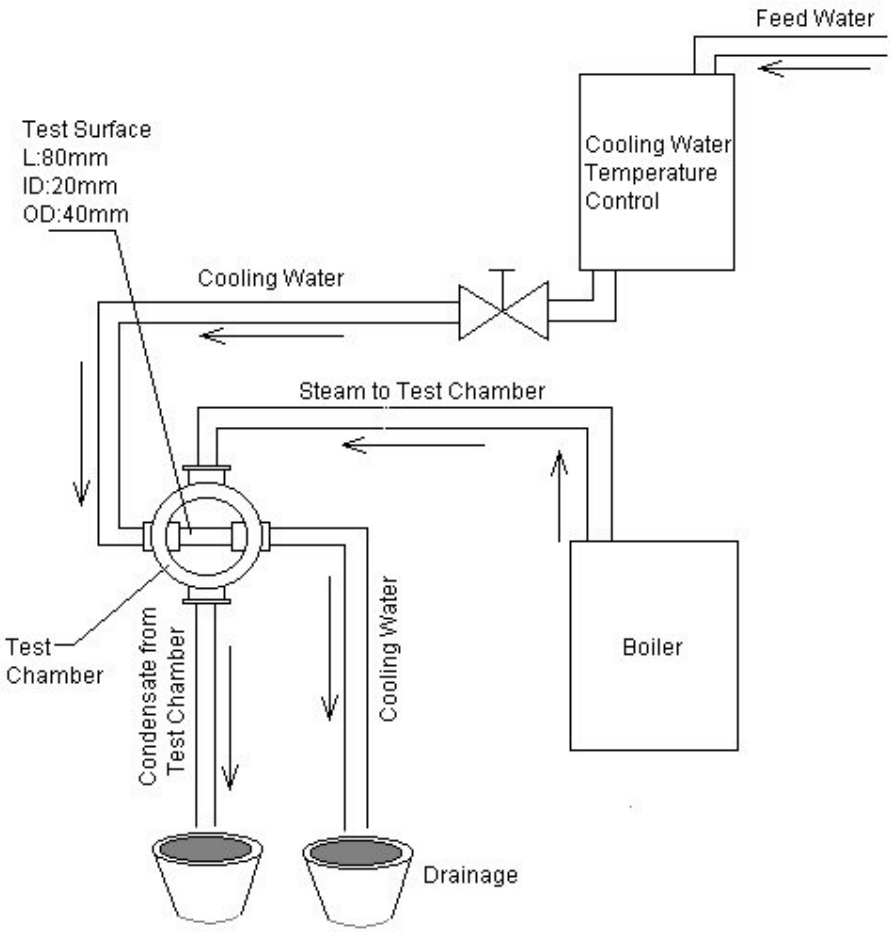

Figure 4.3 Schematic layout of the experimental setup

4.1 Cooling Water Tank

As the steam flows over the horizontal tube (No.4 in Fig 4.1) tested and condenses over it, and heat is transferred from the steam to the tube and then to the cooling water. Therefore it is necessary to supply cold water at a fixed temperature at steady state operation. For this reason, a cooling water tank (denoted as A in Fig 4.2) is placed around the shaft and above the test section (denoted as B in Fig 4.2) to provide cooling water to condensation tube by the gravity. The cooling water could have been supplied directly from the tap but in this case, cooling water temperature control would be more difficult. For this reason a cooling water tank which is kept at a constant temperature is preferred. The dimensions of the tank are 50 cm of height, 30 cm of outer diameter and 9 cm of inner diameter. The tank is filled from the inlet (No.10 in Fig 4.1) at the top and the water that has been heated up to desired temperature is taken from the bottom exit by means of a valve (No.1 in Fig 4.1 or denoted as D in Fig 4.2) connected between the tank and the test section. A small valve has been connected to the tank in order to regulate cooling water flow rate.

Figure 4.4 General view of the cooling water tank

An electric heater (No.11 in Fig 4.1) of 2 kW heating capacity is installed at the bottom of the tank and it is connected to city electric network by well insulated and grounded cables. A ground cable is connected to the metal frame (No.12 in Fig. 4.1) of the apparatus to prevent electric shocks. The tank is well insulated to prevent heat losses as much as possible and it is connected to the shaft by welding.

4.2 Boiler

Steam is generated in a boiler (denoted as C in Fig 4.2) and sent to the test section through a high temperature resistant hose (No.14 in Fig 4.1) from the steam exit at the top. The boiler is made of stainless steel. It is insulated with climaflex in order to minimize heat losses. Dimensions of the boiler are 40 cm of height, 30 cm of outer diameter and 9 cm of inner diameter. Distilled water is used to generate steam in the experiments and it is evaporated by a heater (No.17 in Fig 4.1) which is connected to boiler from bottom side. The electric heater has a power of 2 kW.

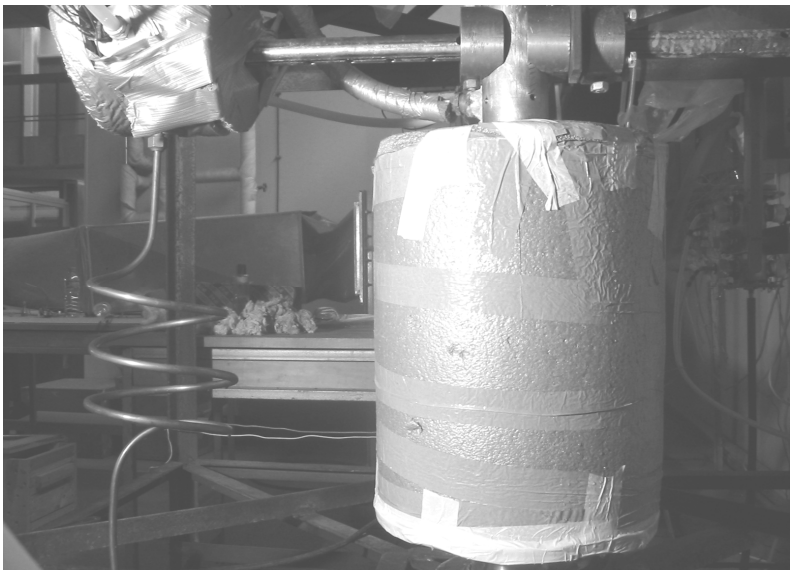

Figure 4.5 General view of the boiler

4.3 Test Section

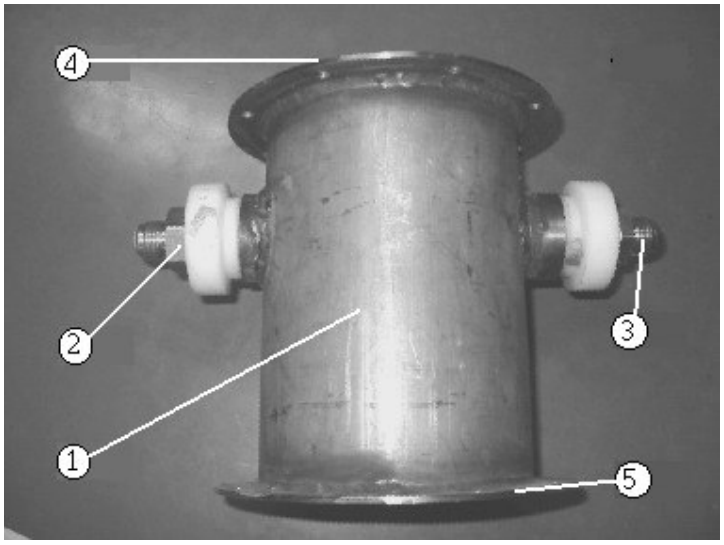

Figure 4.6 General View of the Test Section (1.Main body, 2.Inlet of test section for steam, 3.Exit of test section for steam, 4.Observation window, 5.Flange).

Test section was manufactured in Turkish Railway Factory- Ankara by using an electro-erosion machine and a lathe. The main body (No.1 in Fig 4.6) of the test section is stainless steel pipe which is 107 mm in diameter. The horizontal condensation tube (No.1 in Fig 4.7) should be placed across the main pipe as shown in Figure 4.7. Stainless steel material is used manufacturing the test section in order to prevent corrosion effects of water. Because of the mechanical properties of the stainless steel material, manufacturing of the components of the test section required special equipments and attention. To insert the horizontal tube inside the main pipe, it is necessary to prepare two coaxial holes across the main pipe. Since the wall thickness of the main pipe is small, it is extremely difficult to drill it by using traditional drill techniques with which it is not possible to produce the holes that have the same horizontal axis without damaging the main pipe. Hence, it is decided

to use a boring tool to drill the main pipe in order to keep drill axis in its position without damaging the pipe itself. Boring tool use the principle of drilling the material by moving in vertical and horizantal directions and drilling the material by removing the metal filings from the surface step by step with drills at varying diameters. First , a drill of 48 mm in diameter is prepared to accomplish this task. Then, the blade mounted on the boring tool and, the coaxial holes are obtained on the main pipe. After obtaining the horizontal coaxial hole couple on the main pipe, two pieces of inner stainless steel metal rings are welded on the holes.

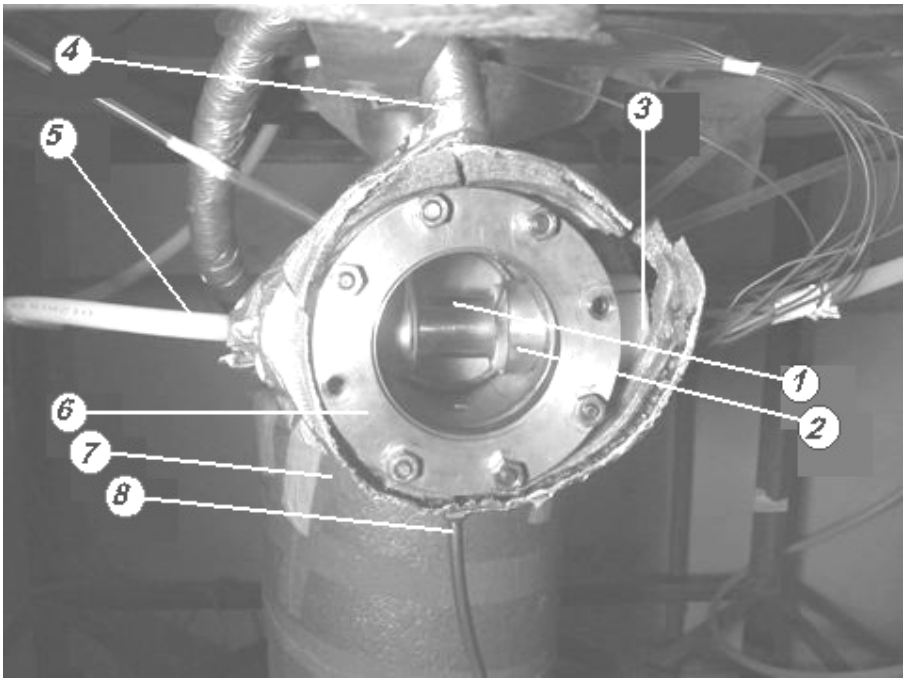

Figure 4.7 Front View of the Test Section (1. Condensation tube main body, 2. Coaxial metal ring, 3. Exit of test section for cooling water, 4. Inlet of test section for steam, 5. Inlet of test section for cooling water, 6. Observation window, 7. Boiler, 8. Exit of test section for steam).

During the welding process, because of high welding temperatures, undesired deformations on the material may occur. A gauge which fits inside the metal rings (No.2 in Fig 4.7) is prepared and screwed into the metal rings to prevent deformations on the material. A sectional view of the gauge and the metal rings is shown in Figure 4.8. After the welding process is completed and the material is cooled, the gauge is unscrewed from the metal rings.

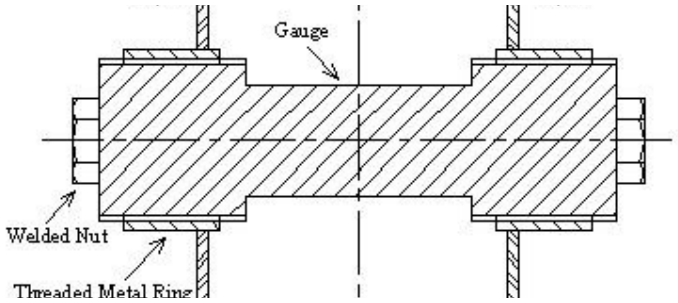

Figure 4.8 Drawing of the gauge and the metal rings

The condensation tube have 20 mm inner diameter and 40 mm outer diameter. It should be compressed from the both ends by Teflon to make sure it stays in its position. Teflon is a functional engineering plastic with metal-like properties made by Dupont (53). It is also a good insulator. Teflon connection component is prepared by using a lathe to provide that the outer surface of the cylindrical component can be tightly screwed into the metal rings (No.2 in Fig 4.7) which were welded on the main pipe (No.1 in Fig 4.6). While one end of Teflon component is connected to a horizontal condensation tube, the other end will be connected to cooling water hose (No.13 in Fig 4.1). Consequently, holes of different sizes are needed for each end of the Teflon. Using the appropriate drills, required holes are bored inside the Teflon component. There is a hole through the teflon part to let the thermocouples pass

inside the test section. The condensation tube is placed between the two Teflon apparatus by using seals and liquid gasket in order to prevent steam leakage to the cooling water. The view of Teflon apparatus is shown in Figure 4.9.

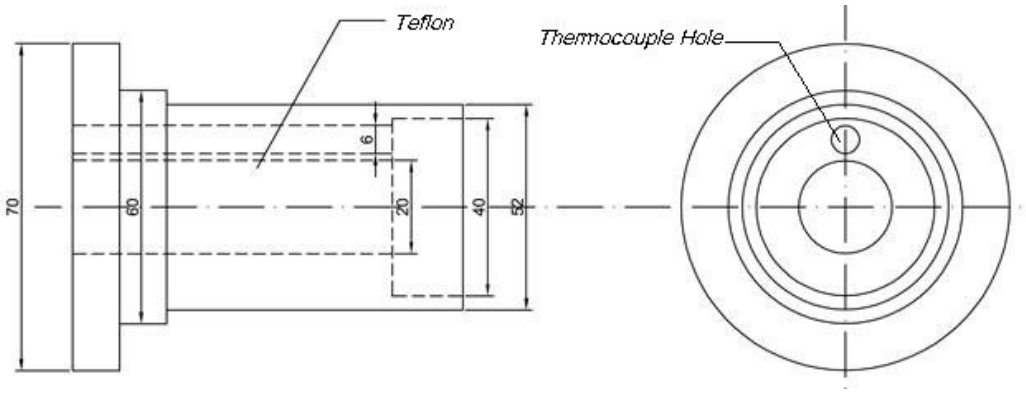

Figure 4.9 Drawing of the teflon component.

Two flanges (No.5 and No.6 in Fig 4.11) are welded on both ends of the test section. During all the welding processes throughout the manufacturing of the test section, specially designed electrodes for the stainless steel are used. Two flanges are mounted on the test section with eight bolts and a rubber seal in order to reach inside the test section whenever it is needed. Since it was necessary to observe the quality of the dropwise condensation taking place on the condenser surface from time to time , a observation window (No.6 in Fig. 4.10 or No.4 in Fig. 4.11) is provided on the test section for this purpose. The center of the front flange is drilled big enough to see the dropwise condensation on the horizantal gold coated surface inside the test section.

The main body (No.1 in Fig. 4.11) of the test section (Ø 107mm) is also drilled on the top and a pipe (Ø 20mm, No.2 in Fig. 4.11) is placed and welded on this hole

so as to provide a connection between the test section and the boiler. The high temperature resistant hose (No.14 in Fig. 4.1), which comes from the boiler, is fastened to the pipe. The bottom of the cylindrical test section is also drilled and a pipe (Ø 20mm, No.3 in Fig. 4.11) is welded here to make the condensate flows out of the setup. The whole test section is covered with an insulation material in order to prevent undesired condensation of steam on the inner surfaces of the setup.

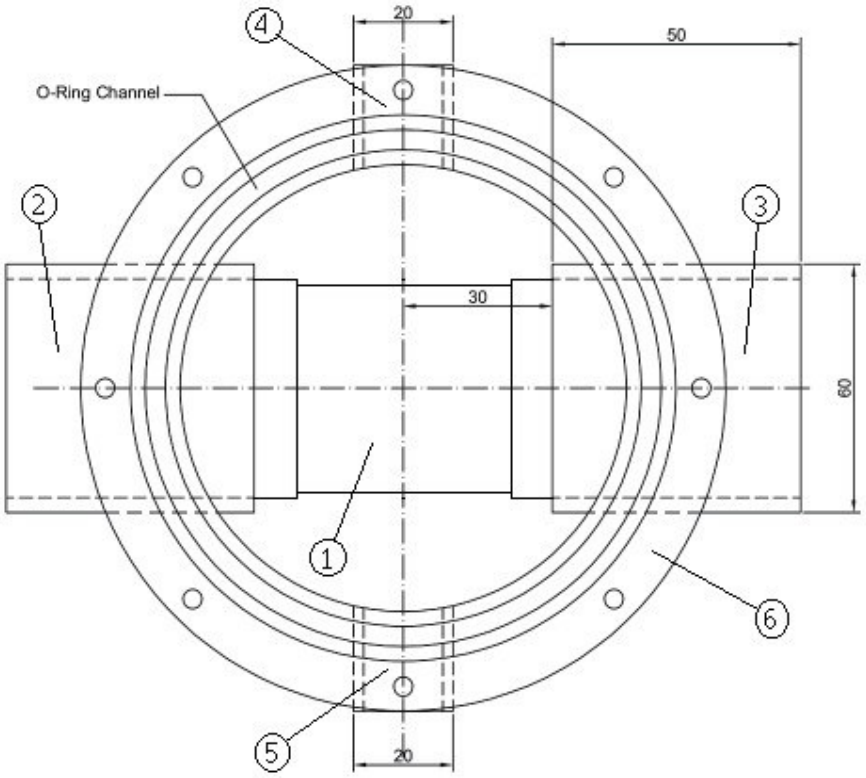

Figure 4.10 Drawing of the test section - front view (1. Gold coated horizantal condensation tube, 2. Inlet of test section for cooling water, 3. Exit of test section for cooling water, 4. Inlet of test section for steam, 5. Exit of test section for condense steam, 6. Observation window).

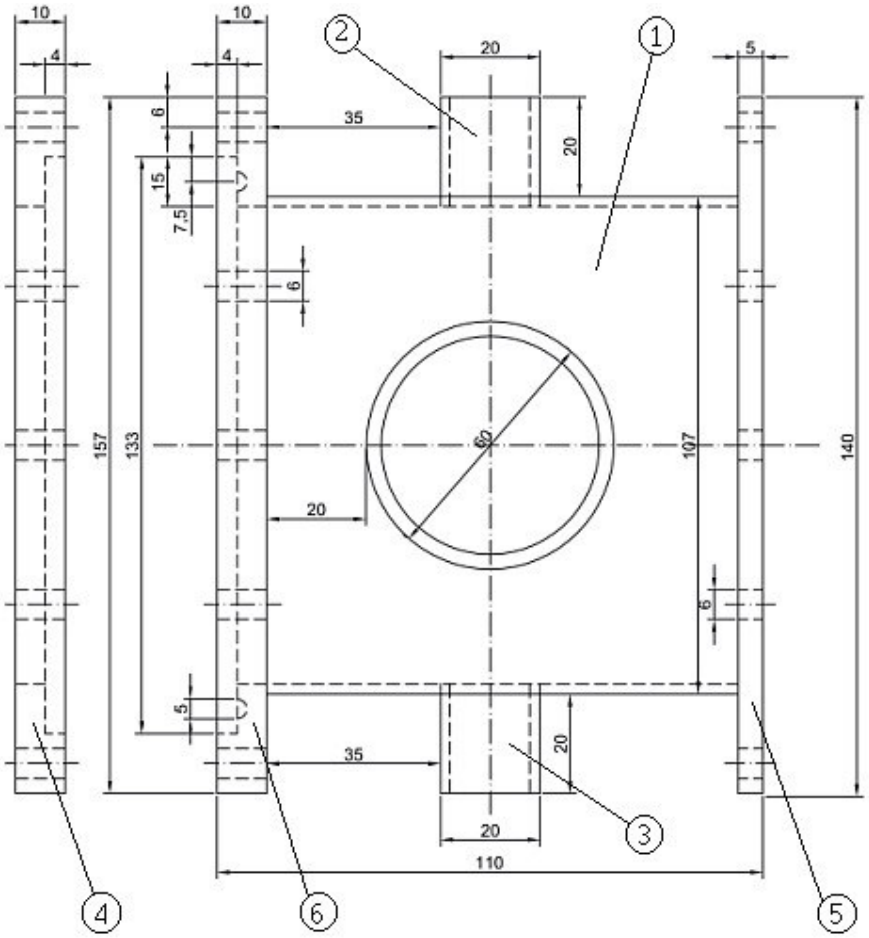

Figure 4.11 Drawing of the test section - lateral view (1. Main body of test section, 2. Inlet of test section for steam, 3. Exit of test section for condense steam, 4. Observation window, 5.Flange, 6.Flange)

4.4 Working Fluid

Water is chosen as the working fluid for this study. The main reason for this selection is that the ultimate goal of dropwise condensation research is to make it applicable to industry, especially to condensers in power plants. Another reason it is inexpensively available in quantity, and is non-toxic. For dropwise condensation

experiments, it is essential that the working fluid be pure enough so as not to significantly effect the experimental results, and distilled water appears to be quite suitable.

4.5 Test Piece

The test piece is shown in Fig. 4.12, and is machined from high purity copper. The temperature measurements for the computation of the heat flux and extrapolation to the surface temperature are made within the cylindrical section. The side surfaces are insulated by a teflon piece. Dropwise condensation occurs on the outer surface. After it is machined, the surface is first polished with fine emery paper. Then, the surface is cleaned by acetone and rubbed by dry cleaning tissue to remove any particles adhering to the surface.

Cooling of the test piece takes place inside of the cylinder. The diameter of the test surface is 40mm. The test surface is coated with gold to a thickness of about $2-3\mu m$. Gold coating is achieved by electroplating techniques. Electroplating is also called electro-deposition. It is the process that produces a thin, metallic coating on the surface of another metal (or any other conductor, e.g., copper) by means of electric current. The metal substrate to be coated is made the cathode in an electrolytic cell where the cations of the electrolyte are the positive ions of the metal to be coated on the surface. When a current is applied, the electrode reaction occurring on the cathode is the reduction of the metal ions to metal. The gold ions can be discharged form a gold solution to form a thin gold coating on the copper condenser surface to produce "hydrophobic behaviour" .

The actual process of electroplating the gold on the measuring tube is carried out in an electroplating bath. The electrolyte contains mostly a salt, dissociated into ions, of the gold. When a dc voltage is applied to the anode, the anode metal (gold) goes into solution as metal ions. These gold ions are attracted by the measuring tube, which functions as a cathode, and are deposited there as a gold coating.

In principle, treatment of the metal surface consists of removing a layer (degreasing or pickling) and applying a layer (electro deposition of gold). Degreasing is the most important initial step in pre-treatment since it ensures that the gold layer can be applied evenly to the surface and will adhere well. Pickling, on the other hand, is used reveal the surface in readiness for the plating charge. In the pickling process, unwanted layers and the like, in particular the oxide layers, are removed from the surface by chemical reaction. These pre-treatment steps are absolutely necessary to obtain a high-quality surface coating.

Figure 4.12 Dropwise condensation on the gold coated condenser surface

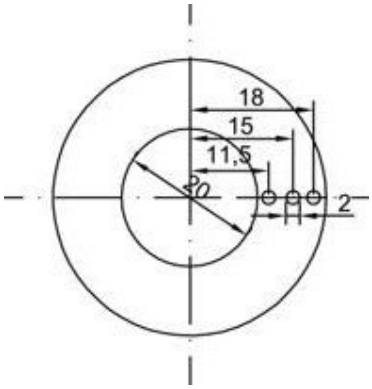

Figure 4.13 The condenser surface - lateral view

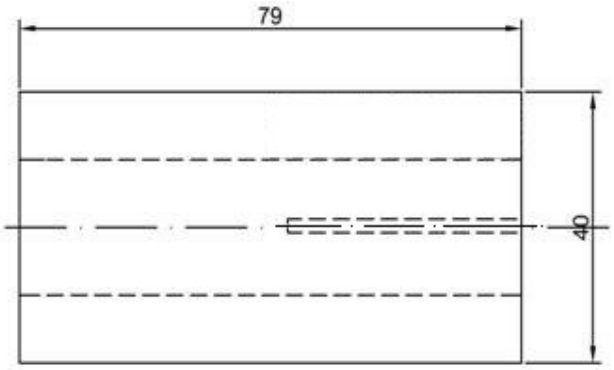

Figure 4.14 The condenser surface - front view

4.6 Temperature Measurement System

The installation of thermocouples has been carried out in the heat transfer laboratory. T type copper-constantan thermocouples are located on six different positions of the setup in order to get temperature measurements.

In order to seal the thermocouples against the steam , thermocouples are covered by a protective sheath. Thermocouples are installed in the condensation tube

by a strong adhesive, named Sun-Fix which is suitable for this kind of applications and also it seals the thermocouples agains the steam.. Once it is applied, three hours are needed for the Sun-fix to be effective. As thermocouple holes are drilling along the copper condensation tube care should be taken because of the mechanical properties and high temperature of copper let the material wrap the driller. After drilling, the thermocouples holes are filled completely with a high thermal conductivity chemical material not to cause any fluctuation while measuring temperature. This chemical material also does not let the holes act as insulator. because of and insulation inside the holes. The thermocouples are stuck inside the holes with Sun-Fix to ensure that temperatures are measured at the right location of condenser tube.

Figure 4.15 Temperature measurement system

One thermocouple is placed on the entrance of cooling water, and another is placed on the exit, in order to get cold water inlet and outlet temperatures (T_{in} and T_{out}) and determine the temperature increase. The third thermocouple is located at the inlet of the steam to the test section to find out the steam temperature, T_{sat}.

The other ends of the thermocouples are connected to the data logger as shown in Fig. 4.15. It provides input for 12 thermocouple probes, each connected to a separate channel but all thermocouples must be of the same type. The instrument can measure the temperature with an accuracy of $0.1°$.

4.6.1 Measuring of The Condenser Surface Temperature :

Three thermocouples are placed along the wall of the condensation tube to determine the temperature distribution there. Once the temperature distribution is determined the surface temperature (T_s) of the tube can be evaluated by using the curve-fitting and interpolation methods. Before the thermocouples are placed in specially prepared holes, these holes are drilled axially at one end of the test section at different distances from the center of the condensation tube, ($r_1 = 11.5$, $r_2 = 15$, $r_3 = 18mm$ as shown in Fig. 4.16).

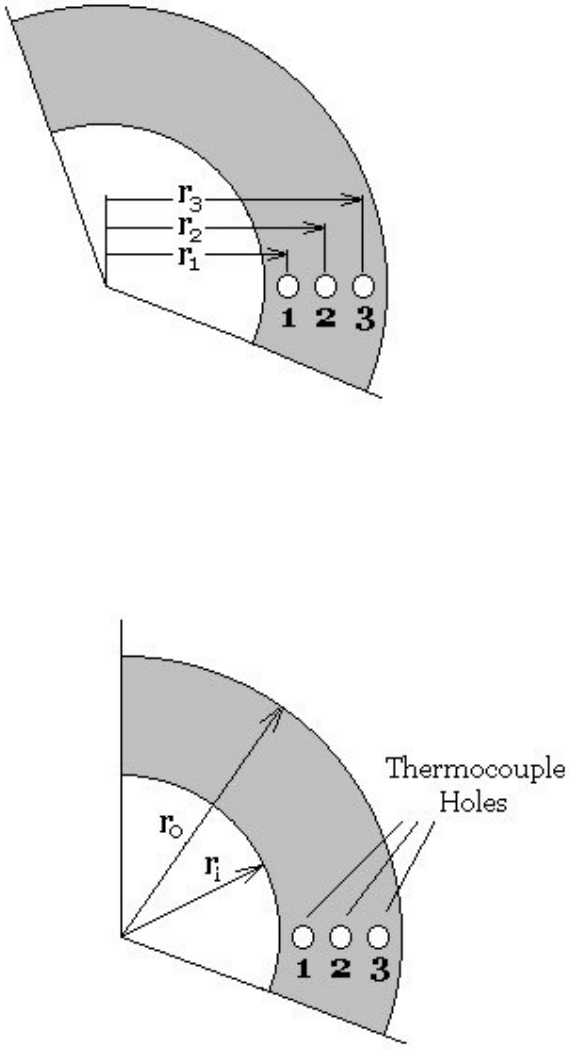

Figure 4.16 The positions of thermocouple holes on the condensation tube.

Temperatures $[T_1, T_2, T_3]$ measured, during experiments by three thermocouples inserted in the wall of the condensation tube are graphed with respect to the radial location as shown in Fig. 4.17. Logarithmic curve-fitting function is employed to the data presented on graphs to be able to find the surface temperature

(T_s) by interpolation. These graphs give the variation of temperatures with respect to the radial distances of thermocouple holes from the center of the condensation tube (11.5 - 15 -18mm). Microsoft Excel program is employed for graphing, curve fitting and interpolation.

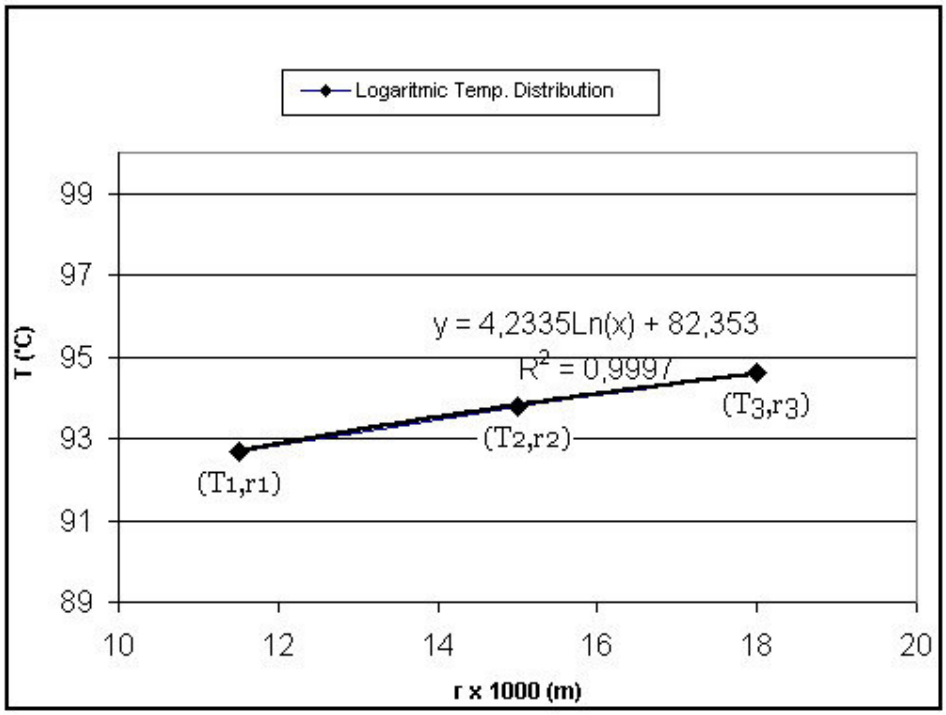

Figure 4.17 A typical variation of temperature value $[T_1, T_2, T_3]$ inside condensation tube with respect to the distance of thermocouple holes from the center of the condensation tube (11.5 - 15 -18mm).

As can be expected variation of temperature distribution in condensation tube changes logaritmically for the radial system studied in the experiments. Curve-fitting function gives an equation which changes logaritmically, e.g. T(r)=5,584*ln(r) + 74,765. This equation can be generalized as $[T(r) = P_1 \ln(r) + R_1]$, while P_1 and R_1

are the constant values to be determined experimentally and by curve fitting techniques.

It is possible to calculate the condenser surface temperature by using the radial distance of the surface from the center of the condensation tube, r = 20mm. The data are taken by three thermocouples $[T_1, T_2, T_3]$, the equations of temperature distribution $[T(r) = P_1 \ln(r) + R_1]$ obtained by curve-fitting function, and the values of condenser surface temperature $[T_s]$ which are calculated by the equations $[T(r)]$ are shown in Table 4.1.

Table 4.1 The temperature values of thermocouples $[T_1, T_2, T_3]$, the equations of temperature distribution $[T(r)]$, condenser surface temperature $[T_s]$.

T1	T2	T3	Equation of Temp.Distribution:T(r)	Ts
88.4	89.9	90.9	5.584*LN(20) + 74.7	91.4
89.4	90.6	91.5	4.683*LN(20) + 77.9	91.9
91.9	92.9	93.7	4.018*LN(20) + 82.0	94.1
91.9	93.1	94.0	4.683*LN(20) + 80.4	94.4
91.9	93.0	93.7	4.026*LN(20) + 82.0	94.1
92.2	93.2	93.9	3.805*LN(20) + 82.9	94.3
92.1	93.3	94.2	4.688*LN(20) + 80.6	94.6
92.7	93.8	94.6	4.239*LN(20) + 82.3	95.0
92.8	93.8	94.6	3.999*LN(20) + 83.0	94.9
91.4	92.4	93.2	4.007*LN(20) + 81.6	93.6
91.4	92.5	93.3	4.249*LN(20) + 81.0	93.7
91.0	91.9	92.6	3.574*LN(20) + 82.2	92.9
93.4	94.5	95.3	4.233*LN(20) + 83.0	95.7
93.1	94.3	95.1	4.467*LN(20) + 82.1	95.5
93.7	94.6	95.4	3.784*LN(20) + 84.4	95.7
94.3	94.9	95.4	2.449*LN(20) + 88.3	95.6
93.8	94.6	95.3	3.342*LN(20) + 85.6	95.6
93.8	94.4	94.9	2.454*LN(20) + 87.8	95.1
93.7	94.4	94.9	2.675*LN(20) + 87.1	95.1
94.2	95.0	95.6	3.130*LN(20) + 86.5	95.9
93.8	94.7	95.3	3.353*LN(20) + 85.6	95.6

4.7 Experimental Procedure

The aim of this study is to measure heat transfer rate and the heat transfer coefficient in dropwise condensation for a horizontal cylindrical surface. As the steam condenses on the horizontal tube, the energy in the form of latent heat is released from the steam conducts through the wall of the cylindrical condenser surface and finally absorbed by the coolant. Since this latent heat given by the steam is equal to the energy taken by the cold water, heat transfer coefficient can be obtained from the equation below:

$$Q = \dot{m} C_p (T_{out} - T_{in}) = hA(T_{sat} - T_{wall}) \qquad (4-1)$$

It is also possible to calculate heat transfer coefficient by using heat conduction equation for radial systems.

$$Q = \frac{2\pi kL(T_3 - T_1)}{\ln\left(\frac{r_3}{r_1}\right)} = hA(T_{sat} - T_{wall}) \qquad (4-2)$$

T_3 : Temperature reading of thermocouple No.3 inside test section shown in Fig. 4.16.

T_1 : Temperature reading of thermocouple No.1 inside test section shown in Fig. 4.16.

k : Thermal conductivity of test section

L : Length of the test section

Experiments are performed at two different stages:

1. Condensation phenomenon on the horizontal tube was investigated at different cooling water inlet temperatures and flow rates to change the surface temperature of the test piece. Experiments of this stage were performed for cooling water inlet temperatures of Ti=20°C, 30°C, 40°C, 50°C, 60°C and 70°C.
2. For each cooling water inlet temperature, the data were taken by varying the flow rate from 0.0105 kg/s to 0.0555 kg/s.

At the start of the experiments, the heater of the boiler was turned on. The heater of the cold water tank was turned on and off according to the cooling water temperature desired in the specific experiment. As soon as cooling water temperature reaches to desired value, the heater is turned off, and boiler is about to begin sending the steam to the setup. A certain period of time is allowed to pass for the test section to be purged and free of noncondensables (air). After the test section is filled up with steam, the valve of the cooling water tank is opened and the water flows over the horizontal condensation tube. Cooling water flow rate is determined by measuring the time necessary to fill a known volume. After the system became stable, temperature and flow rate data are taken.

Parameter varied in the experiments was surface temperature of the condensation tube varied by adjusting the cold water temperature. The data tables obtained from the experiments are given in Appendix A.

CHAPTER 5

RESULTS AND DISCUSSIONS

The results are discussed in three stages; analytical results, experimental results and the comparison of results with previous works. Heat transfer rate, heat flux and heat transfer coefficient are studied by means of the computer program prepared. Furthermore, the effect of the cooling water at varying flow rates and temperatures, the effect of temperature difference between steam and the tube wall on the heat transfer in dropwise condensation, the effect of variation of minimum radius of coalescing droplets (r_{co}), the effect of variation of departing droplet radius (r_{dep}), and the effect of dropsize distribution function constant n are also discussed. The results of the experiments which were conducted at two different stages that are described in Chapter 4 are graphically presented. Experimental results are also compared with the analytical results.

5.1 Analytical Results

A computer code in Mathcad is implemented for the analysis of dropwise condensation of steam. Furthermore, some results has been calculated by using Microsoft-Excel program. It is based on the theoretical model which is developed to calculate heat flux on the condenser surface. Thermophysical properties and

geometric dimensions are set at the beginning of the program. By changing the thermophysical properties, it is possible to examine condensation phenomenon on the horizontal tube for various working fluids. The fundamental geometric parameter is the diameter of the tube. The effect of fractional area constant n on the condenser surface, and the effect of the magnitude of coalescence and departing drop radius on heat flux are also discussed. The parameter that significantly affects condensation rate is the difference between the saturation temperature of steam and the wall temperature of the tube. The results which are obtained for different surface subcoolings (ΔT) are used to study the effect of steam to wall temperature difference on dropwise condensation heat transfer rate, heat flux and heat transfer coefficient.

Since mean heat transfer rate has been already calculated by using the computer program, the mean heat flux and the condensation heat transfer coefficient for different surface subcoolings (ΔT) can be calculated by using Eq. (5-1), and Eq. (5-2) respectively :

$$q'' = \frac{Q}{A} \qquad (5-1)$$

$$h = \frac{Q}{2\pi r L \Delta T} \qquad (5-2)$$

L : The length of cylindrical surface (m).

r : The radius of cylindrical surface (m).

ΔT : Surface subcooling ($^{\circ}C$)

5.1.1 Effect of Steam to Wall Temperature Difference on Condensation Heat Transfer

The theoretical analysis is extended to investigate condensation phenomenon for different surface subcooling $(\Delta T = T_{sat} - T_{wall})$ values. Heat transfer rate for dropwise condensation on a cylindrical surface is calculated using finite angular divisions. Local heat transfer rates are calculated at each angular position on the condenser surface.

For theoretical calculations, a single value of minimum radius for coalescencing droplets is used in all the computations performed here, $r_{co} = 52.10^{-6} m$, and is determined so as to give the best fit for the experimental results. In all computations, the contact angle is taken as 65°. The fractional area constant n in the drop size distribution function for the coalescence region is taken as $n = 1/3$. Since the variation of heat transfer coefficient for different surface subcooling can not be seen easily in some figures, the data tables are also given .

Variation of local heat transfer rate and local heat transfer coefficent on the condenser surface at different surface subcoolings (ΔT) with respect to departing droplet radius (r_{dep}) are presented in Table 5.1 and Table 5.2, respectively. The radius of departing droplet has a significant increase between 81° and 90° on the condenser surface, while the local heat transfer rate decreases sharply. Theoretically the departure size at the top of the cylindrical surface is infinitely large. For that reason, as one gets closer to the top, heat transfer coefficient becomes smaller due to the thermal resistance of the large droplets and at the top heat transfer rate becomes negligibly small.

Table 5.1 Variation of local heat transfer rate on the condenser surface at different surface subcooling (ΔT) with departing droplet radius (r_{dep}).

		Q (Heat Transfer Rate - W/m²)									
α (°)	rdep*100 (m)	ΔT=11	ΔT=10	ΔT=9	ΔT=8	ΔT=7	ΔT=6	ΔT=5	ΔT=4	ΔT=3	ΔT=2
0	0.159	43.02	39.11	35.20	31.29	27.38	23.47	19.56	15.65	11.74	7.83
9	0.160	42.96	39.05	35.15	31.24	27.33	23.42	19.51	15.60	11.69	7.78
18	0.163	42.77	38.88	34.99	31.10	27.21	23.32	19.43	15.54	11.65	7.76
27	0.169	42.40	38.55	34.69	30.84	26.99	23.14	19.29	15.44	11.59	7.74
36	0.177	41.93	38.12	34.31	30.50	26.69	22.88	19.07	15.26	11.45	7.64
45	0.189	41.27	37.52	33.77	30.01	26.26	22.51	18.76	15.01	11.26	7.51
54	0.208	40.30	36.64	32.97	29.31	25.65	21.99	18.33	14.67	11.01	7.35
63	0.237	38.98	35.44	31.89	28.35	24.81	21.27	17.73	14.19	10.65	7.11
72	0.287	37.07	33.70	30.33	26.96	23.59	20.22	16.85	13.48	10.11	6.74
81	0.403	33.79	30.72	27.65	24.57	21.49	18.44	15.37	12.30	9.23	6.16
90	1.376	23.54	21.40	19.26	17.12	14.98	12.84	10.70	8.56	6.41	4.27

It is seen from the Table 5.2 that surface subcooling has very small effect on the local heat transfer coefficient. While the departing droplet radius decreases, the local heat transfer coefficient increases. The variation of departing droplet radius is calculated by using Eq. (3-27), $D_{dep} \approx 1/\sqrt{g\cos\alpha}$.

The variation of local heat transfer coefficient with departing droplet radius is presented in Table 5.2 and Fig. 5.1.

Table 5.2 Variation of local heat transfer coefficient on the condenser surface at different surface subcooling (ΔT) with departing droplet radius (r_{dep}).

		h (Heat Transfer Coefficient - W/m²K)									
α (°)	rdep*100 (m)	ΔT=11	ΔT=10	ΔT=9	ΔT=8	ΔT=7	ΔT=6	ΔT=5	ΔT=4	ΔT=3	ΔT=2
0	0.159	25936	25936	25937	25938	25939	25941	25943	25946	25952	25963
9	0.160	25900	25897	25900	25897	25892	25886	25877	25863	25841	25797
18	0.163	25785	25784	25782	25781	25778	25775	25771	25764	25753	25731
27	0.169	25562	25565	25561	25565	25570	25576	25585	25598	25620	25664
36	0.177	25279	25280	25281	25283	25286	25289	25293	25300	25311	25333
45	0.189	24881	24882	24883	24877	24878	24880	24882	24885	24891	24902
54	0.208	24296	24298	24294	24297	24300	24305	24312	24322	24338	24371
63	0.237	23500	23503	23498	23501	23504	23509	23516	23526	23542	23576
72	0.287	22349	22349	22349	22349	22349	22349	22349	22349	22349	22349
81	0.403	20371	20372	20374	20367	20359	20381	20386	20392	20403	20425
90	1.376	14192	14192	14192	14192	14192	14192	14192	14192	14170	14159

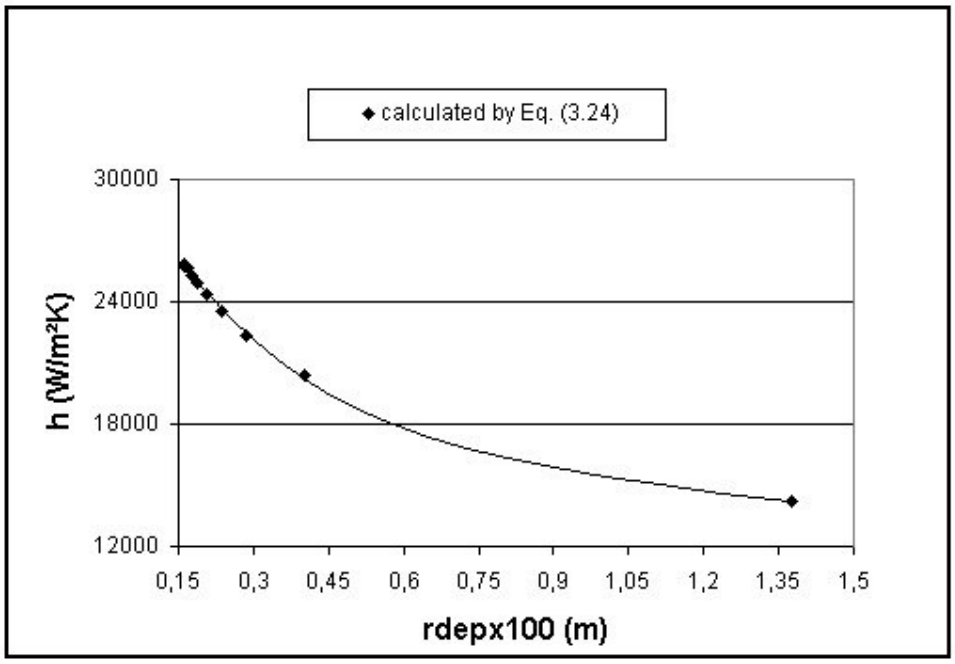

Figure 5.1 Variation of local heat transfer coefficient with departure size.

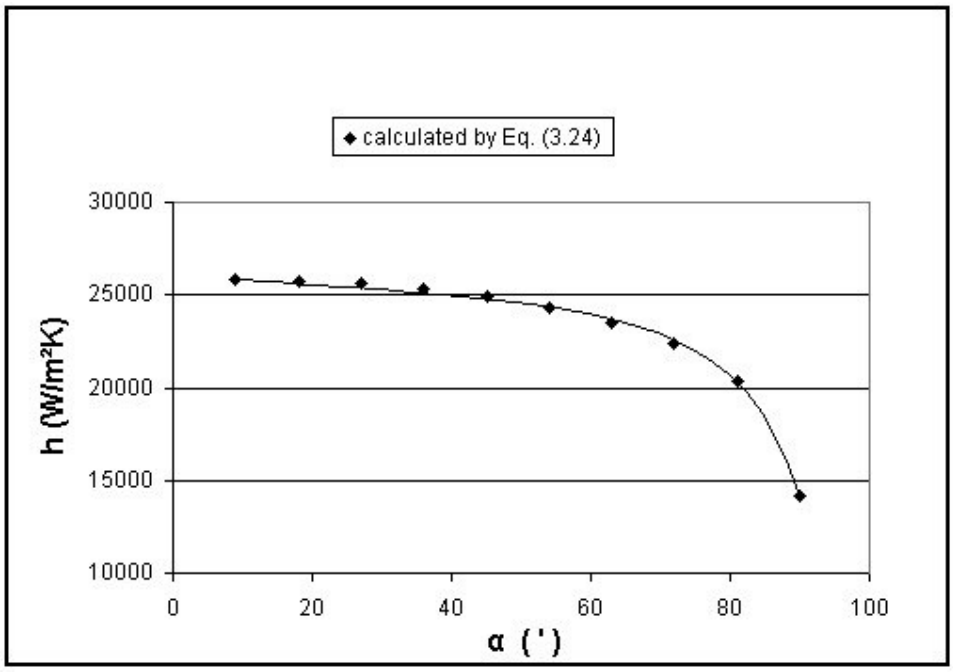

Figure 5.2 Variation of local heat transfer coefficient with angle α.

It is seen in Figure 5.2 that as the angle α increases, the local heat transfer coefficient decreases. The variation of local heat transfer coefficient with angular position shows a significant decrease in local heat transfer coefficient at high values of angular position.

The variation of mean heat flux and mean heat transfer coefficient for entire condenser surface with surface subcooling (ΔT) are presented in Fig 5.3, Fig. 5.4 and in Table 5.3, respectively. Eq. (3-24) is employed in the calculations.

It can be deduced from Table 5.3 that the rate of mean heat transfer increases as the steam to wall temperature difference increases. A small decrease of mean heat transfer coefficient is observed in the table as the surface subcooling is increased. This behavior is due to the fact that the surface is covered by departing droplets more as the surface subcooling and consequently the heat transfer rate and the condensation rate inceases. It can be speculated that as the surface subcooling increases to large values that decrease in the heat transfer coefficient will be more significant.

Table 5.3 Variation of mean heat transfer rate, heat flux and heat transfer coefficient for entire condenser surface with surface subcooling (ΔT).

	ΔT=11	ΔT=10	ΔT=9	ΔT=8	ΔT=7	ΔT=6	ΔT=5	ΔT=4	ΔT=3	ΔT=2
Q (rdep=0.16-1.2)	1630.4	1482.2	1334	1185.8	1037.6	889.46	741.28	593.1	444.9	296.72
q" (rdep=0.16-1.2)	270309	245742	221169	196595	172025	147465	122898	98331	73761	49194
h (rdep=0.16-1.2)	24574	24574	24574	24574	24575	24577	24580	24583	24587	24597

Variation of mean heat flux for different surface subcoolings is presented in Fig. 5.3. It is seen from this figure that a small temperature difference has a considerable effect on mean heat flux and heat flux changes almost linearly with surface subcooling.

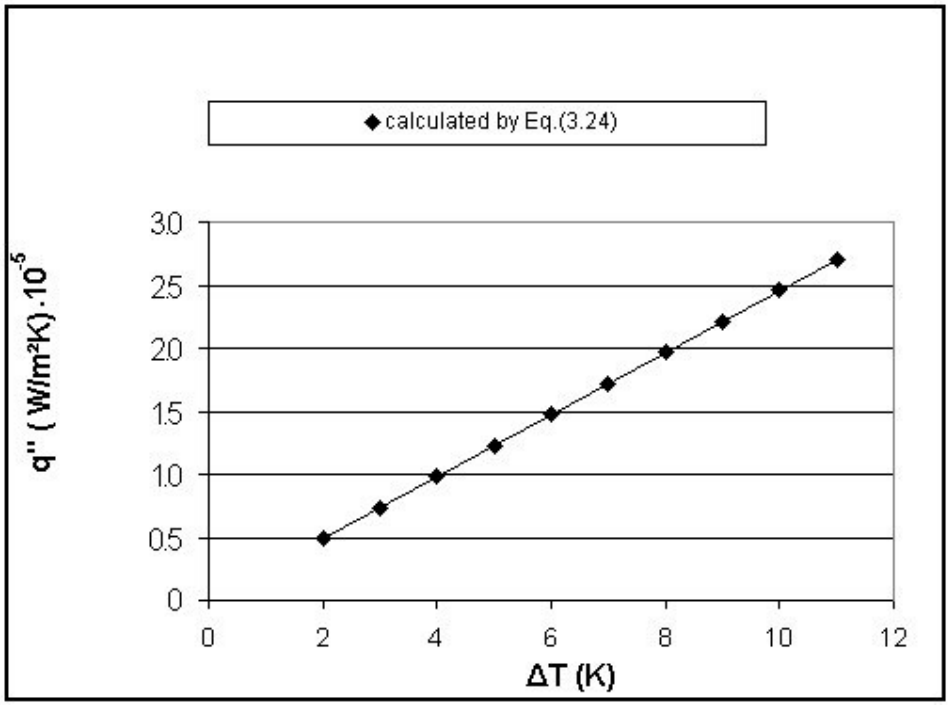

Figure 5.3 Variation of mean heat flux with surface subcooling (ΔT).

Variation of mean heat transfer coefficient for different surface subcoolings (ΔT) is presented in Fig. 5.4. The mean heat transfer coefficient has an insignificiant decrease with increasing (ΔT) as can be seen in Table 5.3. It is also seen that the mean heat transfer coefficient remains nearly constant as surface subcooling is varied in Fig. 5.4. The decreasing tendency in the mean heat transfer coefficient with surface subcoolings can not be observed in Fig. 5.4. Therefore, Table 5.3 is also presented so that the exact values of mean heat transfer coefficient which decreases insignificiantly with increasing surface subcooling is available.

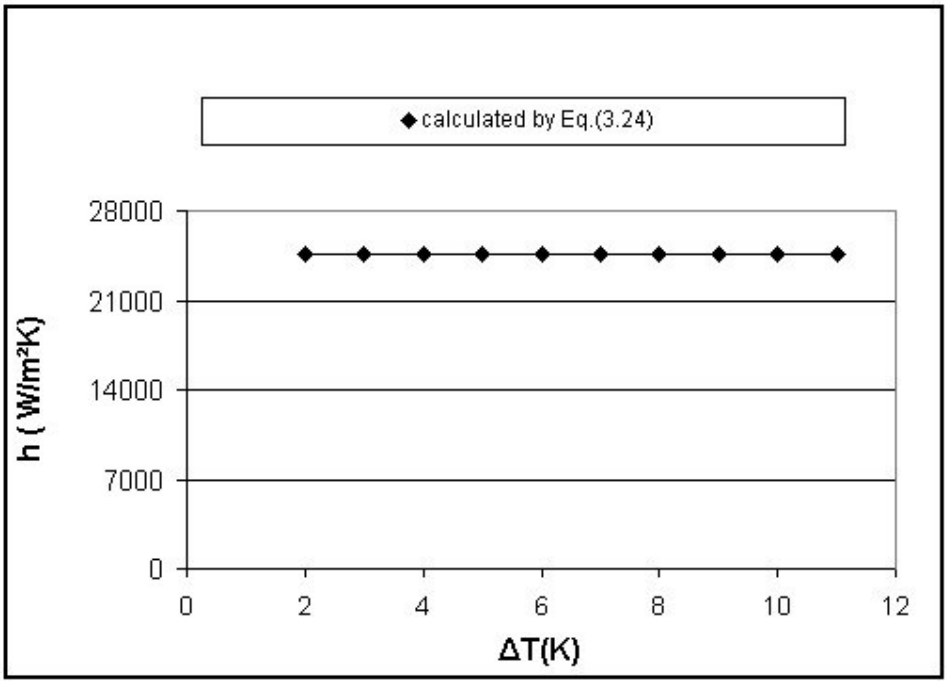

Figure 5.4 Variation of mean heat transfer coefficient with surface subcooling (ΔT).

Filmwise condensation heat transfer coefficient can be calculated by using Eq. (5-3) for the same conditions to compare the heat transfer coefficients for dropwise and filmwise condensation. The results of the calculations that employed the Eq. (5-3) is shown in Table 5.4 and variation of mean heat transfer coefficient for filmwise condensation with surface subcooling (ΔT) is shown in Fig. 5.5.

$$h = C\left[\frac{g\rho_l(\rho_l - \rho_v)k_l^3 h_{fg}}{\mu_l(T_{sat} - T_s)D}\right]^{1/4} \qquad (5-3)$$

C : 0.815 (for the sphere)

C : 0.729 (for the tube)

D : Diameter of condensation tube (m)

Table 5.4 Filmwise condensation heat transfer coefficient (Eq. (5.3))

h (W/m²K)	ΔT (K)
10740	11
11000	10
11290	9
11630	8
12030	7
12500	6
13080	5
13830	4
14860	3
16450	2

It can be deduced from Table 5.4 and Fig. 5.5 that filmwise condensation mean heat transfer coefficient increases as the steam to wall temperature difference decreases.

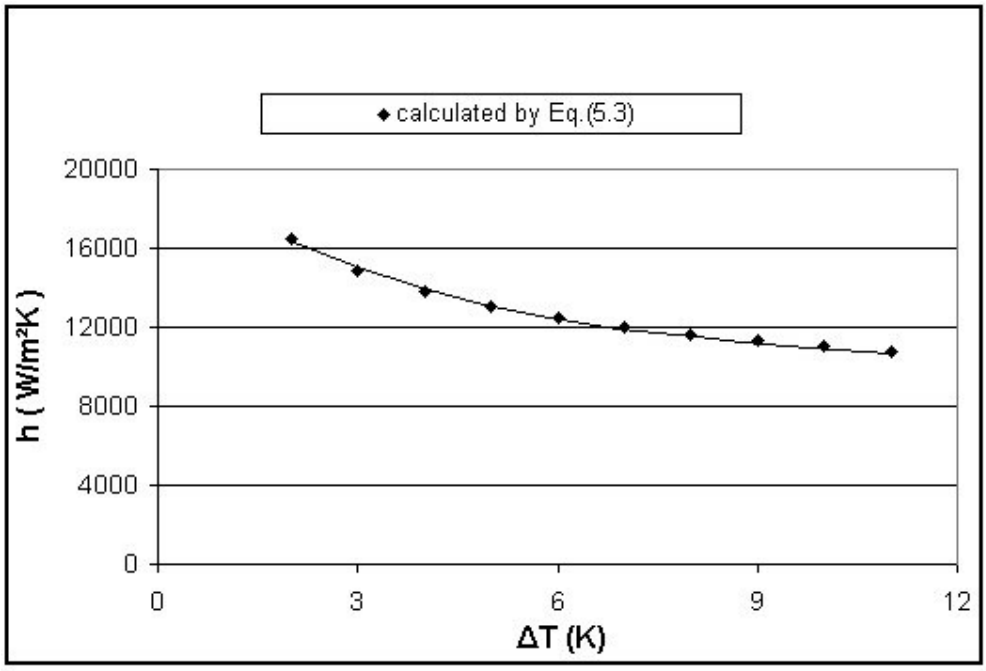

Figure 5.5 Variation of filmwise condensation heat transfer coefficient with surface subcooling (ΔT).

Comparison of filmwise and dropwise condensation heat transfer coefficients will be shown in chapter 5.3.

5.2 Experimental Results

The results of the experiments are obtained for two different stages which are described in Chapter 4. The mean heat transfer rate is obtained from Eq. (5-4), the measured mass flow rate, the inlet and outlet temperatures of the cooling water or by using Eq. (5-5) which calculates the mean heat transfer rate for radial systems.

Condensation heat transfer coefficient is calculated by the convection heat transfer formula Eq. (5-6) :

$$Q = \dot{m} C_p (T_{out} - T_{in}) \qquad (5-4)$$

$$Q = 2.\pi.k.L \frac{(T_3 - T_1)}{\ln\left(r_3 / r_1\right)} \qquad (5-5)$$

$$h_{cond} = \frac{Q}{2\pi \cdot rL(T_{sat} - T_w)} \qquad (5-6)$$

5.2.1 Results of the Experiments Performed at Different Flow Rates and Cooling Water Inlet Temperatures

The experiments were performed at six different inlet temperatures of the cooling water in order to examine the behaviour of the mean heat transfer rate and the mean heat transfer coefficient for different steam to wall temperature differences. The results of the experiments for 20°C, 30°C, 40°C, 50°C, 60°C and 70°C of cooling water temperatures are given in Appendix A.

The main parameter that affects condensation rate is the difference between the saturation temperature of steam and the wall temperature of the tube. The experimental analysis is extended to investigate condensation phenomenon for

different surface subcooling $(\Delta T = T_{sat} - T_{wall})$ values. Since the saturation temperature of steam remains nearly constant, the only way to change ΔT is to change wall temperature of the tube. Cooling water inlet temperature is adjusted so that the wall temperature reaches to the value desired.

Variations of mean heat flux and heat transfer coefficient for different surface subcoolings are presented in Fig. 5.6, Fig. 5.7, respectively. It is seen from the figures that there exist an almost linear relation between the mean heat flux and the surface subcooling and the heat transfer coefficient is almost independent of it.

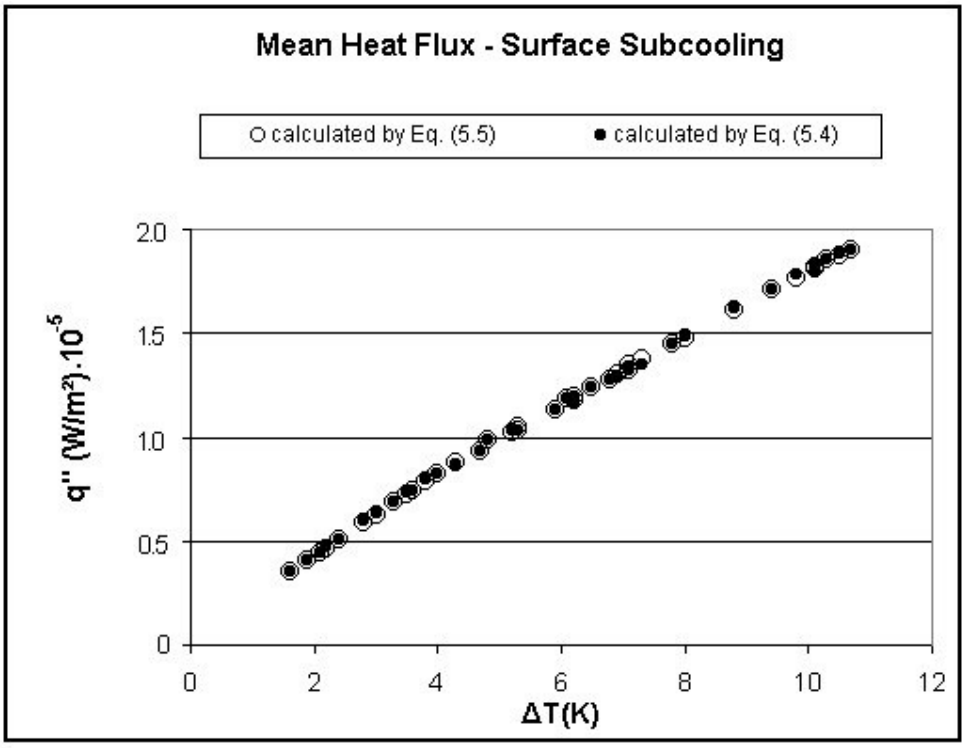

Figure 5.6 Variation of mean heat flux with surface subcooling

The equations (5-4), (5-5), and (5-6) are used to find the mean heat transfer coefficient that presented in Fig. 5.7 and Table 5.5.

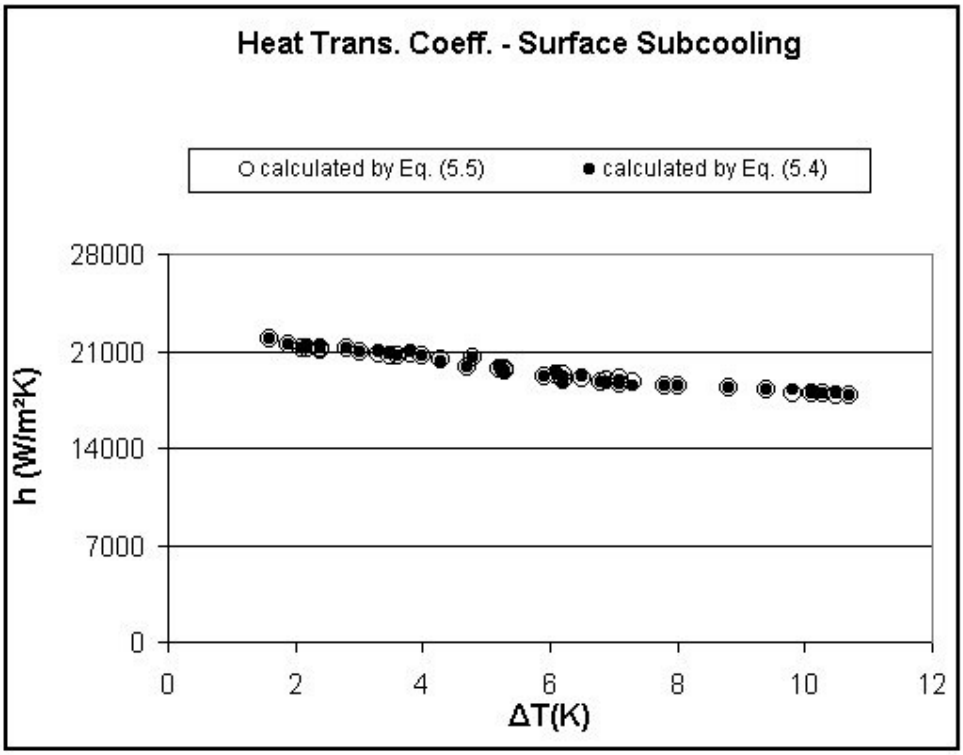

Figure 5.7 Variation of mean heat transfer coefficient with surface subcooling

It is deduced from Figure 5.7 and Table 5.5 that while the mean heat transfer coefficient increases, surface subcooling(ΔT) decreases. Although sweeping effect does not considered in analytical calculations, it can be seen in Fig. 5.7 that it causes a reduction in values of heat transfer coefficient with increasing surface subcooling.

Table 5.5 Variation of mean heat transfer coefficient by experiments at different cooling water inlet temperatures with surface subcoolings (ΔT).

Tin (C°)	ΔT (K)	h1 (W/m²K)	h2 (W/m²K)
20	10.5	17824	17947
20	10.3	17968	17998
20	10.1	18006	18070
20	9.8	18009	18172
20	7.8	18548	18525
20	7.1	18671	18564
20	6.2	18903	18815
30	10.7	17786	17756
30	10.1	17920	17915
30	9.4	18151	18223
30	8.8	18335	18385
30	8	18443	18514
30	7.3	18807	18438
30	7.1	18992	18811
30	6.1	19366	19381
30	5.3	19742	19505
40	6.9	18832	18781
40	6.8	18822	18785
40	6.5	19078	19133
40	6.2	19253	19214
40	5.3	19519	19528
40	5.2	19653	19779
40	4.8	20479	20518
40	3.8	20771	20940

Tin (C°)	ΔT (K)	h1 (W/m²K)	h2 (W/m²K)
50	6.9	18832	18791
50	5.9	19223	19111
50	4.7	19798	19855
50	4.3	20345	20270
50	4	20639	20693
50	3.6	20728	20716
50	3.3	20864	20892
60	2.8	21141	21242
60	2.4	21180	21240
60	2.1	21254	21250
70	3.5	20695	20818
70	3.3	20780	20915
70	3	20927	20982
70	2.4	21113	21272
70	2.2	21140	21384
70	1.9	21456	21422
70	1.6	21839	21881

In Table 5.5,

T_{in} : Cooling Water Inlet Temperature (20 - 70°C)

ΔT : Temperature difference between steam and wall of condensation tube $(\Delta T = T_{sat} - T_{wall})$.

h_1 : Heat transfer coefficient calculated by using Eq. (5-5)

h_2 : Heat transfer coefficient calculated by using Eq. (5-4)

5.3 Comparison of Analytical and Experimental Results

5.3.1 Comparison of Experimental Results with Literature

There are many investigations in dropwise condensation for horizantal cylindrical surfaces. In one of these studies, Zhao et al. (55–58) have successfully applied a practical condenser in the integral heating system in Dalian Power Station in China. The condenser is 800mm of diameter and 3500mm high with 800 brass tubes each having 16mm i.d. and 3000mm long. An overall heat transfer coefficient between 6000 and 8000 W/m²K with 2–3 m/s cooling water velocity has been maintained since its installation October 1989, to the present.

It is seen that the heat transfer coefficients found by the present study are higher than those found by Zhao. The reasons can be the copper condensation tube and gold promoted surface which makes the quality of dropwise condensation better. In their investigation, brass condensation tube and metal organic compound film are used.

Xuehu Ma (66) presented an experimental study that the effect of processing conditions of polymer film on dropwise condensation heat transfer of steam under atmospheric pressure is investigated to find an effective technique to prepare a lasting polymer film that can sustain long-term dropwise condensation pattern. The polytetrafluoroethylene (PTFE) films were coated on the external surfaces of brass tubes by means of the dynamic ion-beam mixed implantation technique, with a variety of surface processing conditions. The surface processing condition is crucial to the adhesion between polymer film and metal substrate. Different substrate material requires different optimal processing condition, and leads to different condensation heat transfer characteristic.

The measured contact angles and condensation modes for various surfaces are presented in Tables 5.6, and 5.7, respectively. Since the measured contact angles for H_2O are higher than 90° in Table 5.6, it is reasonable that dropwise condensation can be observed on these surfaces, but Table 5.7 shows that it is not possible to obtain flawless dropwise condensation all over the condenser surface.

Table 5.6 Contact angle for various surfaces

Surface no.	Contact angle (deg)	
	H_2O	CH_2I_2
B-1	100	45
B-4	109	50
B-6	110	60
B-8	114	63
B-9	104	62
B-10	99	50

Table 5.7 Condensation modes for various surfaces

Surface no.	Condensation mode
B-1	45% DWC
B-2	100% FWC
B-3	100% FWC
B-4	50% DWC
B-5	100% FWC
B-6	90% DWC
B-7	100% FWC
B-8	100% DWC
B-9	60% DWC
B-10	50% DWC

This can be due to the fact that the film covered did not adhere well on the surface and some void form there and also due to the insufficient mechanical strength. The second reason for imperfect dropwise condensation is that the film can not be made thick enough since conduction heat transfer resistance increases excessively. Some organic and dirt contamination over the condenser surface can also be the cause of this problem. Adverse effect of non-condensable gases on heat transfer mechanism in dropwise condensation can also be the reason for imperfect dropwise condensation. As it is explained in chapter 2, surface free energy criterion is better than the contact angle to predict condensation mode since it is not affected by the measuring temperature. It is concluded that contact angle criterion is not reliable value whether dropwise condensation takes place or not on the condensation surface.

Varition of heat transfer coefficient and heat flux with surface subcooling for different surfaces is presented in Fig. 5.8 and Fig. 5.9. The experimental results

indicated that condensation heat transfer coefficient is 1.6–28.6 times larger than that of film condensation values for the brass tubes treated under various conditions.

It is seen that B-1 and B-4 tubes has the same characteristics with the present study in Fig. 5.8.

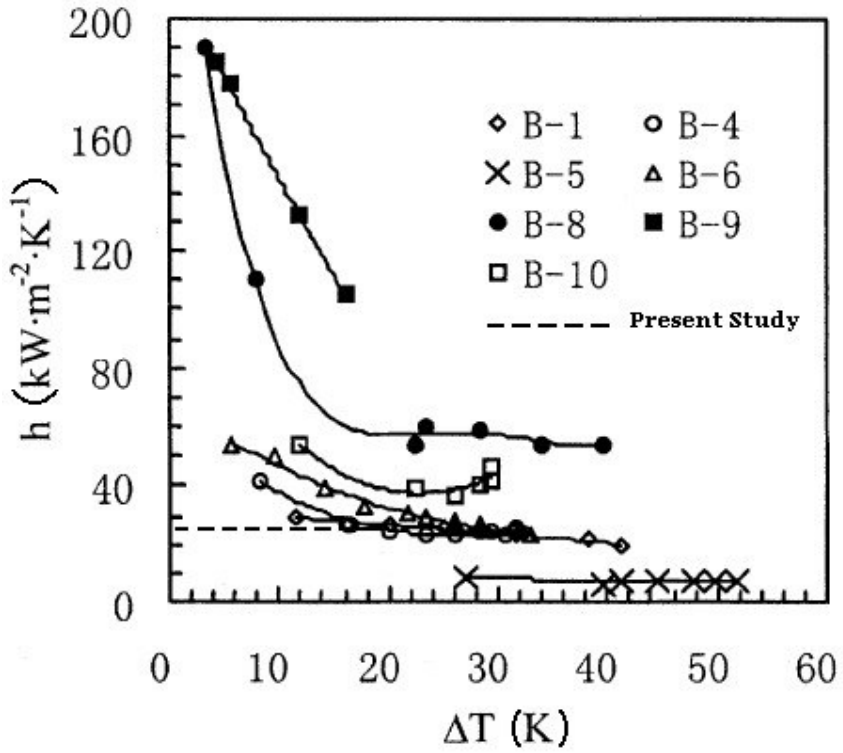

Figure 5.8 Comparison of mean heat transfer coefficient with surface subcooling.

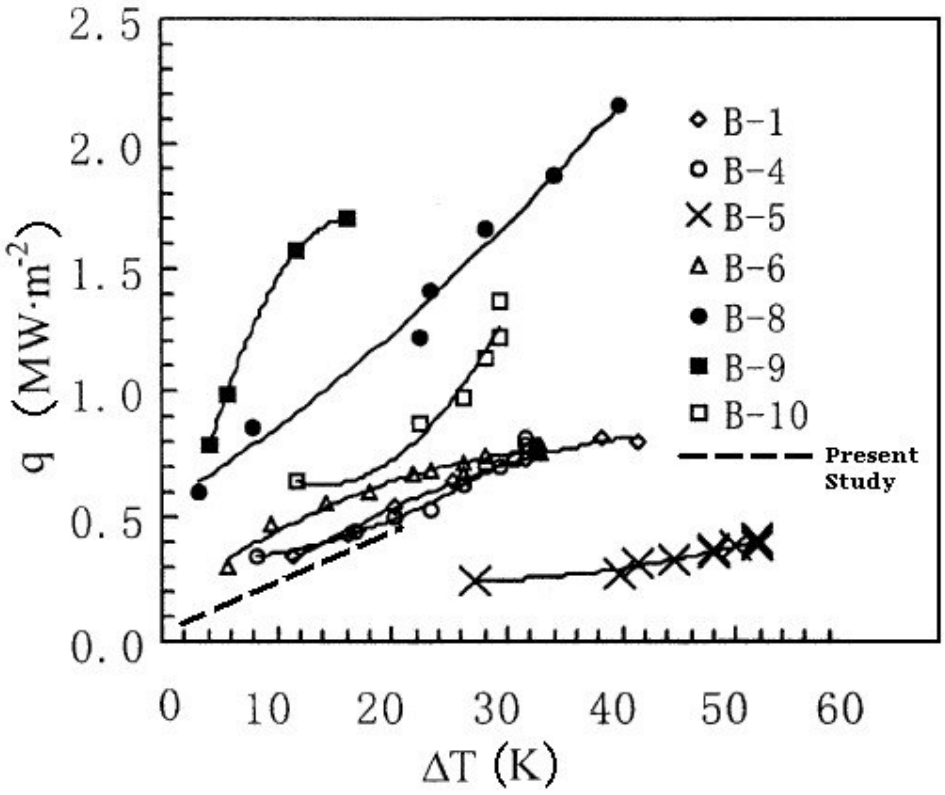

Figure 5.9 Comparison of mean heat flux with surface subcooling.

5.3.2 Comparison of Experimental Results with Analytical Results

The mean heat flux and heat transfer coefficient of condensation tube which were obtained from the experiments conducted and the analytical investigation are presented in Figs. 5.10, 5.11, respectively. Even though experimental results of the present study gives higher heat transfer coefficients than the Zhao's experimental study, they are lower than the analytical results.

The mean heat flux and heat transfer coefficient are calculated for entire condenser surface by using Eq. (3-24) for constant value of $r_{dep} = 0.159 \times 10^{-2} m$. The aim of this calculation is to see how variation of the departure size on a cylindrical surface effects the heat transfer rate. Table 5.8 shows that an increase in

the heat transfer rate and a decrease in the heat transfer coefficient for the large temperature differences take place.

Table 5.8 Variations of mean heat transfer rate, heat flux, and heat transfer coefficient calculated by using Eq. (3-24) for constant value of $r_{dep} = 0.159 \times 10^{-2}$ with respect to surface subcooling.

	ΔT=11	ΔT=10	ΔT=9	ΔT=8	ΔT=7	ΔT=6	ΔT=5	ΔT=4	ΔT=3	ΔT=2
Q (rdep=0.159)	1720.8	1564.4	1408	1251.6	1095.2	938.8	782.4	626	469.6	313.2
q" (rdep=0.159)	285294	259364	233434	207504	181575	155645	129715	103785	77856	51926
h (rdep=0.159)	25936	25936	25937	25938	25939	25941	25943	25946	25952	25963

The symbols and notations used in the Figs. 5.11 and 5.12 are as follows:

(◊) analytic ($r_{dep}: 0.16 - 1.2 \cdot 10^{-2} m$) : The analytical results of heat transfer rate calculated by Eq. (3-24) for varying departing droplet radius (r_{dep}) on the cylindrical condenser surface.

(□) analytic ($r_{dep}: 0.159 \cdot 10^{-2} m$) : The analytical results of heat transfer rate calculated by assuming that departure size is constant and equal to its value on a vertical surface.

(+) calculated by Eq. (5-4) : The experimental results of heat transfer rate calculated by Eq. (5-4). Heat transfer rate is obtained from the measured mass flow rate, the inlet and outlet temperatures of the cooling water.

(●) calculated by Eq. (5-5) : The experimental results of heat transfer rate calculated by employing the Eq. (5-5) which is based on thermal resistance concept.

The comparison of the mean heat flux, and heat transfer coefficient for different wall temperatures are presented in Figs. 5.10 and 5.11, respectively. It is seen from the Fig. 5.10 that a small temperature difference has a considerable effect on the mean heat flux which is calculated by different methods.

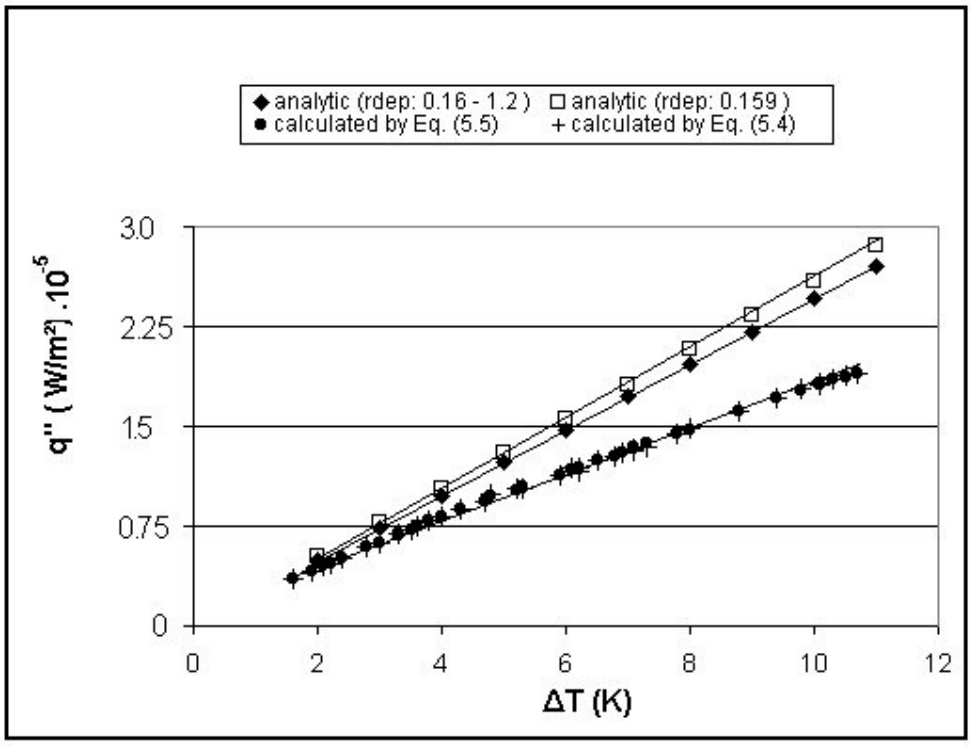

Figure 5.10 Comparison of mean heat flux with surface subcooling.

The dropwise condensation heat transfer coefficient is calculated by using Eq. (3-24) for its constant value of $r_{dep} = 0.159 \times 10^{-2} m$ (on a vertical surface) and its varying values of $r_{dep} = 0.16 \times 10^{-2} mK\ 1.2 \times 10^{-2} m$ (for the cylindrical surfaces). The results of dropwise condensation heat transfer coefficient as a function surface subcooling are shown in Table 5.9 and in Fig. 5.11.

Table 5.9 Comparison of mean heat transfer coefficient calculated by using Eq. (3-24) for different surface subcooling (ΔT) with respect to constant departing droplet radius $r_{dep} = 0.159 \times 10^{-2}$ and varying departing droplet radius $r_{dep} = 0.16 \times 10^{-2} mK\ 1.2 \times 10^{-2} m$.

ΔT (K)	h (r varying)	h (r constant)
11	24573.5	25935.7
10	24574.2	25936.3
9	24574.3	25937.1
8	24574.4	25938.0
7	24575.0	25939.2
6	24577.4	25940.8
5	24579.5	25943.3
4	24582.7	25946.3
3	24586.8	25951.8
2	24596.8	25962.9

It can be deduced from Figure 5.11 that mean heat transfer coefficient increases as the steam to wall temperature difference decreases for the experimental calculations for filmwise condensation. In contrast to increase in the mean heat transfer coefficient for these studies with decreasing temperature differences, a constant value is observed in the mean heat transfer coefficient for the analytical studies which are calculated by Eq. (3-24).

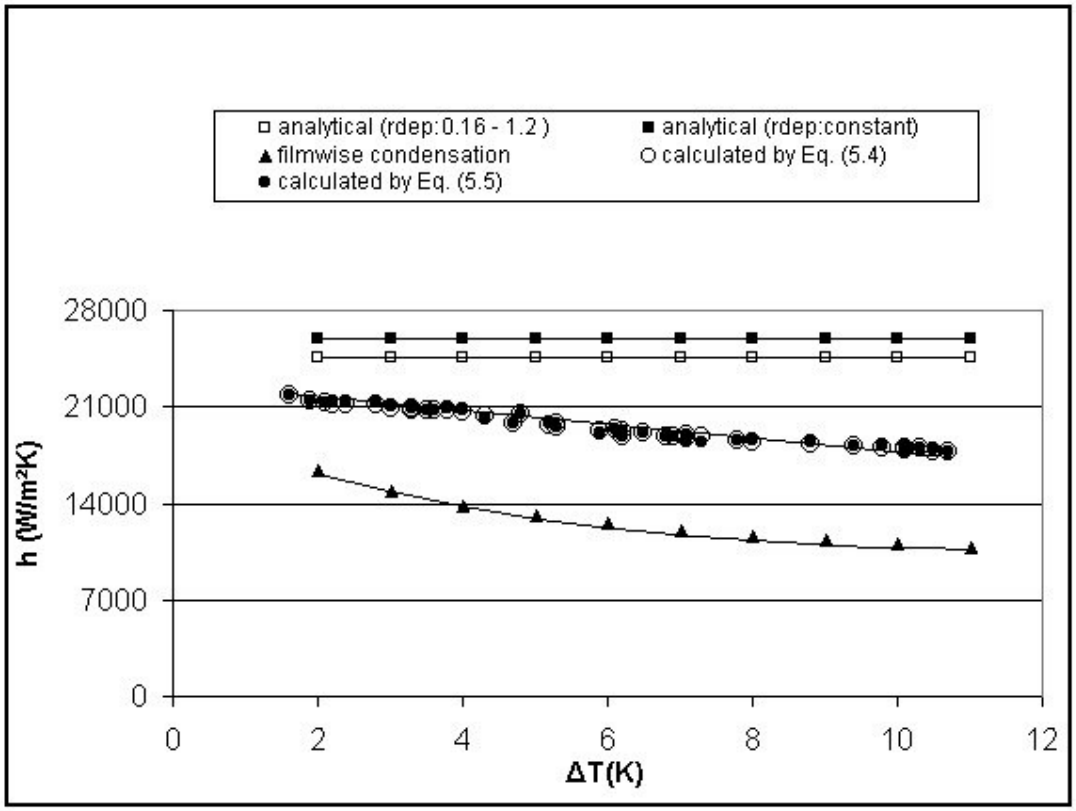

Figure 5.11 Comparison of the mean heat transfer coefficient with surface subcooling.

It is observed in Fig. 5.11 that there is no big difference in the analytical results of the mean heat transfer coefficients which are calculated for constant ($r_{dep} = 0.159 \times 10^{-2}$) and varying ($r_{dep} = 0.16 \times 10^{-2} \text{mK}\ 1.2 \times 10^{-2} \text{m}$) values of departing droplets by using Eq. (3-24). The mean heat transfer coefficient has a small decrease with increasing surface subcooling (ΔT) for the analytical calculations, but the same can not be said for experimental results and mean heat transfer coefficient of filmwise condensation.. The decreasing tendency of mean heat transfer coefficient can be seen better for larger surface subcoolings(ΔT).

Although experimentally measured heat transfer coefficients are higher than the heat transfer coefficients calculated for filmwise condensation, they are smaller than the analytically calculated heat transfer coefficient. The analytically calculated dropwise condensation heat transfer coefficients are almost twice of the heat transfer coefficients obtained by filmwise condensation. Noncondensable gases can be one reason why experimental results are smaller than analytical results. If the radius of the minimum size of the coalescing droplets are taken smaller than $r_{co} = 52 \times 10^{-6} m$ in analytical calculations, higher values for the mean heat transfer coefficient can be obtained.

Variation of mean heat transfer coefficient as a function of departure size which varies a couple of order of magnitude at different fractional area coefficient, n is shown in Table 5.10 and Fig. 5.12. It can be deduced in Table 5.10 that there is no significiant difference in values of mean heat transfer coefficient at different surface subcoolings. Therefore, only the variation of mean heat transfer coefficient for different fractional area coefficient n are compared with departing size droplet radius (r_{dep}) in Fig. 5.12 .

Table 5.10 Comparison of heat transfer coefficient calculated by using Eq. (3-24) for different surface subcooling (ΔT) with departing size droplet radius (r_{dep}).

	h (Heat Transfer Coefficient - W/m²K)									
rdep*100 (m)	ΔT=11	ΔT=10	ΔT=9	ΔT=8	ΔT=7	ΔT=6	ΔT=5	ΔT=4	ΔT=3	ΔT=2
0.0159	30122	30122	30122	30122	30122	30122	30122	30123	30123	30124
0.159	25936	25936	25937	25938	25939	25941	25943	25946	25952	25963
1.59	13550	13550	13550	13550	13550	13551	13551	13552	13553	13555
15.9	6471	6471	6471	6471	6472	6473	6475	6477	6481	6489
159	3024	3024	3024	3024	3025	3025	3025	3025	3026	3027

It can be seen in Fig. 5.12 that while the fractional area constant n increases the mean heat transfer coefficient decreases. Since droplets cover the condensation surface more, as the coefficient n increases the fractional area covered by droplets increases which causes a reduction in heat transfer.

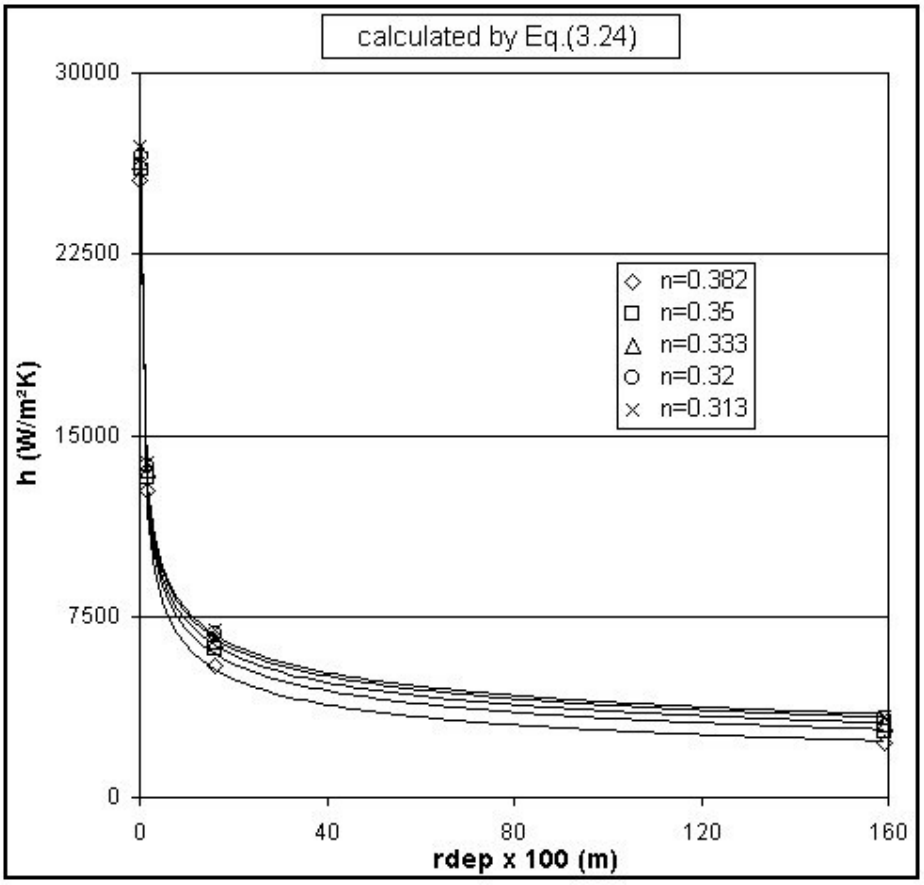

Figure 5.12 Comparison of mean heat transfer coefficient for different fractional area coefficient n with departing size droplet radius (r_{dep}).

The variation of mean heat transfer coefficient presented as a function of coalescence size drop radius (r_{co}) at various fractional area coefficient, n, in Table 5.11 and Fig. 5.13. The values of Table 5.11 show that the surface subcooling (ΔT) has not significiant effect on the mean heat transfer coefficient. Therefore, only the variation of mean heat transfer coefficient for different fractional area coefficient n are presented with coalescence size droplet radius (r_{co}) in Fig. 5.13.

Table 5.11 Comparison of heat transfer coefficient calculated by using Eq. (3-24) for different surface subcoolings (ΔT) with coalescence size droplet radius (r_{co}).

	h (Heat Transfer Coefficient - W/m²K)									
rco*(10^6)	ΔT=11	ΔT=10	ΔT=9	ΔT=8	ΔT=7	ΔT=6	ΔT=5	ΔT=4	ΔT=3	ΔT=2
520	3971	3971	3971	3972	3973	3974	3976	3979	3983	3992
52	25936	25936	25937	25938	25939	25941	25943	25946	25952	25963
5.2	97164	97163	97163	97164	97164	97165	97166	97167	97169	97174
2.6	138225	138222	138223	138224	138224	138226	138227	138230	138235	138243
0.52	289006	288977	288977	288978	288978	288979	288980	288981	288983	288987

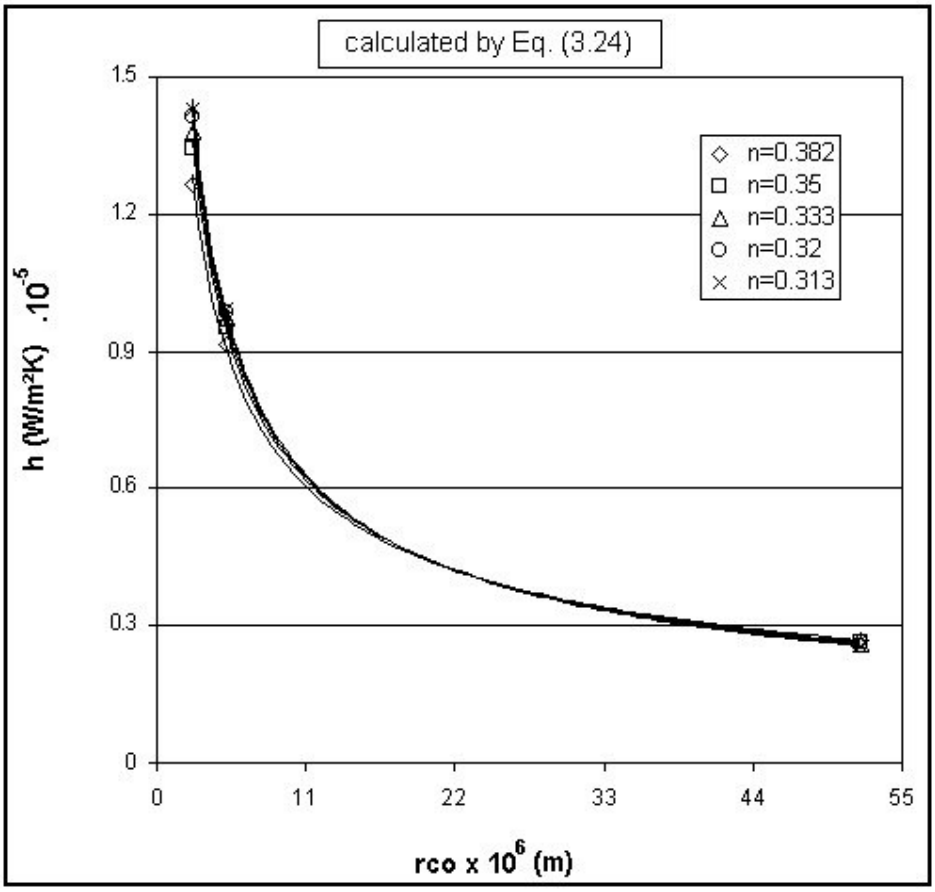

Figure 5.13 Comparison of heat transfer coefficient for different fractional area coefficient n with coalescence size droplet radius (r_{co}).

5.4 Effect of Fractional Area (f_{co}) on Condensation Heat Transfer

Le Fevre and Rose (14) suggested that Eq. (2-1)

$$f_{co}\left(r/r_{max}\right) = 1 - \left(\frac{r}{r_{max}}\right)^{n} \qquad (2-1)$$

can be used for the time average drop size distribution where f_{co} is the fraction of area occupied by droplets in the size range from the radius r to the maximum radius r_{max}. Except as may arise within the empirically determined exponent n, Eq. (2-1) contains no parameters effected by the fluid or solid surface properties. This form of the dropsize distribution is expected to be suitable only for the unsteady drop size distribution which form in the swept region left by a deprating droplet. By appropriately selecting the coefficient n, the same equation can be used to describe a time averaged drop distribution as well.

The experimental results of some researchers, such as Graham and Griffith (67), Tanasawa and Ochiai (68) showed that the coefficient n varies between 0.313-0.350. The theoretical study of Tanaka(15) showed that n should be around 1/3 for the unsteady drop size distribution. Le Fevre and Rose (14) used the same value in Eq. (2-1) in order to compare heat transfer measurements with their analytical model. Rose and Glicksman (52) used a value of 0.382 for their analytical study. Therefore it is constant and a value of 1/3 is used for n in the present study.

Variation of fractional area with coefficent n is presented in Fig. 5.14. It can be seen in the figure that the coefficent n has a significiant effect on the fractional area. While coefficient n increases, the fractional area occupied by droplets also increases that causes a reduction in the mean heat flux.

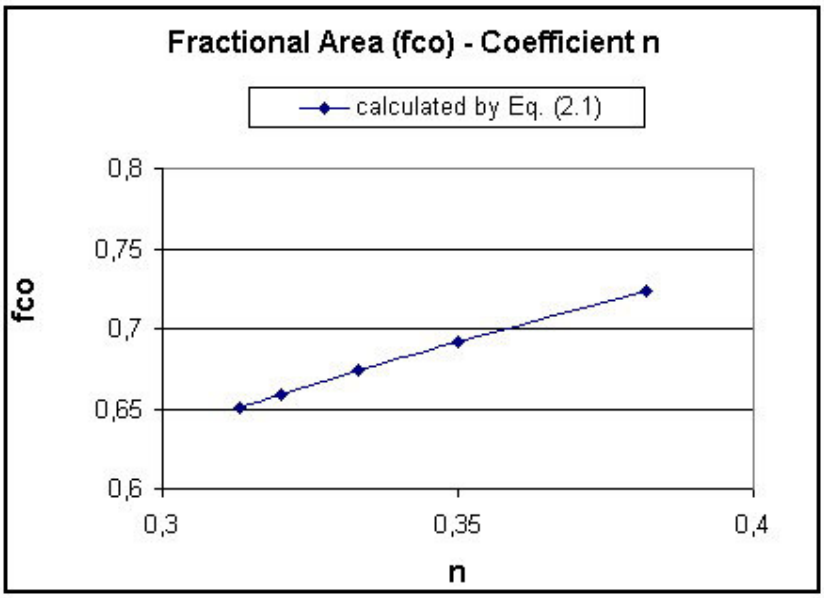

Figure 5.14 Variation of fractional area with coefficent n.

Variation of mean heat transfer coefficient for different values of coefficient n is also presented in Fig. 5.15. It is seen from Fig. 5.15 that as the coefficient n decreases, the mean heat transfer coefficient increases. It is clear that a small increase in fractional area causes a reduction in the mean heat flux since droplets cover the condenser surface.

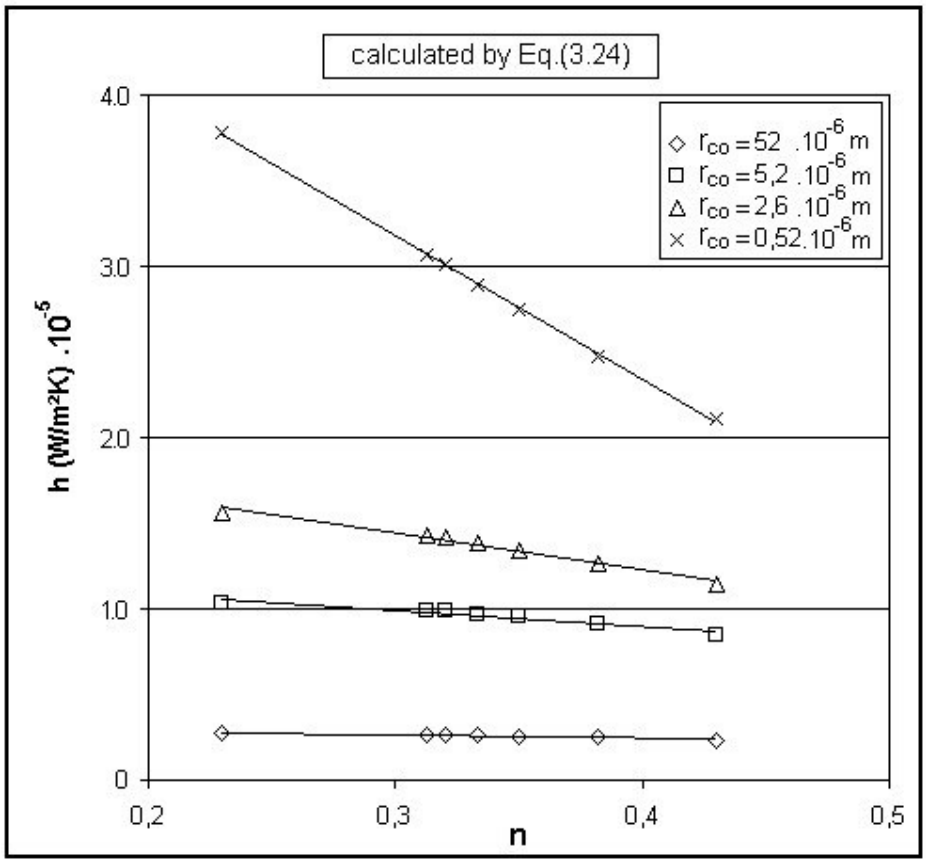

Figure 5.15 Variation of heat transfer coefficient for different coalescence size drop radius with respect to fractional area constant n.

Variations of fractional area with drop radius for different values of n are presented in Fig. 5.16. It is deduced from Fig. 5.16 that while drop radius in coalescence region increases, the fractional area decreases. However it seems that difference in fractional area at different values of n is not significant.

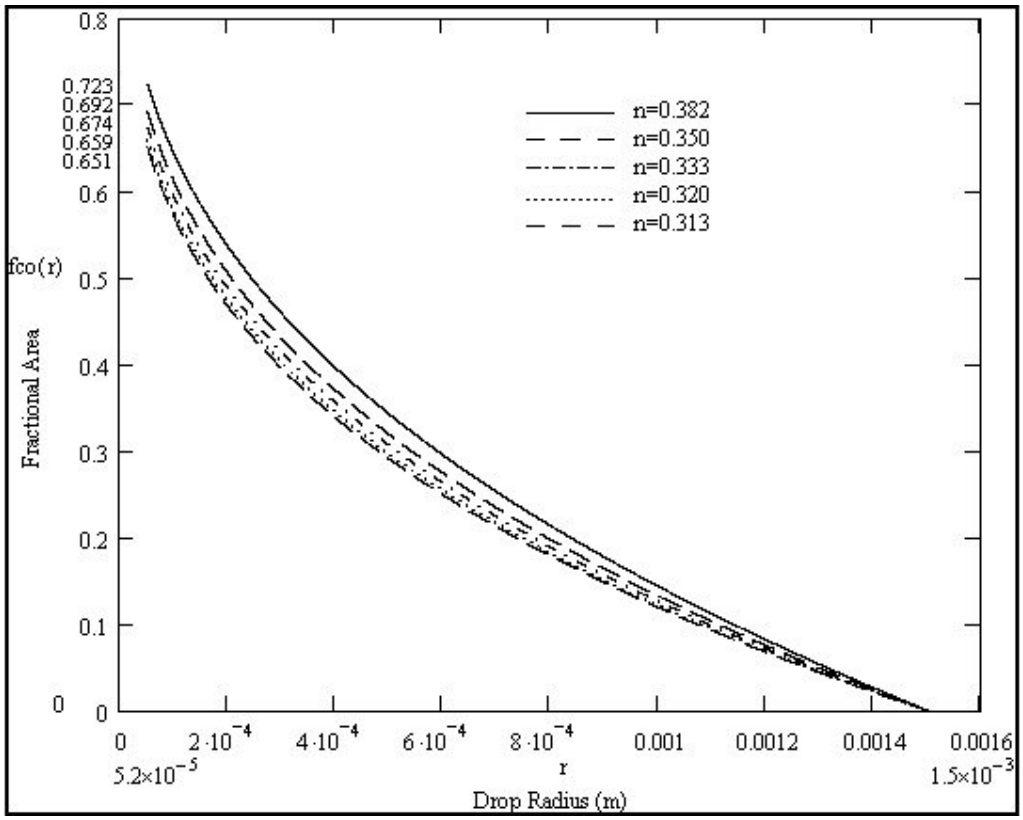

Figure 5.16 Variation of fractional area with drop radius at different fractional coefficient n.

CHAPTER 6

CONCLUSIONS

Analytical and experimental data are presented for condensation of steam on a condensation tube. The conclusions drawn from the present study are as follows:

Condensation rate is higher in dropwise condensation than filmwise condensation at the same surface subcooling (ΔT). Therefore, the condenser surface area can be reduced in a ratio of 1/3 - 1/4 which might result in considerable savings in condenser design.

While the fractional area coefficient n increases, the mean heat flux decreases due to the fractional area occupied by droplets that insulate the condenser surface.

The results of analytical investigation show that the mean heat transfer coefficient decreases by increasing the temperature difference (ΔT) between steam and tube wall.

It is concluded from the experiments that the heat transfer rate is significantly increased by increasing the flow rate of cooling water due to the sweeping effect of steam on the condensate. However, it is seen from experiments that by increasing the temperature of cooling water, the sweeping effect does not have a considerable effect on condensation.

Comparison of the experimental results with the literature show that although the heat transfer coefficients found by the present study are higher than those found by some researchers, they are less than those found by analytical results.

6.1 Recommendations for Future Work

In further studies, the geometry of the condenser tube can be changed, e.g., spherical condenser tube may be constructed to increase the condensation surface.

It is possible to obtain much higher temperature difference between steam to wall by using different working fluids (liquid nitrogen) and some experimental setups.

Various coated surfaces can be prepared to promote dropwise condensation of steam, e.g., a polymer film on the metal substrate may be feasible way for promoting dropwise condensation of organic vapours.

The working fluids may also be changed in advanced studies. Different fluids may be used instead of both steam and the cooling water.

REFERENCES

1. McCormick , J.L. and Baer , E. , '' Dropwise Condensation on Horizantal Surfaces , '' Developments in Mechanics , Pergamon Press , N.Y. , pp. 749-75 (1965) .

2. E. Schmidt, W. Schurig, W. Sellschop, Versuche uber die kondensation von wasserdampf in film — und tropenform, Tech. Mech. Thermodyn. (Forsch. Ing. Wes.) 1 (1930) 53–63.

3. J.L. McCormic, J.W. Westwater, Nucleation sites for dropwise condensation, Chem. Eng. Sci. 20 (1965) 1021**.**

4. Y.J. Song, D.Q. Xu, J.F. Lin, S.X. Tsian, A study on the mechanism of dropwise condensation, Int. J. Heat Mass Transfer 34 (1991) 2827–2832.

5. Jakob , M. , ''Heat Transfer in Evaporation and Condensation – II , '' Mechanical Engineering , 58 , pp. 729 -739 (1936).

6. Emmons , H. , ''The Mechanism of Drop Condensation , ''.Trans. Am. Inst. Chemical Eng. , 35 , p. 109 (1939).

7. Erb. R.A. and Thelen , E. , ''Dropwise Condensation , '' First International Symposium on Water Desalination , Washington , D.C. (Oct. 3-9 , 1965).

8. Eucken , A. , ''Energie – und Stoffaustausch an Grenzflachen , ''Die Naturwissenschaften , 14 , pp. 209-218 (1937).

9. Welch, J.F. and Westwater , J.W. ''Microscobic Study of Dropwise Condensation,'' paper presented at the 1961 International Heat Transfer Conference, Colorado , USA , p. 302.

10. Umur , A. and Griffith , P. , ''Mechanism of Dropwise Condensation ,'' Trans. ASME ,Journal of Heat Transfer , 87C , pp. 275, 282 (1965).

11. Ivanovskii , M.N. , Subbotin , V.I. , and Milovanov , Yu.V. , ''Heat Transfer with Dropwise Condensation of Mercury Vapor'' , Teploenergetika , 14 , p.81 (1967).

12. Glicksman , L.R. and Hunt , A.W. ,''Numerical Simulation of Dropwise Condensation ,'' Int. J. Heat Mass Transfer , 15 , p.2251 (1972).

13. Graham , C. And Griffith , P. , ''Dropsize Distribution and Heat Transfer in Dropwise Condensation , '' Int. J. Heat Mass Transfer ,16 , p.337 (1973).

14. Le Fevre , E.J. and Rose , J.W. , ''A Theory of Heat Transfer by Dropwise Condensation ,'' Proc. of 3rd. Inter. Heat Transfer Conf. , 2 , pp.362 – 375 (1966).

15. Tanaka , H. , ''A Theoretical Study of Dropwise Condensation , '' Journal of Heat Transfer , Trans. ASME , Series C , 97 , pp.72-78 (1975).

16. Fatica N. and Katz , D.L , ''Dropwise Condensation ,'' Chem. Eng. Progress , 45 , No.11 ,pp.661 – 74 (1949).

17. Merte , H. , Jr. ,Yamali , C. '' Profile Departure of Condensation Drops on Vertical Surface '' , Warme und Stoffubertragung (published in 1983).

18. Krischer , S. And Grigull , U. , ''Microscobic Study of Dropwise Condensation ,'' Warme – und Stoffubertragung , 4 , pp.4859 (1971).

19. Othmer , D.F. , ‘’The Condensation of Steam ‘’ Industrial and Engineering Chemistry , 21 , p.576 (1929).

20. Furman ,T. and Hampson , H. ‘’Experimental Investigation into the Effects of Cross Flow with Condensation of Steam and Steam – Gas Mixtures on a Vertical Tube’’ , Proc. Inst. Mech. Engineers , 173 , No.5 , p.147 (1959).

21. Tanner , D.W. , Pope , D. , Potter , C.J. and West , D. , Heat Transfer in Dropwise at Low Steam Pressure in the Absence and Presence of Noncondensable Gas ‘’ , Int.J. Heat Mass Transfer , 11 , pp.181 - 190 (1968).

22. Le fevre , E. J. and Rose , J.W. ‘’An Experimental of Heat Transfer by Dropwise Condensation ‘’ Int. J. Heat Mass Transfer , 8 , pp.1117 – 1133 (1965).

23. Osment , B.D.J. , Tudor , D. , Speirs , R.M.M. and Rugman , W. ‘’Promoters for the Dropwise Condensation of Steam ‘’ Trans. Instn. Chem. Engrs. , 40 ,p.152 (1962).

24. Bromley ,L.A. and Read , S.M. ‘’Dropwise Condensation ‘’ ,AIChE Journal 21 , No.2 , p.391 (1975).

25. Blackman , L.C.F. , Dewar ,M.J.S. ,and Hampson , .H. ‘’An Investigation of Compounds Promoting the Dropwise of Steam’’, Journal of Applied Chemistry , 7 , p.160 (1957).

26. D.C. Zhang, Z.Q. Lin, J.F. Lin, New surface materials for dropwise condensation, in: Proceedings of the 8th International Heat Transfer Conference ’86, Vol. 4, San Francisco, 1986, pp. 1677–1682.

27. D.C. Zhang, Z.Q. Lin, J.F. Lin, New method for achieving dropwise condensation. III. Determination of dropwise-condensation-heat transfer coefficient and life-time tests of heat transfer surfaces, J. Chem. Ind. Eng. (China) 38 (1987) 274–280.

28. Q. Zhao, D.C. Zhang, J.F. Lin, Surface materials with dropwise condensation made by ion implantation technology, Int. J. Heat Mass Transfer 34 (1991) 2833–2835.

29. Y.J. Song, X.H. Ma, D.Q. Xu, J.F. Lin, Condensation of steam on chromium, in: Proceedings of China–Japan Chemical Engineering Conference, Tianjin University Press, Tianjin, 1991, pp. 688–695.

30. S.S. Finnicum, J.W. Westwater, Dropwise condensation of steam on chromium, Int. J. Heat Mass Transfer 32 (1989) 1541–1549.

31. X. Liu, D.Q. Xu, Study of enhancement of condensation heat transfer on Cu-BTA film surface, J. Dalian Univ. Technol. 36 (1996) 162–164.

32. X.F. Guo, L. Bai, Z.Y. Cai, J.F. Lin, Dropwise condensation on a horizontal tube, J. Eng. Thermophys. 11 (1991) 72–75.

33. J.H. Yang, L.X. Cheng, Study on dropwise condensation heat transfer on composite electroplating surface, Chem. Eng. 24 (1996) 38–41.

34. Xin, M.D., Xia, J.L., Heat transfer by dropwise condensation in the two-phase closed thermosiphons, in: Proceedings of the 8th International Heat Transfer Conference ’86, Vol. 4, San Francisco, 1986, pp. 1683–1688**.**

35. X.H. Ma, B.X. Wang, D.Q. Xu, J.F. Lin, Experimental investigation of dropwise condensation lifetime for polymer surfaces, J. Eng. Thermophys. 18 (1997) 196–200.

36. Tanner , D.W. , Pope , D. , Potter , C. J .and West D. , ‘’The Promotion of Dropwise Condensation by Monolayers of Radioative Fatty Acids II. Chromium Surfaces ‘’, Journal of Applied Chemistry , 14 , p.439 (1964).

37. Davies , G. A. , Mojtehedi , W. and Ponter , A. B. , ‘’Measurement of Contact Angles Under Condensation Conditions. The Prediction of Dropwise - Filmwise Transition ‘’ Int.J.Heat Mass Transfer , 14 , p.709 (1971).

38. Smith , T. , ‘‘ The Hydrophilic Nature of a Clean Gold Surface ‘’ Journal of Collaid and Interface Science , 75 , No.1 , p.51 (1980).

39. A.B. Ponter, Contact angles on metal and polymer surfaces in mass transfer environments, Adv. Colloid Interface Sci. 39 (1992) 383 – 395.

40. X.H. Ma, Dropwise condensation on PTFE coated surfaces and the catastrophe transition mechanisms between dropwise and film condensation, Ph.D. Thesis, Dalian University of Technology, (1994).

41. A.W. Adamson, Physical Chemistry of Surfaces, 5th Edition, Wiley, New York, (1990).

42. D.K. Owens, R.C. Wendt, Estimation of the surface free energy of polymers, J. Appl. Polym. Sci. 13 (1967) 1741–1747.

43. Yamali , C. , ‘’Dropwise Condensaiton Under High Gravity and at Large Subcooling ‘’ , Ph.D. Thesis , Univeristy of Michigan (1983).

44. McCormick , J.L. ,and Westwater , J.W. , ‘’Nucleation Sites for Dropwise Condensation ‘’ , Chemical Engineering Science , 20 , pp.1021-1031 (1965).

45. Peterson , A.C.and Westwater , J.W. ,’’Dropwise Condensation of Ethylene and Glycol ‘’ , presented at the 8.National Heat Transfer Conference A.I.Ch.E-A.S.M.E , Los Angeles , California (1965).

46. Ahrendts , J.B. ,’’Der Warmeleitwiederstand eines Kondensattropfens ’’ , Warme – und Stoffubertragung , 5 , pp.239 – 244 (1972).

47. Lorenz , J.J. and Mikic , B.B. , '' The Effect of Thermocapillary Flow on Heat Transfer in Dropwise Condensation ,'' Trans.A.S.M.E. Journal of Heat Transfer , 92 , pp 46- 52 (1970).

48. Sadhal , S.S. and Plesset , M.S. ''Effect of Solid Propertiesand Contact in Dropwise Condensation and Evaporation '' , Trans. ASME ,Journal of Heat Transfer ,101 , pp.48-54 (1979).

49. Hurst , C.J. and Olson , D.R. ,''Conduction through Droplets during Dropwise Condensation , '' J.Heat Transfer ,95 ,pp 12-20 (1973).

50. Rose , J.W. , ''Dropwise Condensation Theory '' , International Journal of Heat and Mass Transfer , 24 , pp.191-194 (1981).

51. Tanaka , H. , ''Measurements of Dropsize Distributions during Transient Dropwise Condensation '' , Trans. A.S.M.E. , Journal of Heat Transfer , 97 , pp.341-346 (1975).

52. Rose , J.W. and Glicksman , L.R., Dropwise Condensation the Distribution of Dropsizes '' , Int. J. Heat Mass Transfer , 16 , pp.411-425 (1973).

53. R/C Dictionary / www.51-50racing.com/dictionary.htm /May 2004

54. McCormick , J.L. and Westwater , J.W. , ''Drop Dynamics and Heat Transfer During Dropwise Condensation of Water Vapor on a Horizantal Surface , '' Chemical Engineering Progress Symposium Series , Vol. 62 , No. 64 , pp. 120-134 (1966) .

55. Q. Zhao, D.C. Zhang, X.B. Zhu, D.Q. Xu, Z.Q. Lin, J.F. Lin , Industrial application of dropwise condensation, Heat Transfer 1990 4 (1990) 391–394.

56. Q. Zhao, B.M. Burnside, Dropwise condensation of steam on ion implanted condenser surfaces, Heat Recovery Syst. CHP 14 (1994) 525–534.

57. Q. Zhao, J.F. Lin, Research progress on industrial application of dropwise condensation, Chem. Ind. Eng. Progress (China) 53 (1991) 17–20.

58. Q. Zhao, D.Q. Xu, Dropwise condensation surface with corrosion resistant properties, Corrosion Rev. 11 (1993) 97–103.

59. Q. Zhao, D.C. Zhang, X.B. Zhu, D.Q. Xu, J.F. Lin, The dropwise condensation condenser design, Nat. J. 14 (3) (1991) 232–233.

60. Yu-Ting Wu, Chun-Xin Yang, Xiu-Gan Yuan, Drop distributions and numerical simulation of dropwise condensation heat transfer, Int. Journal of Heat and Mass Transfer 44 (2001) 4455-4464

61. G.Koch, D.C. Zhang and A.Leipertz, Study on plasma enhanced CVD coated material to promote dropwise condensation of steam, Int. Journal of Heat and Mass Transfer Vol.41 No.13 (1998) 1899-1906

62. Kwang Kim, Advanced Heat Exchangers Using Tunable Nanoscale-Molecular Assembly ,Mechanical Enginnering Depart. and Nevada Ventures Nanoscience program, University of Nevada, Reno

63. Daniel A. Beysens, Phase Transition, Contact Line Dynamics and Drop Coalescence, Equipe du Supercritique pour l'Environnement, les Matériaux et l'Espace Service des Basses Températures, CEA-Grenoble, Grenoble (France) Mailing address: CEA-ESEME, ICMCB, 87, Av. Dr. A. Schweitzer 33608 Pessac Cedex (France)

64. N. Maitia,U, U.B. Desaib, A.K. Raya, Application of mathematical morphology in measurement of droplet size distribution in dropwise condensation ,Th,n Solid Films, 376 (2000) 16-25.

65. B.M. Burnside, H.A. Hadi,Digital computer simulation of dropwise condensation from equilibrium droplet to detectable size, International Journal of Heat and Mass Transfer 42 (1999) 3137-3146.

66. Xuehu Ma, Jiabin Chen, Dunqi Xu, Jifang Lin, Chunsheng Ren, Zhenhu Long , Influence of processing conditions of polymer film on dropwise condensation heat transfer, International Journal of Heat and Mass Transfer 45 (2002) 3405–3411.

67. C.Graham, P.Griffith, Drop size distributions and heat transfer in dropwise condensation, Int. Journal Heat Mass Transfer 16 (1973) 337-346.

68. I.Tanasawa, J.Ochiai, An experimental study on dropwise condensation, Bull. JSME 16 (98) (1972) 1184-1197.

69. The Engineering Physical Sciences Research Council, PRESSURE DROP AND HEAT TRANSFER DISTRIBUTIONS AROUND A BUNDLE OF PLASMATREATED TUBES CONDENSING DROPWISE, Department of Mechanical and Chemical Engineering Heriot-Watt University Riccarton Edinburgh EH14 4AS

.

APPENDIX A

RESULTS OF THE EXPERIMENTS

Table A.1 Experimental Data and Results for $T_{in} = 20°C$

T1 (℃)	T2 (℃)	T3 (℃)	Ts (℃)	m (kg/s)	ΔT (℃)	Q1 (W)	h1 (W/m²K)	Q2 (W)	h2 (W/m²K)
82,2	84,9	86,4	87,50	0,0535	10,49	1128,4	17825	1136,2	17948
82,5	85	86,7	87,67	0,0483	10,33	1119,6	17969	1121,4	17998
82,9	85,4	87,1	87,81	0,0384	10,18	1106,2	18007	1110,2	18071
83,4	85,9	87,4	88,18	0,0319	9,81	1066,2	18010	1075,9	18172
86,1	88,2	89,4	90,18	0,0230	7,81	874,3	18549	873,2	18526
87,3	89,3	90,3	90,89	0,0157	7,10	799,7	18672	795,1	18564
88,6	90,2	91,2	91,80	0,0116	6,19	706,4	18903	703,1	18816

Table A.2 Experimental Data and Results for $T_{in} = 30°C$

T1 (℃)	T2 (℃)	T3 (℃)	Ts (℃)	m (kg/s)	ΔT (℃)	Q1 (W)	h1 (W/m²K)	Q2 (W)	h2 (W/m²K)
81,9	84,8	86,2	87,31	0,0517	10,68	1146,2	17787	1144,3	17757
82,7	85,3	86,8	87,88	0,0428	10,11	1092,9	17921	1092,6	17916
83,8	85,9	87,7	88,62	0,0357	9,37	1026,3	18151	1030,9	18233
84,6	86,7	88,2	89,20	0,0326	8,79	972,9	18336	975,6	18386
85,8	87,7	89,1	89,97	0,0272	8,02	893,0	18444	896,4	18514
87	89	90,1	90,71	0,0211	7,28	826,3	18808	810,1	18439
87,2	89,1	90,3	90,90	0,0205	7,09	813,0	18992	805,2	18811
88,5	90,4	91,2	91,83	0,0174	6,16	719,7	19366	720,3	19381
89,7	91,2	92,1	92,62	0,0148	5,37	639,7	19742	632,1	19506

Table A.3 Experimental Data and Results for $T_{in} = 40°C$

T1 (℃)	T2 (℃)	T3 (℃)	Ts (℃)	m (kg/s)	ΔT (℃)	Q1 (W)	h1 (W/m²K)	Q2 (W)	h2 (W/m²K)
86,7	88,4	89,6	91,07	0,0555	6,92	786,38	18832	784,27	18781
87,6	89,3	90,5	91,19	0,0441	6,80	773,06	18822	771,53	18785
87,8	89,6	90,6	91,51	0,0394	6,48	746,40	19079	748,53	19133
88,2	89,3	90,9	91,80	0,0340	6,19	719,74	19253	718,29	19214
89,5	90,8	91,8	92,67	0,0254	5,32	626,44	19519	626,74	19529
89,7	90,9	92	92,82	0,0238	5,17	613,11	19653	617,05	19779
90,4	91,8	92,6	93,25	0,0211	4,74	586,45	20480	587,58	20519
91,8	92,9	93,6	94,17	0,0153	3,82	479,83	20771	483,75	20941

Table A.4 Experimental Data and Results for $T_{in} = 50°C$

T1 (℃)	T2 (℃)	T3 (℃)	Ts (℃)	m (kg/s)	ΔT (℃)	Q1 (W)	h1 (W/m²K)	Q2 (W)	h2 (W/m²K)
87,3	89,4	90,3	91,07	0,0517	6,92	786,38	18832	784,67	18791
88,8	90,3	91,4	92,02	0,0405	5,97	693,08	19224	689,04	19111
90,4	91,8	92,5	93,23	0,0258	4,76	568,68	19798	570,34	19856
91,0	92,3	93,0	93,65	0,0211	4,34	533,14	20345	531,20	20271
91,3	92,6	93,2	94,00	0,0172	3,99	497,60	20639	498,89	20693
91,9	92,8	93,6	94,37	0,0140	3,62	453,17	20729	452,90	20717
92,4	93,4	93,9	94,68	0,0113	3,31	417,63	20864	418,20	20893

Table A.5 Experimental Data and Results for $T_{in} = 60°C$

T1 (℃)	T2 (℃)	T3 (℃)	Ts (℃)	m (kg/s)	ΔT (℃)	Q1 (W)	h1 (W/m²K)	Q2 (W)	h2 (W/m²K)
92,6	93,7	93,9	95,21	0,0254	2,78	355,43	21142	357,11	21242
93,1	93,9	94,3	95,54	0,0185	2,45	313,22	21181	314,09	21240
94,4	94,8	95,4	95,85	0,0107	2,14	275,45	21254	275,41	21251

Table A.6 Experimental Data and Results for $T_{in} = 70°C$

T1 (℃)	T2 (℃)	T3 (℃)	Ts (℃)	m (kg/s)	ΔT (℃)	Q1 (W)	h1 (W/m²K)	Q2 (W)	h2 (W/m²K)
92,3	93,3	94	94,47	0,05	3,52	439,84	20695	442,47	20819
92,9	93,8	94,4	94,70	0,0394	3,29	413,18	20781	415,85	20915
93,1	93,8	94,5	94,97	0,0340	3,02	382,08	20928	383,09	20983
93,9	94,6	95,0	95,55	0,0192	2,44	311,00	21113	313,34	21273
94,1	94,8	95,1	95,80	0,0156	2,19	279,90	21141	283,12	21384
94,3	94,8	95,3	96,04	0,0130	1,95	253,24	21456	252,84	21422
94,6	94,4	95,4	96,38	0,0105	1,61	213,25	21839	213,66	21881

APPENDIX B

MATHCAD PROGRAM SOURCE

$T_{sat} := 371K$ $\quad P_v := 0.954 \cdot 10^{5} \frac{N}{m^2}$ $\quad h_{fg} := 2261 \cdot 10^{3} \frac{J}{kg}$

$T_s := 364K$ $\quad \rho_l := 959.693 \frac{kg}{m^3}$ $\quad k_f := 679 \cdot 10^{-3} \frac{W}{m \cdot K}$

$r_{co} := 2.6 \cdot 10^{-6} m$ $\quad \sigma := 59.3 \cdot 10^{-3} \frac{N}{m}$ $\quad C_p := 4180 \frac{J}{kg \cdot K}$

$r_{dep} := 0.25 \cdot 10^{-2} m$ $\quad G := 461.9 \frac{J}{kg \cdot K}$ $\quad \theta := 1.134$

$\gamma := 1$ $\quad M := \frac{1}{3}$ $\quad g := 9.81 \frac{m}{s^2}$

for $n \in 1..10000$

$Ts \leftarrow 360$

$rdep \leftarrow 0.159 \cdot 10^{-2}$

$rco \leftarrow 52 \cdot 10^{-6}$

$\sigma \leftarrow 59.3 \cdot 10^{-3}$

$m \leftarrow \frac{1}{3}$

$hfg \leftarrow 2261317$

$Pv \leftarrow 0.954 \cdot 10^{5}$

$\theta \leftarrow 1.134$

$\rho l \leftarrow 959.693$

$\gamma \leftarrow 1$

$Tsat \leftarrow 371$

$\Delta Tt \leftarrow (Tsat - Ts)$

$B \leftarrow \frac{kf \cdot Tsat}{\theta \cdot K1}$

$K1 \leftarrow \left(\frac{2 \cdot \gamma}{2 - \gamma}\right) \cdot \left(\frac{1}{2 \cdot \pi}\right)^{\frac{1}{2}} \cdot \frac{(hfg)^2 \cdot Pv}{G^{\frac{3}{2}} \cdot (Tsat)^{\frac{3}{2}}}$

$K2 \leftarrow \frac{2 \cdot Tsat \cdot \sigma}{hfg \cdot \rho l}$

$a_n \leftarrow rco \cdot e^{\frac{\ln(rdep) - \ln(rco)}{10000} \cdot n}$

$R \leftarrow \frac{a_n}{\sin(\theta)}$

$a_0 \leftarrow rco$

$df_n \leftarrow m \cdot \left[\frac{\left[\frac{a_n + a_{(n-1)}}{2}\right]}{rdep}\right]^{m-1} \cdot \frac{\left(a_n - a_{n-1}\right)}{rdep}$

$$qdpa_n \leftarrow \frac{2 \cdot K1 \cdot B}{(a_n)^2 \cdot Tsat} \cdot \left(a_n \cdot \Delta Tt - K2 \cdot \sin(\theta)\right) \cdot \left(-\cos(\theta) + \frac{a_n + B \cdot \cos(\theta)}{a_n} \cdot \ln\left(\frac{a_n + B}{B}\right)\right)$$

for $j \in 1..10000$

$sumx_j \leftarrow df_j \cdot qdpa_j$

for $k \in 0..9999$

$sumx_0 \leftarrow 0$

$sumx_{k+1} \leftarrow sumx_{k+1} + sumx_k$

$sumx_{10000} \cdot \left(48 \cdot 10^{-3} \cdot 3.142 \cdot 10^{-3}\right)$